POLITECNICO
MILANO 1863

SCUOLA DI INGEGNERIA INDUSTRIALE
E DELL'INFORMAZIONE

Thermohydraulic performance analysis of the submerged-containment PCCS concept for SMRs under severe LOCA conditions

Tesi di Laurea Magistrale in
Nuclear Engineering - Ingegneria Nucleare

Author: **Jason Gabriel Ulises Treufo Quiroz**

Student ID: 245541
Advisor: Prof. Marco Pellegrini
Academic Year: 2025-26

Abstract

Passive safety systems operate without active controls. They rely instead on fundamental physical principles such as natural circulation, condensation, and heat transfer. The Passive Containment Cooling System (PCCS) adopted in the NuScale and Nuward SMR designs submerges the steel containment vessel in a water pool to remove heat. This thesis investigates the submerged-containment PCCS concept through thermohydraulic simulations using GOTHIC under a severe Loss of Coolant Accident (LOCA), when the containment is externally cooled by air and water. The case study corresponds to the new test facility at Becker Technologies GmbH. The model was developed following Nuclear Energy Agency (NEA) recommendations. Steam injection, hydrogen injection, pool water injection, and pool temperature were varied to assess their influence on peak pressure, peak temperature, hydrogen concentration, and condensation rate. Initial conditions were 101.325 kPa and 20 °C, with all control volumes filled with air. In the base case, peak pressure reached approximately 1200 kPa due to the competition between steam injection and heat removal by condensation. The peak temperature was 188 °C, corresponding to saturation conditions. Gas and temperature stratification was developed due to buoyancy effects. The containment atmosphere was characterized by an upper hydrogen-rich region, a middle steam-rich condensing region, and a lower air-rich region. The average condensation rate was 0.1105 kg/s (99.45% of the steam injection rate), with a maximum of 0.1463 kg/s, which represents the cooling capability limits of the system. The parametric study showed that the condensation rate depends primarily on the steam injection rate, while hydrogen had no statistically significant effect due to the stratification. Two characteristic factors were introduced: the characteristic (or peak) time, defined as the time when condensation equals the steam injection, and the volumetric gas-phase energy as an indicator of the cooling capability of the system. Finally, it was determined that the system remains in a safe condition when the volumetric energy do not exceed the limit of 13720 kJ/m^3.

Keywords: Severe Accidents, SMR, PCCS, Thermohydraulics, GOTHIC.

Abstract in lingua italiana

I sistemi di sicurezza passiva operano senza controlli attivi. Si basano invece su principi fisici fondamentali come la circolazione naturale, la condensazione e il trasferimento di calore. Il Passive Containment Cooling System (PCCS) adottato nei progetti SMR di NuScale e Nuward prevede l'immersione del vessel di contenimento in acciaio in una piscina d'acqua per la rimozione del calore. La presente tesi analizza il concetto di PCCS a contenimento sommerso mediante simulazioni termo-idrauliche con il codice GOTHIC in condizioni di grave Loss of Coolant Accident (LOCA), quando il contenimento è raffreddato esternamente da aria e acqua. Il caso di studio riguarda il nuovo impianto sperimentale di Becker Technologies GmbH. Il modello è stato sviluppato secondo le raccomandazioni della Nuclear Energy Agency (NEA). Sono state variate la portata di iniezione di vapore, l'iniezione di idrogeno e le condizioni della piscina per valutarne l'influenza su pressione e temperatura di picco, concentrazione di idrogeno e tasso di condensazione. Le condizioni iniziali erano 101325 kPa e 20 °C, con volumi riempiti d'aria. Nel caso base, la pressione di picco ha raggiunto circa 1200 kPa per la competizione tra iniezione di vapore e rimozione di calore per condensazione; la temperatura massima è stata di 188 °C, corrispondente alla saturazione. Si è sviluppata una marcata stratificazione termo-compositiva: regione superiore ricca di idrogeno, intermedia ricca di vapore in condensazione e inferiore ricca di aria. Il tasso medio di condensazione è risultato pari a 0.1105 kg/s (99.45% della portata di vapore), con un massimo di 0.1463 kg/s, rappresentativo del limite di raffreddamento. Lo studio parametrico ha mostrato che il tasso di condensazione dipende principalmente dalla portata di vapore, mentre l'idrogeno non presenta un effetto statisticamente significativo. Sono stati introdotti due parametri caratteristici: il tempo caratteristico (quando condensazione e iniezione si eguagliano) e l'energia volumetrica della fase gassosa quale indicatore della capacità di raffreddamento. Il sistema rimane in condizioni sicure finché tale energia non supera 13720 kJ/m^3.

Parole chiave: Incidenti gravi, SMR, PCCS, Thermohydraulics, GOTHIC.

Contents

Introduction

Nuclear safety has been one of the major issues to be studied since the inception of the nuclear industry [1]. The development and design of advanced nuclear reactors are intended to increase their reliability and safety by means of system redundancy, minimization of system components, non-reliance on external power sources, and integral long term decay heat removal and containment cooling systems [2].

In this context, passive safety systems are engineered features designed to perform safety functions without the need for active controls, operator intervention, or external power supplies [3]. Instead, they rely on fundamental physical principles such as gravity-driven flow, natural circulation, condensation, and heat conduction to operate automatically under accident conditions [3, 4]. Current reactor designs incorporating these mechanisms include the Isolation Condenser System (ICS) implemented in the BWRX-300, which removes decay heat through natural circulation to heat exchangers submerged in a water pool, and the Passive Containment Cooling System (PCCS) adopted in NuScale and Nuward Small Modular Reactors (SMRs) (see Figure 1), where the containment vessel is fully submerged in a water pool for passive heat removal [4].

Alternative PCCS concepts are also reported in the literature. For example, the PCCS of the AP300 which consists of an elevated water tank that discharges water over the containment vessel, forming an external water film. As the containment heats up, the water film evaporates and the resulting vapor is carried away by buoyancy-driven air flow, similarly to a natural draft cooling tower [4].

This thesis will focus on the submerged-containment PCCS concept implemented in designs such as the NuScale and Nuward SMRs. A suitable definition of this PCCS concept is provided by the U.S. Nuclear Regulatory Commission (US NRC) as an engineered safety system capable of transferring heat directly from the steel containment vessel to the external environment. The operability of this system relies primarily on steam condensation to prevent that the containment pressure and temperature exceed the design values during a postulated design-basis accidents, e.g. a loss-of-coolant accident (LOCA) [5].

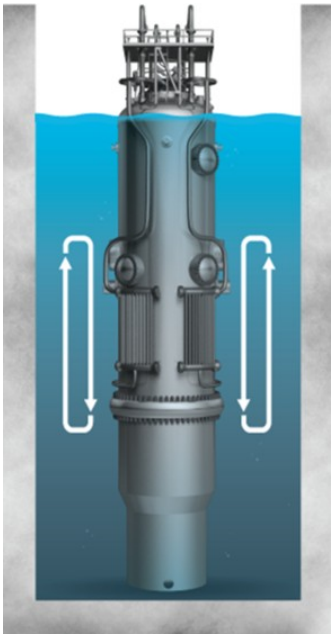

Figure 1: NuScale power module [6].

The origin and development of passive safety systems is of long data, as documented in various publications of the International Atomic Energy Agency (IAEA) [3, 7, 8]. However, their widespread adoption in reactor design have been intensified considerably in recent years. Particularly, this has been triggered by the occurrence of major nuclear accidents such as the Fukushima Daiichi nuclear disaster and the increasing concerns of the population [9]. The Fukushima accident exposed vulnerabilities of current NPP designs highlighting the need for enhanced systems to increase the plant resilience, specially when subjected to beyond design basis accidents and prolonged station blackout conditions [9, 10]. In response, nuclear regulatory authorities adapted NPP design criteria and safety requirements for acceptability, including design extension conditions [11]. These conditions include scenarios that may lead to significant core degradation and that may jeopardize the integrity of the physical barriers, i.e. severe accidents [11]. Within this reinforced regulatory environment, passive safety systems have gained renewed relevance, as their reliance on fundamental physical principles and reduced dependence on external power sources directly address these vulnerabilities.

Considering the strict requirements applied, such passive systems must undergo comprehensive evaluation prior to large-scale commercial deployment [12]. Accordingly, the main objective of this thesis is to study the fundamental physics behind the submerged-containment PCCS concept adopted in some SMRs, and assess its performance, through thermohydraulic simulations, under a severe LOCA. For this purpose, the new experi-

mental test facility at Becker Technologies GmbH is modeled and analyzed. This facility is designed to provide high-resolution experimental data on the transient evolution of accidents and to support the validation of the SMR-PCCS concepts with a large external water pool.

The creation of the plant model will follow most of the Nuclear Energy Agency recommendations to carry out a safety analysis with CFD tools. Starting with the specification of the accidental scenario, the description of the plant and the phenomena identification ranking table (PIRT). The plant model is created with the CFD-type code GOTHIC. The selection of the physical models follows the results of the PIRT table and preliminary assessment of the phenomena. Then, the plant model is assessed through a verification step to confirm that the model was well implemented. Finally, the plant model is evaluated at different boundary conditions (e.g. steam mass flow injection, hydrogen mass flow injection, external water temperature, etc.) to carry out a parametric analysis. The parametric analysis aims to determine under which accidental conditions the PCCS is a reliable system that effectively maintains the containment in a safe condition. The levels of the parameters to be varied were determined by a standard design of experiment (DOE) technique, which allowed to distinguish the significant effects over the plant response.

Objectives

The main objective of this thesis was to study the fundamental physics behind the submerged-containment PCCS concept adopted in some SMRs (such as, NuScale or Nuward), and assess its performance, through thermohydraulic simulations, under a severe Loss-of-Coolant Accident.

The specific objectives were:

- To analyze the thermohydraulic phenomena inside the containment when it is externally cooled by natural convection with air and water.
- To model and evaluate a generic SMR-PCCS test facility under typical accident conditions, and to design the thermohydraulic experiments to be conducted during its commissioning.
- To determine the limitations of the submerged-containment concept, considered as the maximum cooling capability that the design offers and that can effectively maintain the containment in a safe state.
- To study the distribution and evolution of combustible gas mixtures with hydrogen within the containment.

Scope

The plant under investigation corresponds to the new test facility at Becker Technologies GmbH, which purpose is to provide thermohydraulic experimental data for the validation of new SMR passive safety concepts with large water pools. The facility does not intend to represent a specific SMR design but to be a cornerstone for the safety passive system evolution. Therefore, the proposed accident sequence and operating conditions are constrained by the experimental capabilities of the facility and their standard procedures. Furthermore, as the test facility is still under construction during the execution of this thesis work and there is no experimental data available, a validation of the model is not foreseen.

1 Framework

1.1. Safety in Nuclear Power Plants

The Fundamental Safety Principles of the International Atomic Energy Agency (IAEA) establish one fundamental safety objective and ten safety principles that provide the basis for requirements and measures for the protection of people and the environment against radiation risks and for the safety of facilities and activities that give rise to radiation risks [11]. The primary means of preventing and mitigating the consequences of accidents is 'defence in depth'. Defence in depth is implemented primarily through the combination of a number of consecutive and independent levels of protection that would have to fail before harmful effects could be caused to people or to the environment. If one level of protection or barrier were to fail, the subsequent level or barrier would be available [13]. Defence in depth is achieved primarily by means of four successive barriers which prevent the release of radioactive material i.e. fuel matrix, cladding, primary coolant boundary and containment [14]. In consequence, the last physical barrier during an accidental condition to prevent the release of radioactive material to the environment is the containment, and its safety assessment is of primary concern.

In the frame of nuclear safety, there are two main approaches to perform safety analysis, a deterministic and a probabilistic approach [15]. In particular, the objective of a Deterministic Safety Analysis (DSA) of a Nuclear Power Plant (NPP) is to confirm that the safety functions can be performed with the necessary reliability and that the necessary structures, systems and components are capable and sufficiently effective to keep the releases of radioactive material from the plant below acceptable limits [16], specially in postulated accidental conditions [15].

The development and design of advanced nuclear reactors are intended to increase their reliability and safety by means of system redundancy, minimization of system components, non-reliance on external power sources, and integral long term decay heat removal and containment cooling systems. Specifically, the next generation of advanced nuclear reactor designs include: (1) low volumetric heat generation rates; (2) reliance solely on natural

forces, such as gravity and pressurization for safety system operation; and (3) dependence on natural phenomena, such as natural convection and condensation, for safety system performance [2].

1.2. A new safety concept in Small Modular Reactors: the Passive Containment Cooling System

Small Modular Reactors (SMRs) are advanced reactors with a power capacity of typically up to 300 MW(e) per unit [17]. They are characterized by the possibility to be factory-built, to be transported by modules to the plant site, and to be flexible scaled up in terms of power capacity [18]. By 2024, more than eighty (80) SMR designs were under development and deployment at different stages [17]. The development of SMRs and the improvement of the passive safety systems led to the development of the so-called Passive Containment Cooling System (PCCS) [1]. In the literature are found different PCCS, such as the PCCS of the AP300 which consists of an elevated water tank that discharges water over the containment vessel, forming an external water film, and the PCCS of NuScale which consists of a submerged containment vessel in a water pool [4]. Specifically, the submerged containment concept will be analyzed here.

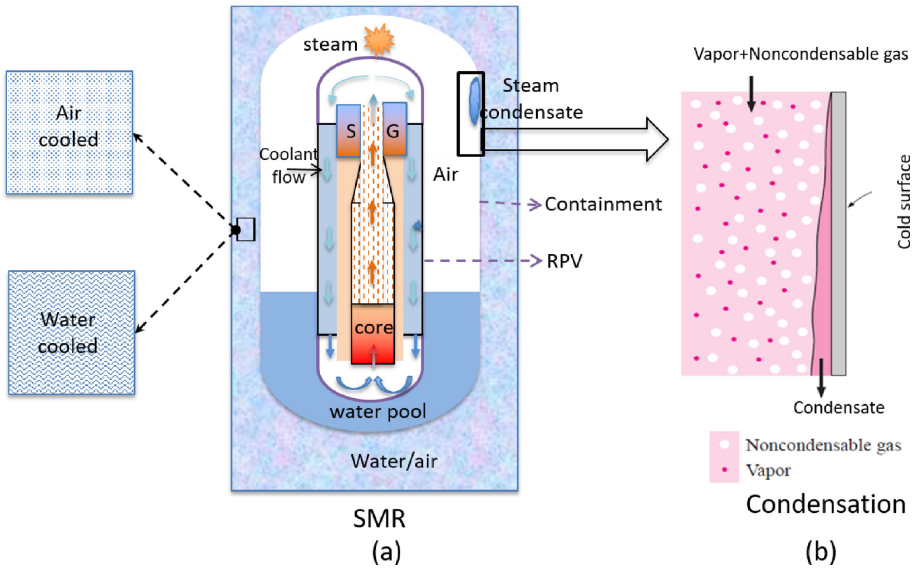

Figure 1.1: (a) Scheme of PCCS of SMR. (b) Condensation inside the containment [19]

The submerged-containment PCCS is an engineered safety system which is capable of transferring heat directly from the steel containment vessel to the external environment. This heat transfer removes the thermal energy from the containment atmosphere following a postulated design-basis accident (e.g. a loss-of-coolant accident (LOCA) or main

steam line break (MSLB) accident), and it prevents the containment from exceeding the design pressure and temperature [5]. The PCCS relies on the condensation of the steam (coming from water flashing in the event of a postulated accident) on the steel containment vessel walls to reduce the containment temperature and pressure (Figure 1.1) [1]. By this mechanisms, the PCCS also limits releases of radioactivity (post-accident) by reducing the pressure differential between the containment atmosphere and the external environment, thereby diminishing the driving force for leakage of fission products from the containment to the atmosphere [5].

1.3. Classification of plant states and progression of a severe accident

The Figure 1.2 shows the different plant states currently considered during the design phase of a NPP. These plant states are grouped and classified depending on the operational conditions of the plant. That is to say, a normal operation is an operation within the specified operational limits of the plant, while a design extension condition is an accidental condition [1] that is not considered for design basis accidents [2] but that are still considered in the design process of the facility. For example, severe accidents which involve significant core degradation are part of a design extension condition [20].

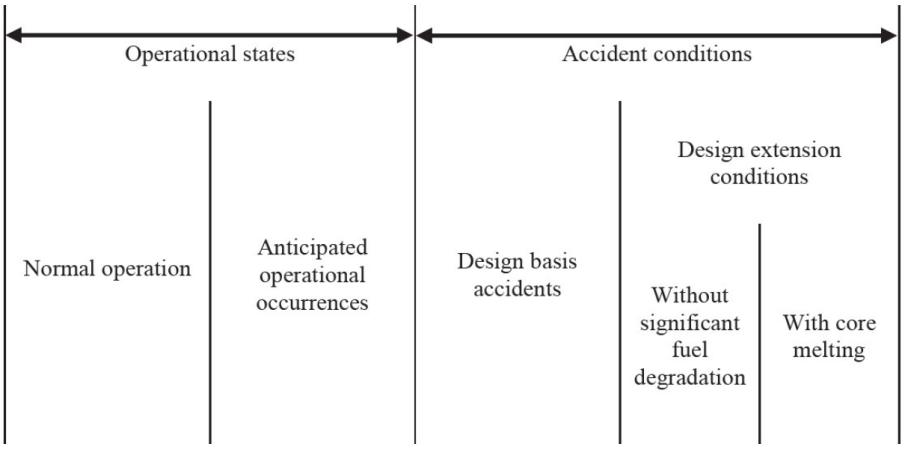

Figure 1.2: Plant states of a nuclear power plant considered in the design phase [20].

[1] According to the IAEA accident conditions are deviations from normal operation that are less frequent and more severe than anticipated operational occurrences, where an anticipated operational occurrence is a deviation that do not cause any significant damage to items important to safety and that can be ensured and maintained stable for a long time.

[2] A design basis accident (DBA) is a postulated accident leading to accident conditions for which a facility is designed (e.g. a LOCA or MSLB) in accordance with established design criteria and conservative methodology, and for which releases of radioactive material are kept within acceptable limits [20].

Due to the increasing demands for safety, the IAEA adapted the NPP design criteria and included the design extension conditions as part of the requirements for acceptability [11]. Before, the designer was required to include only explicit defenses in the plant for DBAs [15]. Nowadays, additional safety features are required to include also those very low probable plant states that are beyond DBAs, i.e. conditions that may lead to significant core degradation and that may jeopardize the integrity of the barriers, e.g. severe accidents [11].

Severe accidents can evolve from postulated accidents that were not controlled in early stages. They can include very complex physicochemical and radiological phenomena that can take place at different stages of the accident [21]. In the case of an accident sequence with sustained loss of core cooling, the accident progression can involve two phases: the in-vessel phase and the ex-vessel phase [14]. The in-vessel phase covers core heat-up, fuel degradation, and core material relocation inside the reactor pressure vessel (RPV). From the failure of the RPV and subsequent release of molten corium into the containment corresponds to the ex-vessel phase [21]. An example of the in-vessel phase sequence for LWR goes as follows [14]:

1. Overheating of fuel and cladding.
2. Onset of exothermic oxidation of the cladding, accompanied by production of hydrogen.
3. Damage to and melting of the fuel cladding.
4. Rapid increase in hydrogen production, with a possible challenge to containment integrity due to deflagration/detonation.
5. Melting of the cladding, fuel and core materials and downward relocation of the corium.
6. Interaction of the molten corium with the residual water in the RPV.
7. Potential steam explosions caused by a molten corium–water reaction.
8. Heating of the RPV by the molten corium.

The ex-vessel phase considers the thermal and chemical interaction between core debris and containment structures, and containment transport of radioactive substances [21]. At this phase, several phenomena might be observed in the containment, for example, (a) heat-up by high pressure ejection of corium from the vessel (direct containment heating (DCH)), (b) hydrogen combustion (produced in both, the in-vessel phase and the ex-vessel phase), (c) containment foundations melting due to Molten-Corium Concrete Interaction (MMCI), and (d) containment failure due to long term pressurization and/or temperature increase [14].

1.4. Containment thermohydraulic phenomena during a severe accident

In the progression of a severe accident, a wide spectrum of different phenomena may occur within the containment. These phenomena are classified in the following four groups [21]:

1. Related to thermohydraulics;
2. Related to fission product and aerosol behaviour;
3. Related to melt behaviour;
4. Related to technical systems activation.

As the subject of this thesis is the PCCS thermohydraulics, we will focus on this group. In particular, the thermohydraulic phenomena is classified in five sub-processes according to the main processes occurring inside the containment, i.e. sources and sinks, pressurization/depressurization, transport (gas/water flows), heat and mass transfer, and hydrogen distribution and combustion [21]. A brief description of each sub-process is provided here:

- **Sources and sinks**

  It refers to the sources and sinks affecting the containment thermohydraulic. During a SA there are mass and energy (water, steam and hydrogen) inlets from several sources, such as the primary circuit at the break location or from discharges through relief valves into the containment volume. This mass injection can be two phase flows (steam and liquid) or single phase flows (such as, liquid water, superheated steam or hydrogen). The sinks are related to containment leakages, such as filtered vents or cracks in the containment walls [21].

- **Pressurization/depressurization**

  Pressurization and depressurization refers to the changes in the containment pressure which are driven by the sources and sinks described previously. An example of pressurization occurs when there is steam injection in the containment due to a large LOCA, which might increase the pressure up to 4 bar in less than one minute. On the other hand, the opening of a vent is an example of a depressurization process. Other example of depressurization can be the result of mass and energy exchange within the containment atmosphere, as is the case of wall condensation [21].

- **Transport (gas/water flows)**

  Transport refers to those processes where fluids move from one defined region to another, usually involving flows between compartments, such as convective loops between interconnected compartments. Transport may also occur in a same com-

partment between different components, such as between the condensate pool and the atmosphere [21].

- **Heat and mass transfer**

  Heat and mass transfer refers to the exchange of mass and energy occurring within the containment or between the containment and the external environment. Inside the containment is possible to have mass and energy transfer processes that can lead to condensate accumulation. For example, when the steam exchange heat with the internal structures or the initially cold atmosphere (e.g. air). Other heat exchange processes will only lead to temperature rising without mass transfer, such as the heating of air and hydrogen. The mass and energy exchange can drive the appearance of other phenomena, such as mixing or stratification inside the containment. A mixing process refers to the combination of fluids with different characteristics to form a fluid with homogeneous properties. While the stratification refers to the separation of different fluid by layers. Typical conduction, convection and radiation mechanisms are present [21].

- **Hydrogen distribution and combustion**

  The oxidation of metals, such as zirconium in the fuel cladding, with steam is the dominant source of hydrogen during a severe accident in water cooled reactors [21]. Another sources of hydrogen during the in-vessel phase are steel–steam reaction and boron carbide–steam reaction [22]. The production of hydrogen can reach up to 2 kg/s during the core degradation stage [22].

  As hydrogen is produced, it starts mixing with the steam and air in the containment atmosphere. However, its distribution is not uniform in the atmosphere of the containment, as various phenomena take place e.g. buoyancy, molecular diffusion, steam condensation, effects of containment layout, location of hydrogen release, safety systems, etc. This non-homogeneous distribution leads to high local hydrogen concentrations which are higher than the limit of flammability [22]. Accordingly, the prediction of the hydrogen distribution during the progression of a severe accident, and the implementation of safety actions, such as the installation of Passive Autocatalytic Recombiners (PARs), to avoid combustible atmosphere is a crucial subject in nuclear safety.

  For the combustion of hydrogen two conditions should be satisfied during the progression of an accident. Firstly, the gas mixture of the atmosphere should be combustible. Secondly, the presence of an ignition source [22]. However, as the likeli-

hood of ignition depends on the accident sequence, which is an stochastic process, it is considered that ignition may occur anywhere in the containment at any time when there is a combustible mixture [21]. In consequence, the aim is to avoid the combustible mixtures inside the containment.

The Shapiro diagram of Figure 1.3 can be used to determine whether the air–hydrogen-steam mixture in the containment is combustible or not. In a dry atmosphere (steam 0% v/v), for example, combustion is possible when the hydrogen volume fraction is between 4 and 78%. The hydrogen fraction range gets narrow as the steam fraction increases, meaning that the probability of combustion gets lower as there is more steam present. For steam fractions over 62%, combustion is not possible anymore.

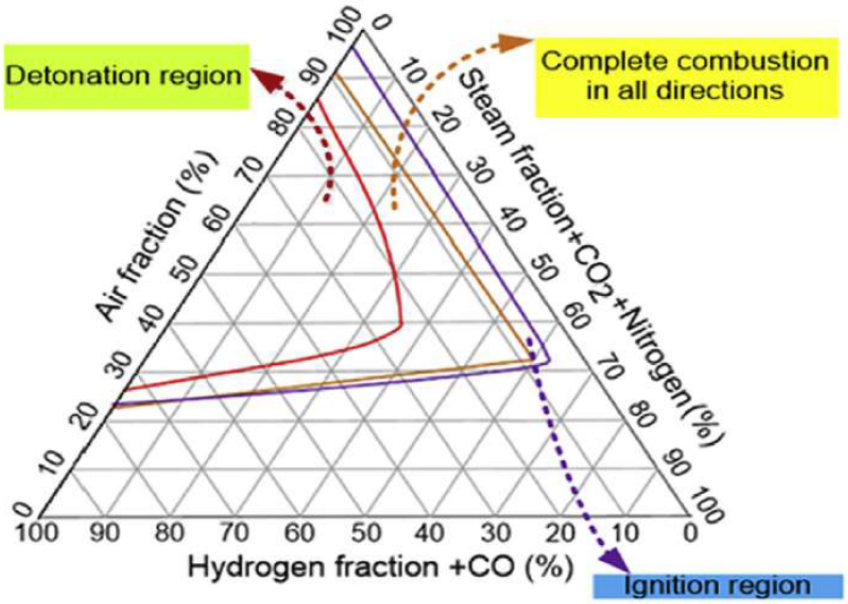

Figure 1.3: Shapiro diagram for air–hydrogen–steam mixture with additional gases [22]

1.5. Thermohydraulic simulations in nuclear applications

The safety assessment of a NPP under a specific postulated accidental scenario, which has the potential to lead to a radioactive release to the environment, has to be carried out by computational simulations [16]. For this purpose, the Nuclear Energy Agency provides a guideline to perform safety analysis with CFD tools, which consists of 6 steps [23] (Figure 1.4). Each step follows certain recommendations to deliver a specific output, which must be documented. For example, the first step makes use of the phenomena identification ranking table (PIRT) approach to isolate the problem, and its output is the PIRT table. Then, the physical model selection is based on the PIRT results and

preliminary calculations such as the Rayleigh number for the turbulence regime.

Accordingly, the creation of the plant model will follow most of the NEA recommendations for CFD studies. This includes the identification and evaluation of the related phenomena and the verification of the model. As indicated previously, the validation is excluded from this thesis due to the lack of experimental data. Once the plant model is created, a parametric analysis will be carried out to evaluate the system response (e.g. maximum pressure) under different accident conditions (e.g. steam injection). This will have the objective of determining the limitations of the submerged-containment PCCS concept, i.e. under which accident conditions the design is capable of effectively cooling the system and maintain it in a safe condition. The parametric analysis also has the aim of identifying the significant input parameters that determine the system's responses. To do this a standard design of experiment (DOE) technique is used to define the more appropriate combination of the input parameters. Finally, the design of the commissioning test will also be accomplished through this method.

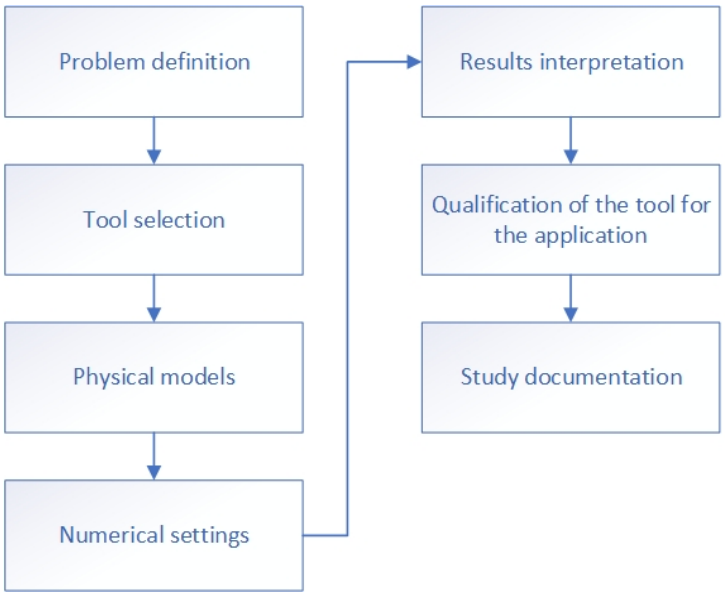

Figure 1.4: Recommended steps to perform a CFD study in nuclear applications (ref. [23])

1.6. New SMR-PCCS test facility for thermohydraulic research

The new facility at Becker Technologies GmbH, shown in Figure 1.5, aims to provide a benchmark for the investigation of SMR-PCCS with large external water pool. In this new facility several tests will be carried out to deliver precise experimental data about the transient evolution of a LOCA event, and to validate the performance of the PCCS

under severe accidental scenarios.

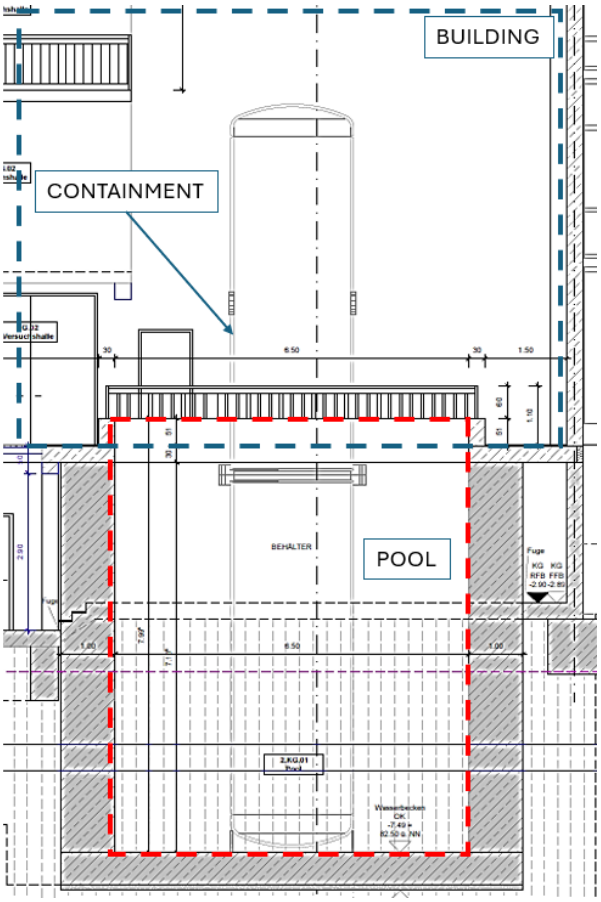

Figure 1.5: New SMR-PCCS test facility.

The commissioning tests of the facility are aimed to qualify the installed instrumentation and data acquisition system, as well as to generate qualitative data on the thermal-hydraulic performance of a SMR-PCCS system. For this task, it is required to study the plant beforehand through simulations to obtain preliminary information about the plant response. These simulations will not only provide valuable information of the plant response, but also they will be used to design the commissioning tests and to assess the performance of a generic SMR-PCCS system. The commissioning tests will be carried out with the containment initially surrounded by air rather than water at the start of the experiments (see Figure 1.6). The steam injection is located in the upper third section of the vessel and it represents the LOCA break point. The pool filling will start following the steam injection. The tests continue with the injection of helium to study the hydrogen distribution, its effects over the condensing conditions and the hydrogen stratification. In addition, the completely new test facility offers the rare opportunity for a "double-blind benchmark", since no modeling experience with this specific geometry, the vessel and the

extended infrastructure, will be available at this time.

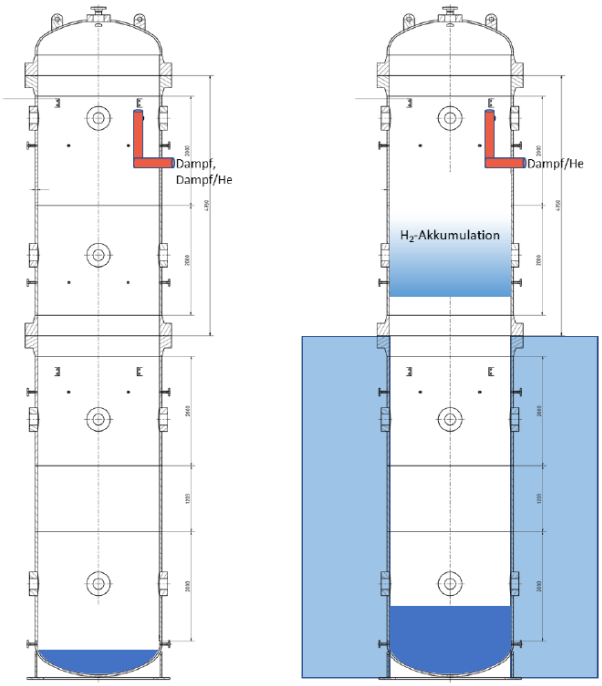

Figure 1.6: Proposed commissioning tests of the new SMR-PCCS test facility.

2 | Case Study: Analysis of the passive safety concept in a test facility

Following the Best Practice Guidelines of the NEA for thermohydraulic simulations. The first stage of this thesis is to describe the problem to be solved and to create a PIRT table. For this purpose, the elaboration of the PIRT table starts with the specification of the accidental scenario and the description of the plant [24]. Then, the phenomena is identified and ranked. The identification and ranking of the phenomena was done by taking as reference PIRT tables of similar plants [25, 26].

2.1. Scenario specification

The accidental scenario to be modeled (properly fitted with the execution of experimental activities) corresponds to a severe loss of coolant accident (LOCA) with release of steam and hydrogen into the containment. The proposed scenario can be divided into three main stages: break out, in-vessel progression and long-term cooling. The accidental scenario is classified in the in-vessel phase because it doesn't considered any phenomena related to direct contact between the core debris and the containment. Furthermore, the combustion of hydrogen is also excluded from this work. The proposed scenario is described as follows:

1. **Break out (BO)**: The accident starts with the rupture of a pipe of coolant inside the containment. As soon as the pipe breaks, the steam is released into the containment leading to a fast pressurization. Due to the initial dry condition and low temperature of the containment, the steam condensates leading to a depressurization phase.

2. **In-vessel progression (IP)**: After some hours of the break out, the core starts to degrade and hydrogen is released into the containment. The hydrogen accumulates inside the containment and it mixes with the steam and non-condensable gases present. At this phase is expected a second increment of the pressure inside the containment and a reduction of the condensation rate as consequence of the additional barrier for the steam at the condensate boundary layer.

3. **Long-term cooling (LT)**: The long progression of the accident leads to a quasi-stationary condition between the heating, caused by the steam injection, and the cooling, caused by the external cooling driven by the heat transfer to air and water by natural convection.

The proposed scenario is further adapted to be in compliance with the experimental tests to be designed and, subsequently, to be carried out by Becker Technologies. Therefore, the model needs to consider also some restrictions that are part of a controlled experiment, such as, the capacity of the plant (steam, hydrogen and water injection) and practical procedures (such as, constant mass flow injections). The main characteristics of the experiments considered in the model are listed here:

- All mass flow injections are constant in time (steam, water and hydrogen).
- Hydrogen injection starts exactly 6 hours after the break for all tests conditions [1].
- The total amount of hydrogen is limited to 3.5 kg.
- The steam and water flow rates are limited to a maximum of 500 kg/h and 5 kg/s, respectively.
- The total experimental time is approximately 12-16 hours depending on the pool filling time.

The nominal conditions of the plant are provided here. The PIRT table made later considers these values as reference.

Table 2.1: Nominal conditions of the plant

Parameter	Mass flow rate	Temperature
Steam injection	400 kg/h	100 °C
Water injection	4.25 kg/s	20 °C
Hydrogen injection	2.25 g/s	20 °C

2.2. Plant description

The facility at Becker corresponds to a SMR-type containment of 12 [m] height with a diameter of 2.2 [m], a pool of 7 [m] height with a diameter of 6.5 [m], and an upper room of around 12 [m] per side. A front view of the facility is provided in Figure 1.5. The plant was divided as indicated in the figure to guide the PIRT analysis. This division is also in accordance with the definitions of the IAEA [21] [2]. Accordingly, each component is

[1] The real experiments consider helium instead of hydrogen due to safety reasons.

[2] The constituents of an atmosphere are predominantly gases, although two phase mixtures, liquid droplets and solid particles, may be present during a transient. The constituents of a pool are predom-

described as follows:

- **Containment**: It corresponds to the vessel wall that separates the interior from the exterior space and communicates with the atmosphere or pool through a surface.
- **Atmosphere**: The open volume or free flow volume for gases. It excludes an existing pool of water or a pool of water that may form during an accident [27].
- **Pool**: Open structure intended to contain liquid water.

2.3. Phenomena Identification and Ranking Table

The aim of this stage is to identify and rank the physical phenomena during the proposed accidental scenario, which will be later used as a guidance for the model construction. The construction of the PIRT table was done with the methodologies of Yang et al. and the Nuclear Energy Agency. The global steps are summarized in Figure 2.1.

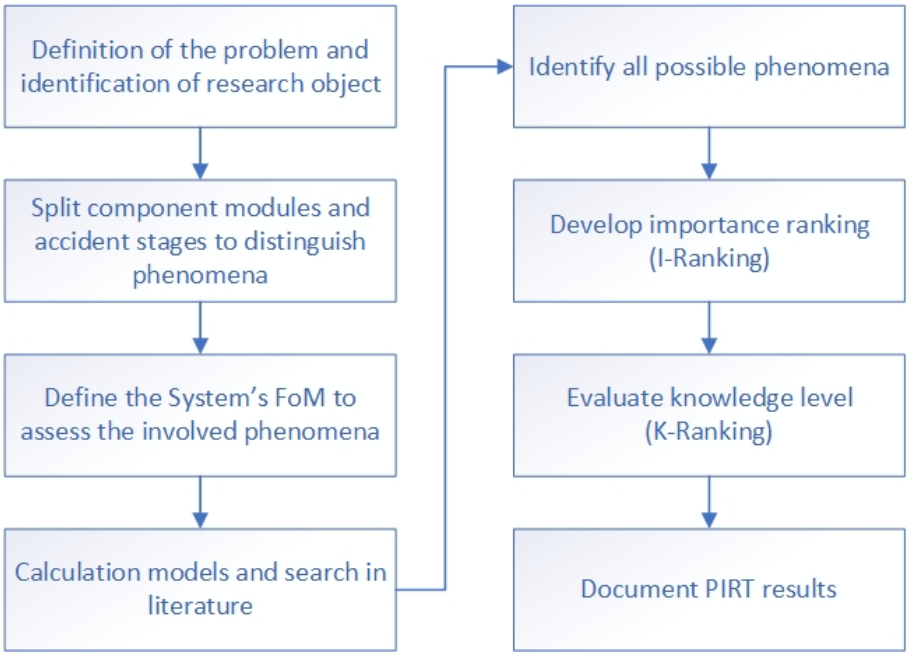

Figure 2.1: Steps of PIRT Table construction.

Following the steps of Figure 2.1, the problem is defined as the performance assessment of the PCCS as an effective safety system for SMR under a severe LOCA accident, i.e. it will be determined under which accidental conditions the PCCS might effectively work and bring the SMR to a safe condition. The research object is the SMR-PCCS test facility

inantly liquids, although two-phase mixtures, gas bubbles and solid particles, may be present during a transient. In certain cases, one component may transform into another component, for example, water runs onto a structure (dry floor) forming a pool, or a pool is drained away leaving a structure.

at Becker Technologies. And, the component modules are the containment, pool and atmosphere; while the stages of the accident are the break out, in-vessel progression and long term cooling.

The performance of the SMR-PCCS system is assessed with respect to some key parameters that can capture the functional objectives of the containment and the passive cooling system simultaneously. That is to say, the functional objective of the containment is to provide confinement of radioactive substances in operational states and in accident conditions [11]. While, the functional objective of the passive cooling system is to reduce the containment temperature and pressure following a postulated design basis accident by removing thermal energy from the containment atmosphere [5]. In consequence, the key parameters that might trigger these functional objectives (referred as the Figure of Merits (FoM) of the system) were defined as the peak pressure, peak temperature, peak hydrogen concentration and average condensation rate.

The evaluation of the phenomena, and subsequent evaluation of accidental conditions, was done with respect to these FoMs. The phenomena identification was done for all the three plant's component at the three accident stages taking as reference the PIRT of Yang et al., while the rankings were assigned by taking the reference values of Yang et al. and Morin et al.. The result is summarized in the Table 2.4. Furthermore, the ranking values are defined in the following Tables.

Table 2.2: Importance level ranking definitions (I-Ranking)[23]

Ranking	**Description**
High (H)	Significant or dominant influence on FoM
Medium (M)	Moderate influence on FoM
Low (L)	Small influence on FoM (including the possibility that the phenomenon is not present or possible)

Table 2.3: Knowledge level ranking definitions (K-Ranking) [23]

Ranking	**Description**
Known (K)	Phenomenon is well understood and can be accurately modeled
Partially Known (P)	Phenomenon is understood, however, can only be modeled with moderate uncertainty
Unknown (U)	Phenomenon is not well understood. Modeling is currently either not possible or is possible only with large uncertainty

Table 2.4: PIRT of the thermohydraulic phenomena of a generic SMR-PCCS system

Component	Id	Phenomena	I-Ranking			K-Ranking	ref.
			B.O.	I.P.	L.T.		
Containment	1	Pressure distribution	H	H	M	0	[28]
	2	Pressure fluctuation	H	H	H	H	[21]
	3	Thermal stratification	L	H	H	L	[21]
	4	Components stratification	L	H	H	L	[21]
	5	Non-condensable gas distribution	L	H	H	L	[21]
	6	Pressure-driven flow	H	M	M	M	[21]
	7	Steam condensation	L	H	H	L	[21]
	8	Condensate accumulation	L	M	H	L	[21]
	9	Natural convection	L	M	H	L	[21]
	10	Thermal radiation	L	H	H	L	[21]
	11	Hydrogen absorption	L	L	L	0	[28]
	12	Hydrogen adsorption	L	M	M	0	[28]
	13	Thermal conduction	L	H	H	H	[21]
Pool	14	Thermal stratification	L	H	H	0	[28]
	15	Pressure distribution	L	L	L	0	[28]
	16	Evaporation	L	H	H	L	[21]
	17	Natural convection	L	H	H	0	[28]
Atmosphere	18	Thermal stratification	L	H	H	0	[28]
	19	Natural convection	L	H	H	0	[28]
	20	Thermal radiation	L	M	M	0	[28]

- B.O.: Break out, I.P.: In-vessel Progression and L.T.: Long-term containment cooling.

2.3.1. Simulation of high-ranked critical phenomena

For the simulation of the plant, the attention has to be in the phenomena for which there is less information and it is more important, as indicated in Table 2.5. Phenomena such as condensation, natural convection, heat exchange with structures, and the temperature stratification inside the containment are generally predicted with large uncertainty margins [21]. Therefore, its correct simulation is important for the results of risk analyses. Accordingly, a description of the most critical phenomena for this study is provided here.

Table 2.5: Determination of phenomena for further consideration [23]

K-Ranking level	I-Ranking Level		
	High (H)	**Middle (M)**	**Low (L)**
Known (K)	NO	NO	NO
Partially Known (P)	NO	NO	NO
Unknown (U)	YES	YES	NO

- **Gas and Thermal stratification**

  The energy exchange between the atmosphere, the pool and the structures controls the resulting flows which will contribute to the mixing of the atmosphere (or the partial displacement of the existing atmosphere). Simulation of stratification may give rise to problems in lumped parameter approaches. Therefore, a good knowledge of the facility is necessary for the elaboration of an appropriate nodalization. It is required sufficient nodalization of the containment to account for possible stratification effects, and to ensure that the heat sinks are properly distributed in the compartments [21].

  On the other hand, the distribution of hydrogen and oxygen in the containment is determined by the location of the sources and by the transport processes. For a realistic assessment, it is important to: (i) minimize the effects of numerical diffusion; and (ii) consider plume effects that may lead to incomplete mixing near the source. The CFD models should account for the proper geometry of the containment volumes, including obstacles and, therefore, should preferably be fully three dimensional to address issues of plume behaviour and associated entrainment [21].

  Furthermore, it is necessary to include the transport of non-condensable species by at least one additional conservation equation to properly predict the hydrogen distribution and account for the risk of combustible mixtures [21].

- **Steam condensation**

  The key phenomenon in the operation of the PCCS is steam condensation in the presence of non-condensable gases such as air or a mixture of air and hydrogen. The presence of non-condensable gases significantly reduces the condensation rate and condensation heat transfer performance. Moreover, SMRs require efficient steam condensation to reduce the size of the containment structure [18].

  The general categories of numerical approaches to condensation heat transfer anal-

ysis suitable for an SMR are empirical, resistance layer, and theoretical. The empirical models are algebraic models that were developed using test data from a large-scale integral effects test (IET) or a small-scale separate effects test (SET). The resistance-layer models are algebraic models that use a heat and mass transfer analogy or a diffusion layer approach to develop a simplified model. The theoretical models are numerical models that solve some conservation equations in either only the liquid phase, only the gas phase, or in both phases [18].

- **Natural convection**

  The general impact of the natural circulation of coolant or steam in the reactor coolant system and vessel is to reduce temperature gradients in the core and vessel by moving heat from the hotter channels to the cooler channels and structures. However, the natural circulation is strongly affected by the design of the plant. In addition, hydrogen enhances natural convection and heat transfer but reduces steam condensation. For a fluid component, the interior processes usually are convection but they can also include conduction and diffusion under certain circumstances. Suitable correlations are required for both forced and natural convection [21].

- **Radiation heat transfer**

  Thermal radiation may also be a significant heat transfer process. Radiative cooling may be important in aerosol processes; aerosols also absorb and scatter thermal radiation. Thermal radiation is modeled in most of the codes but usually the models cannot deal with scattering media (e.g. water droplets) or large cavities with strong absorption by the gas. The lack of appropriate radiative heat transfer models will lead to an incorrect temperature distribution in the vessel [21].

Exclusions:

Boiling models were excluded from the plant model because of the following reasons:

- At the beginning, the vessel is externally surrounded by air instead of water. Therefore, there is no chance of boiling.
- The pool starts to be filled after the LOCA break, and when full it covers 7.5 of 12 [m]. Considering that the pool level will increase at a rate of 8.7 mm/min (at the nominal rate of 4.25 kg/s), the condensate accumulates at the bottom and there will be temperature stratification inside the containment. It is expected that the lower section of the containment will have a temperature lower than the inner saturation temperature. In consequence, assuming that the temperature of the condensate pool inside the containment is at 100 [°C], and that the saturation temperature for the

water in the external pool is also 100 [°C]. The inequality $\Delta T_{surf.} > \Delta T_{sat.} + \Delta T_{ONB}$, that determines if there is sub-cooled nucleate boiling, will not be satisfied.

- As the simulation progresses, it is expected that the hottest point of the containment will be located in its upper section, possibly closed to the breaking point (around 7.5 [m]). This section will be cooled at all times by natural convection with air and thermal radiation with the external walls.
- The pool is constantly filled with water at a temperature between 15-25°C, which will keep the pool at a low temperature.
- Adding boiling models will increase the computing time unnecessarily.

2.4. Model development with GOTHIC

The simulation tool selected for this study was GOTHIC (Generation of Thermal-Hydraulic Information for Containments), which is a general thermal-hydraulics code applicable for the design, licensing, safety and operating analysis of NPP containment and other confinement buildings [29].

The plant model was built in 3D to capture the specific geometry of the facility. The selection of the physical models is in accordance with the PIRT results and the qualification report of GOTHIC, which compiles a set of experiments and analytical results that validates the models for its applicability in containment analysis [30]. In this section, it is reported the main features of GOTHIC such as the governing equations and the most important physical models used. The specific methodology for the plant model construction, the design of experiments and the parametric analysis is detailed in the Methodology Chapter.

2.4.1. Governing equations solved in GOTHIC

Mass conservation

Mass conservations equations are solved for five phases: drops, liquid, ice, mist and steam, and for each non-condensing gas component. The steam/gas mixture, hereafter referred to as the vapor phase, can be in the form of bubbles or a continuous vapor region. The liquid phase can be in the form of pools, films or large chunks found in slug flow. The general form of the mass balance solved by GOTHIC is [31],

$$\underbrace{\frac{\partial}{\partial t}\int_V \Theta\alpha_\phi\rho_{\phi\zeta}\,dV}_{\text{storage}} = \underbrace{-\int_A \Psi\alpha_\phi\rho_{\phi\zeta}\,\vec{u}_\phi\cdot\vec{n}\,dA}_{\text{convection}} + \underbrace{\int_{A_f}\Psi\alpha_\phi\rho_\phi D^c_\phi\vec{\nabla}\left(\frac{\rho_{\phi\zeta}}{\rho_\phi}\right)\cdot\vec{n}\,dA}_{\text{diffusion}} + \underbrace{\int_{A_w} s^c_{\phi\zeta}\,dA}_{\text{boundary source}} + \underbrace{\int_{A_{I_\phi}} S^c_{\phi\zeta}\,dA_{I_\phi}}_{\text{interface source}} + \underbrace{E^c_{\phi\zeta}}_{\text{equipment source}} + \underbrace{C^c_{\phi\zeta}}_{\text{combustion source}} \tag{2.1}$$

Where:

ϕ : Phase. It takes on the values v (vapor), l (liquid), d (drops) and i (ice).
ζ : Vapor's component - s (steam), n (single non-condensing gas), and g (non-condensing gas mixture).
Θ : Volume porosity factor.
Ψ : Area porosity factor.
α : Volume fraction.
ρ : Density.
$\vec{u}$: Velocity.
$\vec{n}$: Outward normal vector to the surface dA.
A_f : Portion of the total surface area in contact with adjacent fluid volumes.
D^c : Mass diffusion coefficient, including turbulence effects only.
s^c : Mass source per unit area generated at bounding wall, A_w.
S^c : Mass source per unit area coming from the interfacial area, A_I.
E^c : Mass source from engineered safety equipment.
C^c : Mass source from hydrogen combustion.

Energy conservation

Energy conservation equations are solved for three fluid phases: drops, liquid and vapor/mist, and for solid thermal conductors. The fluid energy equation is solved for enthalpy, so the equation is written in terms of enthalpy rather than internal energy. The fluid energy equation solved in GOTHIC is [31],

$$\begin{aligned}
&\underbrace{\frac{\partial}{\partial t}\int_V \Theta\alpha_\phi\left(\rho_\phi(h+ke)_\phi - P\right)\,dV}_{\text{storage}} = -\underbrace{\int_A \Psi\alpha_\phi\rho_\phi(h+ke)_\phi\;\vec{u}_\phi\cdot\vec{n}\,dA}_{\text{convection}} \\
&\quad\underbrace{-\int_V \Theta P\frac{\partial}{\partial t}\alpha_\phi\,dV}_{\text{work}} + \underbrace{\int_{A_f}\Psi\alpha_\phi\rho_\phi c_{p\phi}D^e_\phi\vec{\nabla}T_\phi\cdot\vec{n}\,dA}_{\text{thermal diffusion}} \\
&\quad\underbrace{+\sum_\zeta\int_{A_f}\Psi\alpha_\phi\rho_\phi D^c_\phi\vec{\nabla}\left(\frac{\rho_{\phi\zeta}}{\rho_\phi}\right)h_{\phi\zeta}\cdot\vec{n}\,dA}_{\text{mass diffusion}} + \underbrace{\int_{A_w}s^e_\phi\,dA}_{\text{boundary source}} \\
&\quad\underbrace{+\int_{A_{I_\phi}}S^e_\phi\,dA_{I_\phi}}_{\text{interface source}} + \underbrace{E^e_\phi}_{\text{equipment source}} + \underbrace{C^e_\phi}_{\text{combustion source}}
\end{aligned} \tag{2.2}$$

Where:

h : Enthalpy.
ke : Kinetic energy ($ke_\phi = u_\phi^2/2$)
P : Static pressure.
D^e : Thermal diffusion coefficient.
s^e : Energy source per unit area generated at bounding wall, A_w.
S^e : Energy source per unit area coming from the interfacial area, A_I.
E^e : Energy source from engineered safety equipment.
C^e : Energy source from hydrogen combustion.

Kinetic energy is included or neglected by user selection, and all other energy forms not explicitly represented above are neglected. Viscous dissipation is also neglected. All components of the vapor are assumed to be at the same temperature. The enthalpy in the vapor energy is the mixture energy of the steam, non-condensing gas mixture and the mist. The energy transported with the mass through mass diffusion is included only for the vapor [31].

The energy equation for the solid conductors is [31],

$$\underbrace{\int_{V_{cn}}\rho_{cn}c_{p,cn}\frac{\partial T_{cn}}{\partial t}\,dV_{cn}}_{\text{storage}} = \underbrace{\int_{A_i}D^e_{cn}\vec{\nabla}T_{cn}\cdot\vec{n}\,dA}_{\text{thermal diffusion}} + \underbrace{\int_{A_b}s^e_{cn}\,dA}_{\text{boundary source}} \tag{2.3}$$

Where:

cn : It refers to a particular conductor.
V_{cn} : Conductor volume.
A_i : Internal surface area between conductors.
D^e_{cn} : Thermal diffusion coefficient (conductivity).
A_b : External surface area of the conductor at the interface with a fluid phase.

Momentum conservation

Momentum conservation equations are solved for three phases: drops, liquid and vapor. The general equation solved in GOTHIC is [31],

$$\underbrace{\frac{\partial}{\partial t}\int_V \Theta\alpha_\phi\rho_\phi\vec{u}_\phi\,dV}_{\text{storage}} = -\underbrace{\int_A \Psi\alpha_\phi\rho_\phi\vec{u}_\phi(\vec{u}_\phi\cdot\vec{n})\,dA}_{\text{convection}} + \underbrace{\int_{A_f}\Psi\alpha_\phi\boldsymbol{\sigma_\phi}\cdot\vec{n}\,dA}_{\text{surface stress}} + \underbrace{\int_V \Theta\vec{g}\alpha_\phi\rho_\phi\,dV}_{\text{body force}} + \underbrace{\int_{A_w}\vec{s^m_\phi}\,dA}_{\text{boundary source}} + \underbrace{\int_{A_{I_\phi}}\vec{S^m_\phi}\,dA_{I_\phi}}_{\text{interface source}} + \underbrace{\vec{E^m_\phi}}_{\text{equipment source}} \tag{2.4}$$

Where:

$\boldsymbol{\sigma_\phi}$: Stress tensor. It includes the static pressure, the viscous and Reynolds stress terms.
$\vec{g}$: Gravitational acceleration.
$\vec{s^m_\phi}$: Momentum source per unit area generated at bounding wall, A_w.
$\vec{S^m_\phi}$: Momentum source per unit area coming from the interfacial area, A_I
$\vec{E^m}$: Momentum source from engineered safety equipment.

All components of the vapor are assumed to move at the same velocity. The density in the vapor momentum equation includes the steam and gas component densities, (each at their own partial pressure) and the mist macroscopic density (i.e., mist mass per unit vapor volume) [31].

2.4.2. Physical models

The performance of the PCCS to reduce the containment pressure is mostly determined by the condensation process. GOTHIC offers five different options to calculate the con-

densation inside the containment, as shown in Figure 2.2.

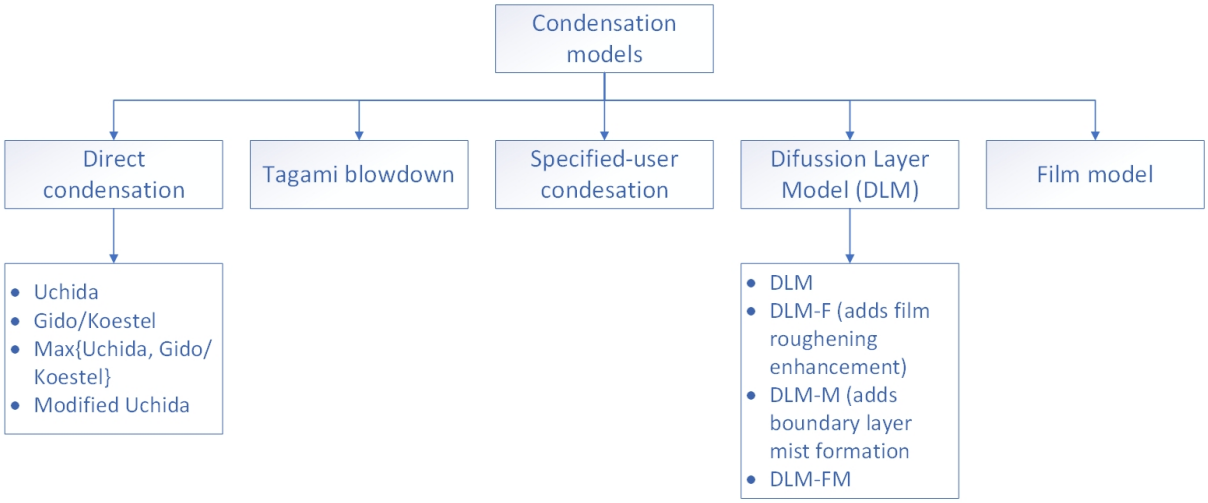

Figure 2.2: Condensation options available in GOTHIC.

For the plant model construction, it was used the models DLM and DLM-FM because they were validated by GOTHIC for several experiments, geometries and conditions, including the test facility MISTRA of similar size [30].

Diffusion Layer Model (DLM)

The diffusion layer model assumes that a liquid film builds up on the wall from the condensing steam, and that the transfer of heat and mass to the film surface is controlled by diffusion through a boundary layer, see Figure 2.3. Where, the condensing wall is at a temperature T_w, the bulk vapor is at temperature T_b, χ_b is the steam mole fraction in the bulk and χ_i is the steam mole fraction at the interface. The presence of non-condensing gases in the boundary layer increases the resistance for the (steam-) mass transfer reducing the condensation rate [31].

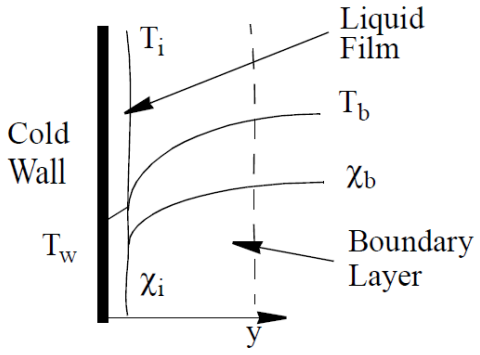

Figure 2.3: Conceptual scheme of the DLM condensation model (ref. [31])

The condensation rate due to diffusion and bulk transport through the boundary layer is given by [31],

$$\Gamma_d^{"} = -\lambda_t \frac{M_s Sh D_{sg} \bar{c}}{D_h} ln\left(\frac{1-x_i}{1-x_b}\right) \tag{2.5}$$

Where:

$\Gamma_d^{"}$: Condensation rate per unit area.
λ_t : User specified multiplier.
M_s : Steam molecular weight.
Sh : Sherwood number.
D_{sg} : Binary diffusion coefficient for the steam in the gas mixture.
$\bar{c}$: Molar concentration of steam-gas mixture in the boundary layer.
D_h : Cell hydraulic diameter.
x_i : Steam molar fraction in the boundary layer.
x_b : Steam molar fraction in the bulk fluid.

The heat and mass transfer enhancement due to roughness of the condensate film applies a scaling factor, λ_h, to the natural convection Nusselt and Sherwood numbers. The scaling factor has a lower limit of 1.0 and an upper limit of 4.0 [31],

$$\lambda_h = c_f g_f\left(\chi_g\right) Re_f^{n_f} \tag{2.6}$$

Where:

χ_g : Volume concentration of non-condensing gas.
Re_f : Film Reynold's number.
c_f : Model's constant ($= 0.2$).
n_f : Model's constant ($= 0.2$).
$g_f\left(\chi_g\right)$: Polynomial function of χ_g.

On the other hand, the formation of mist in the boundary layer affects the mass and energy balance by including a balance equation for the mist in the model.

2.4.3. Numerical solution

Mass and energy equations are solved for each sub-volume so that the three-dimensional distribution of mass and energy is obtained. Momentum equations are solved at the boundaries of each sub-volume to obtain the flow pattern within the room. For subdivided volumes, equations for the flow field are solved using a staggered difference scheme on an Eulerian mesh. Velocities are obtained at mesh cell faces and state variables (e.g., pressure, density, enthalpy, gas concentration, and phase volume fractions) are obtained at mesh cell centers. The mesh cell is characterized by nominal dimensions ΔX, ΔY and ΔZ and volume and area porosity factors. This cell is the control volume for the scalar continuity and energy equations. The cells of a subdivided volume are numbered sequentially, progressing through the X-planes, Y-planes and then Z-planes [29].

3 | Methodologies

In this chapter are detailed the steps for the construction of the plant model, the strategy for the design of the commissioning tests and parametric study. Furthermore, it is included a preliminary phenomena assessment to sustain some of the physical models selection.

3.1. Preliminary phenomena assessment

3.1.1. Turbulence regime

For natural convection systems, the turbulence regime is determined with the Rayleigh number (eq. (3.1)), where values larger than 10^9 are representative of turbulent regimes [32]. As inside the containment is expected to have higher levels of turbulence because of the mass injections, the Rayleigh number was only estimated for the containment external fluids, i.e. water and air. For this purpose, the values of the containment wall and fluids temperature were assumed. Furthermore, several properties were considered constants to simplify the calculation, e.g. density, thermal heat capacity, conductivity, etc. The containment height exposed to each external fluid was fixed at the pool depth.

$$Ra_H = \frac{g\beta\Delta T H^3}{\alpha\nu} \tag{3.1}$$

Where:

g : Gravitational acceleration.
β : Thermal expansion coefficient.
ΔT : Temperature difference.
H : Height.
α : Thermal diffusivity.
ν : Kinematic viscosity.

The results of the estimation are given in Table 3.1. They indicate that both external fluids have Rayleigh numbers larger than 10^9. In consequence, a proper turbulent model

must be enabled in the model.

Table 3.1: Estimation of Rayleigh number for the external air and water

Property	Variable	Unit	Air	Water
Containment external diameter	D_{ext}	m	2.3	2.3
Exposed containment height	H	m	4.5	7.5
Assumed containment external temperature	T_s	°C	40	30
Assumed external fluid temperature	T_∞	°C	25	25
Density	ρ	kg/m^3	1.184	997
Specific heat	c_p	J/kg-K	1007	4180
Thermal conductivity	k	W/m-K	0.02551	0.607
Thermal diffusivity	α	m^2/s	2.14E-05	1.46E-07
Dynamic viscosity	μ	kg/m-s	1.85E-05	8.91E-04
Kinematic viscosity	ν	m^2/s	1.56E-05	8.94E-07
Prandtl Number	Pr	-	7.30E-01	6.14E+00
Thermal expansion coefficient	β	1/K	3.35E-03	2.47E-04
Rayleigh Number	Ra_H	-	1.35E+11	3.93E+13

3.1.2. Heat transfers mechanisms

The heat transfer by radiation might be an important factor to cool down the containment in the non-submerged section, specially, in the very beginning of the accident. Therefore, assuming that this mechanism is not relevant might negatively affect the performance of our simulation. As a mean to determine the inclusion (or exclusion) of surface-to-surface thermal radiation in the model, an estimation of the heat transfer by convection and radiation from the external containment walls to the building walls was done. For this estimation, the temperature of the surfaces and the external air were assumed.

The Nusselt number was calculated for the external air using the equation (3.2). This correlation is valid for externally cooled vertical cylinders with $D/H > Ra_H^{-0.25}$ and $Pr \gtrsim 1$ [32] [1]. After obtaining the heat transfer coefficient, the convective heat flux was obtained with equation (3.3). The radiative heat transfer was calculated with equation (3.4).

[1]Even though the Prandtl number of air is lower than 1, the correlation was still used, since the motivation was not to obtain a precise result but to understand the radiation:convection proportion.

$$\overline{Nu}_H = \frac{4}{3}\left[\frac{7Ra_H Pr}{5(20+21Pr)}\right]^{0.25} + \frac{4(272+315Pr)H}{35(64+63Pr)D} \tag{3.2}$$

$$q_{conv} = h(T_1 - T_\infty) \tag{3.3}$$

$$q_{rad} = \epsilon\sigma(T_1^4 - T_2^4) \tag{3.4}$$

Where:

Ra_H : Rayleigh number.
H : Height.
D : Diameter.
h : Heat transfer coefficient ($h = \frac{Nu \cdot k}{D}$).
T_1 : Containment wall temperature.
T_2 : Building wall temperature.
T_∞ : Fluid temperature (air).
ϵ : Emissivity.
σ : Stefan-Boltzmann constant ($5.67 * 10^{-8}$ $[W/(m^2K^4)]$).

Table 3.2: Estimation of heat transfer

Property	**Variable**	**Unit**	**Thermal Radiation**	**Natural Convection**
Nusselt Number	Nu_H	-	-	334.0
Heat transfer coefficient	h	$W/m^2 - K$	-	1.89
Emissivity	ϵ	-	0.5 [33]	-
Assumed containment external temperature	T_s	K	313	313
Assumed external fluid temperature	T_∞	K	-	298
Assumed concrete walls temperature	T_{ext}	K	293	-
Heat flux	q	W/m^2	63.16	28.40

According to the results of Table 3.2 the heat transfer by radiation is relevant, and it

might be even more important that the natural convection with air. In consequence, the surface-to-surface thermal radiation will be included in the model.

3.2. GOTHIC Model construction

A general view of the model construction sequence is provided in Figure 3.1. The sequence followed here is aligned with the recommendations of the GOTHIC User's Manual [29]. The superior title in the boxes indicates the menu label in GOTHIC, e.g., the turbulence parameters are set in the "Control Volumes" menu, and the radiation parameters are set in the "Thermal Conductors" menu.

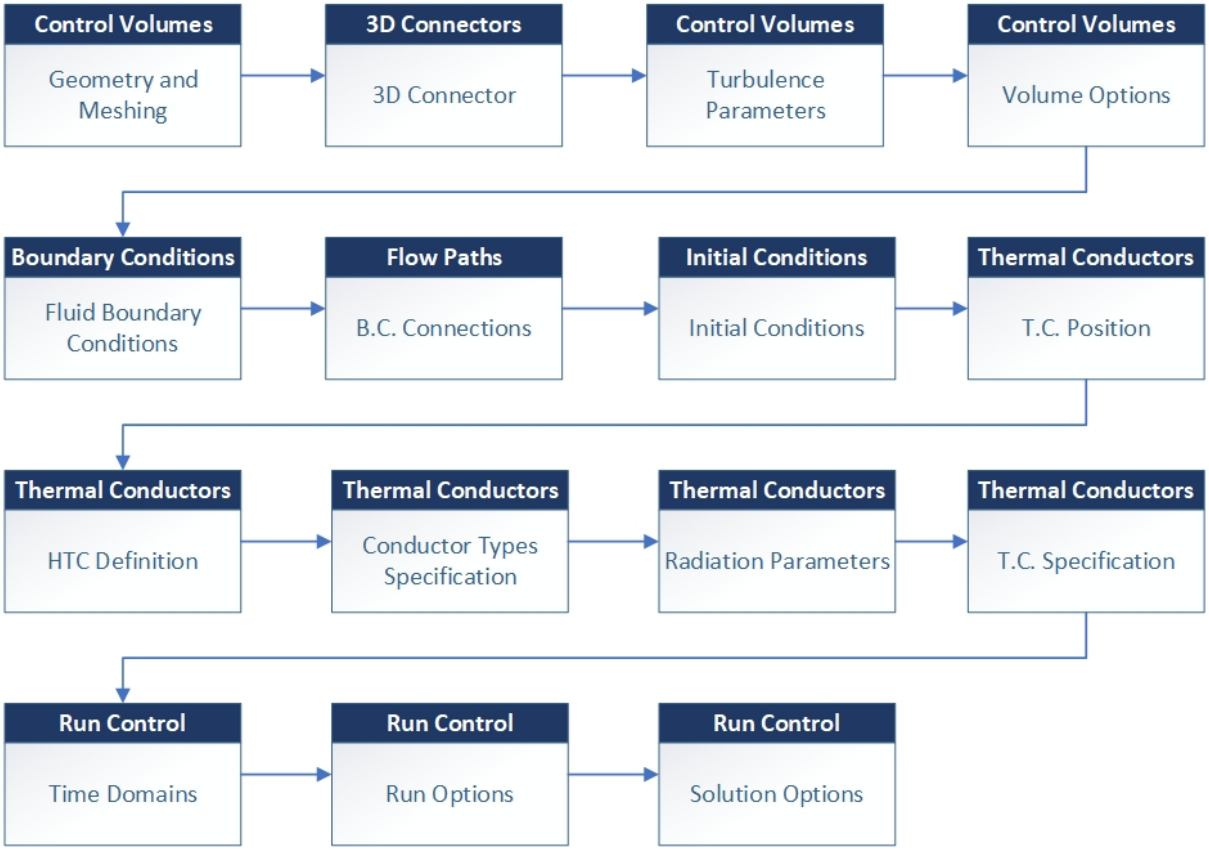

Figure 3.1: GOTHIC Model construction sequence.

3.2.1. Geometry and meshing

The principal element of a GOTHIC model is the control volume, described as a space or subsystem occupied by a fluid with certain fluid conditions (temperature, density, gas concentrations, etc.) [29]. The model was built with 3 control volumes: the containment, pool and room. As the purpose of this simulation is to study the flow patterns and temperature distribution of the PCCS, these control volumes were further divided in

several sub-volumes. In Figure 3.2 are identified the three (sub-divided) control volumes (1s, 2s and 3s), and other elements that will be identified in next sections.

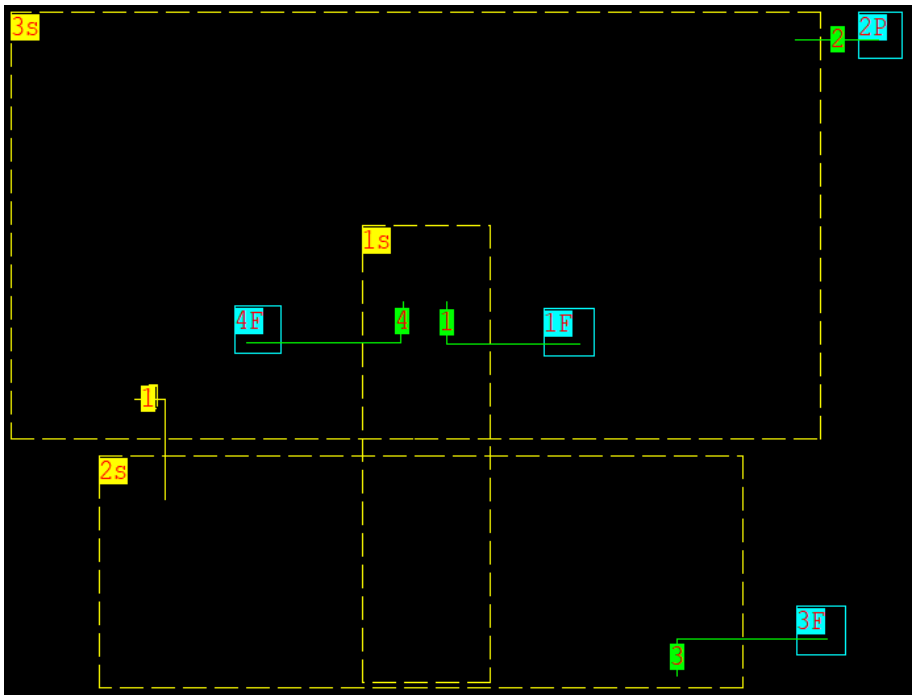

Figure 3.2: GOTHIC Model representation

The dimensions of each control volume are given in Table 3.3. These dimensions were obtained from the facility drawings (see referential Figure 1.5). Moreover, the final model geometry was simplified with the intention of limiting the time calculation and fit in with the code versatility. For example, the containment was built with hemispherical heads instead of semi-elliptical ones. Also, the external containment geometry only included the biggest union flanges, and all other minor connections for pipes or instrumentation were excluded.

Table 3.3: Control volume dimensions

Id.	Description	Volume (m^3)	Height (m)	Diam. or Side (m)
1s	Containment	46	12.0	2.22
2s	Pool	220	7.5	6.50
3s	Room	1711	12.0	12.00

The meshing in GOTHIC is Eulerian and it is aligned with the cartesian coordinate axis. The meshing of adjacent control volumes must also be aligned and match between each

other to do a conformal mesh. If adjacent cells belonging to different control volumes are not matched, it might lead to numerical errors. Also, as recommended in the User's Manual the cell size difference must be kept lower than 2, as well as the aspect ratio [2]. Accordingly, the smallest sub-volume unit was inside the containment and had a side of 0.5 (m), while the largest one was in the room and had a size of 0.9 (m). A referential image of the containment sub-division is given in Figure 3.3. The blockages (gray regions) are model elements to give shape and delimit the control volume's space. The presence of blockages affect the volume and area porosity factors, e.g. if a blockage cover half of a face of a control volume, then only the half of that face would exchange mass and energy with the surroundings.

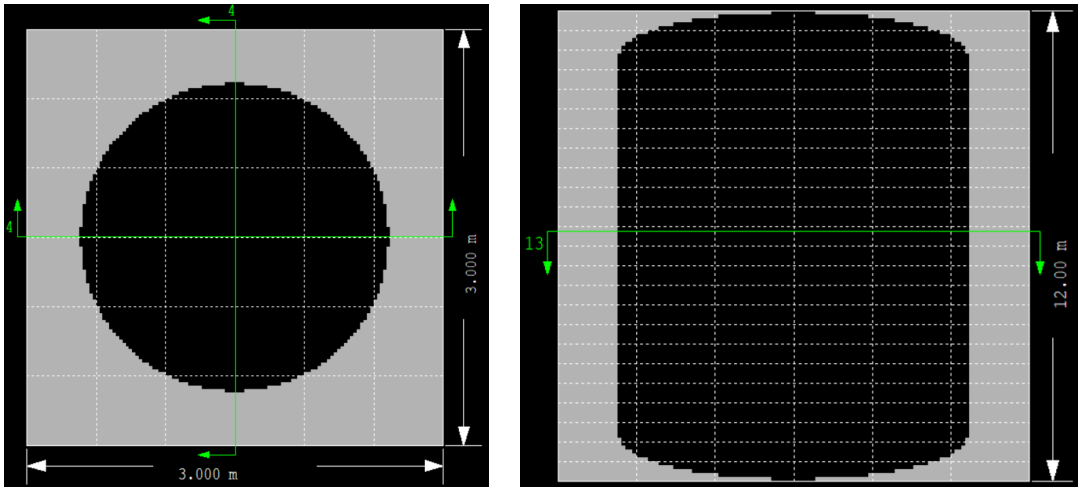

Figure 3.3: Sub-division of containment. Top and front view.

Finally, adjacent control volumes can be communicated through different elements depending if they transfer mass or not. The top face of the pool control volume was connected to the bottom face of the room control volume through a so-called "3D-Connector". This element enables the continuity between both control volumes. On the other hand, the containment interior was connected to the pool and room through "Thermal Conductors" which represent the containment wall allowing only energy transfer.

3.2.2. 3D connector

When two adjacent control volumes share an open face (such as a doorframe), the continuity of the mass, energy and momentum is enabled with a 3D-Connector. To join both control volumes, the sub-volume faces must match between each other. The built model

[2]Large changes in cell size and high aspect ratio may increase run time and be characterized by exceptional mass and energy errors [29]

has one 3D-Connector between the pool and room, and it is indicated by the yellow box connector line "1" in Figure 3.2. The connector is extended over all the common faces of the corresponding sub-volumes (Figure 3.4), i.e. all the bottom faces of the sub-volumes in the room are connected with the top faces of the sub-volumes in the pool. Those open faces of the room that are joint with a closed face in the pool (represented as blockages), as occurred with the room ground, there is not mass transfer. As it will be seen later, this surface can be associated with a thermal boundary condition.

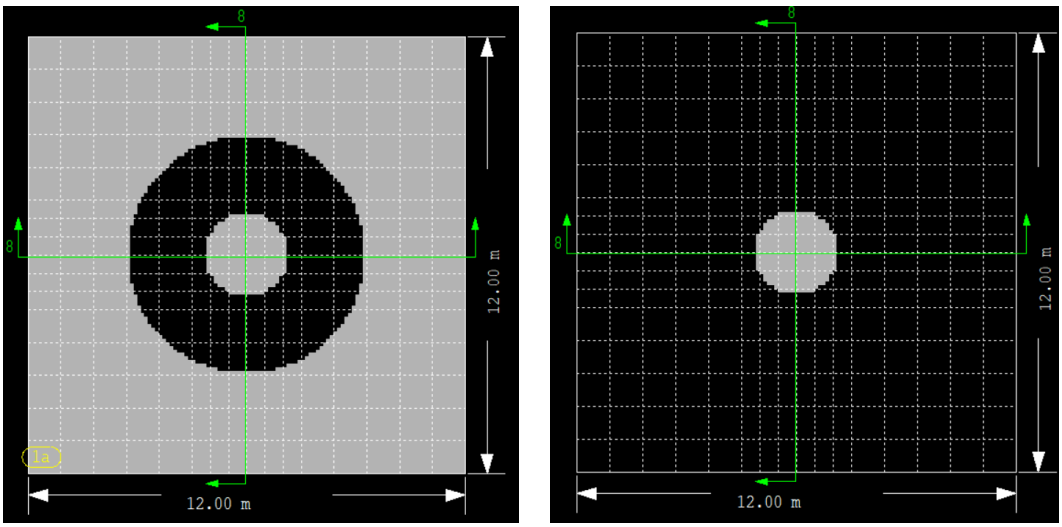

Figure 3.4: Extension of 3D connector at the shared surface between Pool-top face and Room-bottom face

3.2.3. Turbulence Parameters

GOTHIC offers 5 different turbulent models, namely, mixing length (MIX-L), k-epsilon standard (ke-STD), k-epsilon with the re-normalized group source (ke-RG), with a second and a third order approximation for the Reynold stress term (ke-NL2 and ke-NL3, respectively). The model selected was ke-NL2 to have a higher precision at a reasonable computing cost [3].

Under this menu, it is also needed to enable the molecular diffusion within the control volumes. This mechanism was enabled in all control volumes due to the presence of multiphase flows. Furthermore, the phase option "Two" must be set to apply the selected turbulent model to both phases (liquid and vapor). Table 3.4 shows the overall settings.

[3]GOTHIC allows the selection of different turbulent models for different control volumes, and even for different phases. However, this was avoided as it might affect the overall result precision.

Table 3.4: Turbulence parameters specification

Id.	Molecular Diffusion	Turbulence Model	Phase Option
1s	Yes	ke-NL2	Two
2s	Yes	ke-NL2	Two
3s	Yes	ke-NL2	Two

3.2.4. Volume Options

A few other additional options have to be defined to complete the volume settings. The considered options in the model are indicated in Table 3.5. A description of these options is given below:

- **Surface wave damping factor**: This parameter is set to ease the time step for tracking liquid surface waves. Generally, a value of 0.1 is used to eliminate the surface waves and allow greater time steps, while a value of 1.0 restricts the time step. Given that GOTHIC does not automatically limit the time step for pool surface stability, this value has to be checked manually to assure that the solution is not affected by nonphysical surface waves [31].

  This parameter was key for the model convergence, and it had to be set by trial and error. An incorrect value of these parameter made the model to fail or diverged.

- **Pool detection option**: This option is associated with the flow regime of our simulation, and it can be set as local, global or none. The global option includes the detection of liquid surface in horizontally adjacent cells, while local only considers vertically cells. If a surface level is detected in a cell, the interphase drag, heat and mass transfer coefficient are set appropriately. Otherwise, the interface coefficients are based on single phase, bubbly or film flow [29].

- **Gas tracking**: By default this option is ON. In some special cases as boiling, where there should only be present water and steam, it is recommended to turn this option OFF to discard any non-condensing gas that might be accumulating as part of the numerical solution or from flow connections.

- **Burn model**: Hydrogen burn models are available to predict the ignition and/or propagation of burning hydrogen [29]. This option was not activated since the real experimental activities will be performed with helium instead of hydrogen.

Table 3.5: Volume options specification

Id.	Surf. Wave Damp. Factor	Pool Det. Option	Gas Tracking	Burn model
1s	0.85	Global	On	None
2s	0.85	Global	On	None
3s	0.85	Global	On	None

3.2.5. Fluid Boundary Conditions

The built model includes 4 fluid boundary conditions[4] which are identified by a light blue square in the Figure 3.2. In GOTHIC, the fluid boundary conditions are specified by the pressure, temperature, flow and elevation. When necessary, the boundary conditions can also be a function of time.

Table 3.6: Fluid boundary conditions

Id.	Description	Pressure (kPa)	Temp. (°C)	Flow (kg/s)	Elev. (m)
1F	Steam injection	101.325	100	1	7.75
2P	Atmospheric Pressure	101.325	20	-	18
3F	Water injection	101.325	20	1	1
4F	Hydrogen injection	101.325	20	1	7.75

When one of the entries is represented by a function, as is the case of the flow, the number entered corresponds to a multiplier (in this case 1). The flows were described by functions because they might be framed to a short period (as the case of hydrogen), or they can lead to a numerical error when starting instantly at the time 0 as it can occur with the steam injection. As indicated in Table 3.15, the flow injections are constants and their values were set in each simulation model as described below:

- The constant value of each mass injection was set within a 10 seconds frame.
- The steam injection started 5 seconds after the beginning of the simulation.
- The water injection started 12 seconds after the beginning of the simulation.
- The hydrogen injection started 6 hours after the beginning of the simulation.

[4]Thermal boundary conditions are specified in the Thermal Conductors Menu.

3.2.6. Boundary Conditions connection

The connection of the B.C. to the control volumes is done by a flow path element, represented by a green line in Figure 3.2. The flow paths can represent an open section in a wall or a pipe inside a control volume. To fully specify them in GOTHIC is required to indicate the elevation of both extremes, the profile height at the extremes (which in our case is coincident with the hydraulic diameter), the flow area, the hydraulic diameter, the length, among other options. The specification of the elements considered in the model is given in Table 3.7.

Table 3.7: Flow paths specification

Id.	Description	Flow Area (m^2)	Hyd. Diam. (m)	Length (m)	Elev. (m)
1	Steam pipeline	0.013	0.1282	1	7.75
2	Vent to atmosphere	0.1	0.1	0.5	18
3	Water pipeline	0.00309	0.06268	1	1
4	Hydrogen pipeline	0.00216	0.05248	1	7.75

The dimensions of the pipe were not changed between different simulation cases, and their diameter were selected with the aim of obtaining velocities in a typical range for the three flow levels specified in Table 3.14. The nominal pipe dimensions of the model and the calculated velocities are given in Table 3.8. The flow path "vent to atmosphere" is fictitious and its only role was to maintain the atmospheric pressure inside the room.

Table 3.8: Pipe dimensions and selection

Description	Unit	Steam Line	Water Line	Hydrogen Line
Pipe size	mm	DN125	DN65	DN50
Pipe schedule	-	STD 40s	STD 40s	STD 40s
Low level velocity	m/s	10.8	1.1	9.1
Nominal level velocity	m/s	14.4	1.4	13.7
High level velocity	m/s	18.0	1.6	18.2

3.2.7. Initial Conditions

The initial conditions are specified in Table 3.9. The three control volumes were started with the same initial conditions and filled with air (M=28.97 g/gmol). The initial condi-

tions were not changed during the parametric study.

Table 3.9: Initial conditions

Id.	Total Pressure (kPa)	Vapor Temp. (°C)	Liquid Temp. (°C)	Relative Humidity (%)	Liq. Vol. Fraction
1s	101.325	20	20	40	0
2s	101.325	20	20	40	0
3s	101.325	20	20	40	0

3.2.8. Thermal Conductors Positioning

The first step to include heat transfer mechanisms in the model is to position the "thermal conductors". In GOTHIC a thermal conductor represent the surface where occurs heat exchange and it can be associated with convective/radiative heat transfer mechanisms or with thermal boundary conditions. If they are not included properly, the model will not perform any heat transfer calculation. Therefore, all the surfaces of the model must be able to transfer heat with the facing fluid, which can be air, water or steam depending on its location. The pool and room walls were associated with thermal boundary conditions by specifying a value for the heat transfer (e.g. 0 at the mid-plane of the wall) or a temperature (e.g. as environmental temperature at the external side of the walls).

The thermal conductors are specified with several features such as the material, internal sub-divisions (to calculate the wall temperature profile), and the heat transfer coefficients (HTC) associated at the surface. Each thermal conductor has two side (such as, the two sides of a wall), and they can be specified as required. For example, one side can be associated with a HTC that includes condensation models, while the other side can be specified as a thermal boundary condition. All these features are detailed in the next sections.

The built model includes a total of 27 spanned thermal conductors (see Figure 3.5), i.e. thermal conductors that cover several sub-volume faces [5]. These spanned thermal conductors can only cover orthogonal planes. Therefore, in order to cover all the perimeter of the containment, the thermal conductors were spanned over vertical stripes (see Figure 3.6). The room and pool walls were covered automatically by GOTHIC with less number of spanned thermal conductors.

[5]In GOTHIC is possible to specify thermal conductors for each face of a sub-volume cell.

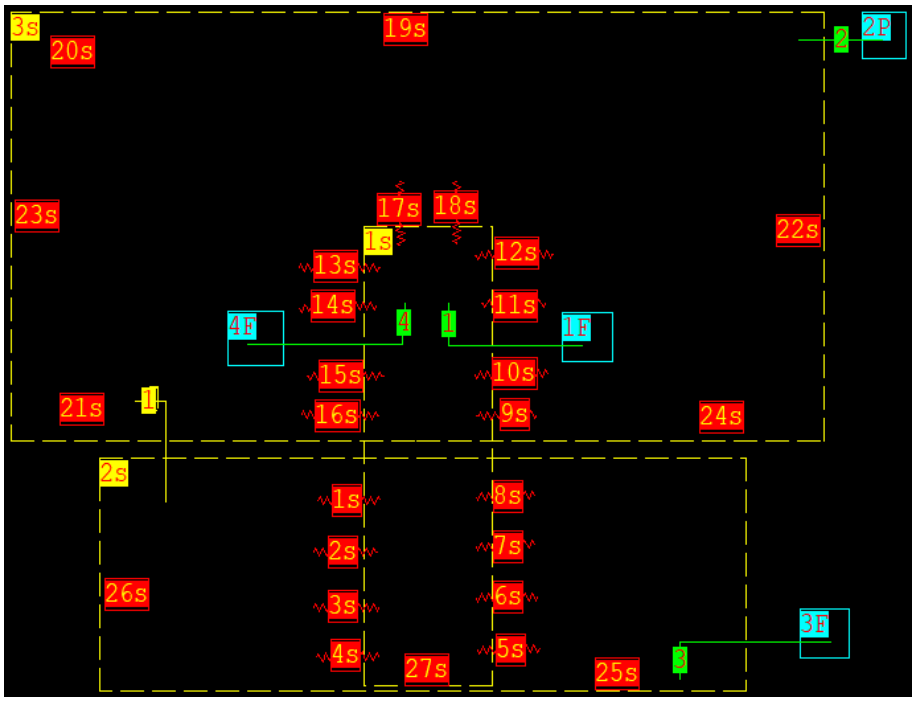

Figure 3.5: GOTHIC Model with indication of the thermal conductors

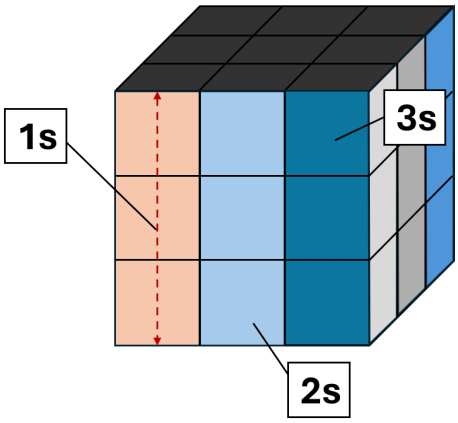

Figure 3.6: Scheme of thermal conductors spanning

In Table 3.10 is given a description of the thermal conductors position, its type and the associated HTC. As seen in the table, each conductor connects two control volumes, or in some cases, connects a control volume with a thermal boundary condition. The conductor type refers to the wall specifications such as materials, thickness and subdivisions (detailed in next section).

Table 3.10: Thermal conductors specifications

Id.	Vol. A	HTC A	Vol. B	HTC B	Cond. Type
1s-8s	Containment shell	1	Pool	4	1
9s-16s	Containment shell	1	Room	6	1
17s-18s	Containment top	2	Room	7	1
19s	Room ceiling	8	B.C.	9	4
20s	Room north wall	6	B.C.	9	4
21s	Room south wall	6	B.C.	9	4
22s	Room east wall	6	B.C.	9	4
23s	Room west wall	6	B.C.	9	4
24s	Room floor	7	B.C.	9	4
25s	Pool floor	5	B.C.	10	3
26s	Pool wall	4	B.C.	10	3
27s	Containment bottom	3	B.C.	10	2

3.2.9. Heat Transfer Coefficients Definition

There were defined 10 different HTC types. These HTC differ between them in the inclusion of certain characteristics, as it might be the condensation model, the orientation of the faces, or if they are specified as thermal boundary conditions. Their specification is given in Table 3.11.

Table 3.11: Heat Transfer Coefficients specifications

Id	H.T. Option	Nominal Value	Cond./Conv. Option	Cond. Option	Nat. Conv. Option	Rad. Option	Phase Option
1	Direct	-	ADD	DLM-FM	Vert. Surf.	ON	Split
2	Direct	-	ADD	DLM-FM	Face Down	ON	Split
3	Direct	-	ADD	DLM-FM	Face Up	ON	Split
4	Direct	-	ADD	DLM	Vert. Surf.	OFF	Split
5	Direct	-	ADD	DLM	Face Up	OFF	Split
6	Direct	-	ADD	DLM	Vert. Surf.	OFF	Vapor
7	Direct	-	ADD	DLM	Face Up	OFF	Vapor
8	Direct	-	ADD	DLM	Face Down	OFF	Vapor
9	Sp Heat Flux	0	-	-	-	-	-
10	Sp Temp	10	-	-	-	-	-

A brief description of the entered options is given below according to the User's Manual [29]:

- **Heat Transfer Option**: The Direct option was the predominant since it is recommended one for modeling containment. It is also recommended when wall condensation is expected. The Sp Heat Flux and Sp Temp are used for defining thermal boundary conditions.
- **Condensation/Convection Option**: ADD combines the condensation heat transfer with any convection and radiation heat transfer also specified.
- **Condensation Option**: DLM states for Diffusion Layer Model. The diffusion layer model calculates the condensation rate and sensible heat transfer rate using heat/mass transfer analogies. The DLM-FM includes options for the formation of mist in the boundary layer and an enhancement due to roughness of the condensate film.
- **Natural Convection Option**: It defines the correlation to be used to calculate the natural convection heat transfer coefficient. Each correlation is based on Nusselt number as a function of Rayleigh number, Ra. There are seven user selectable correlations which depend on orientation and geometry.
- **Radiation Option**: This option enables the radiation heat transfer to the vapor phase [6], which is expected to be important between the steam and the internal side of the containment.
- **Phase Option**: Here is specified to which phase is applicable the defined HTC. The SPLIT option allows to recognize between the Liquid and Vapor phase fractions that are in contact with the conductor. Other options, such as Vapor, make the model to consider that the entire conductor is in contact with that phase.

3.2.10. Conductor Types Specification

The conductor type refers to the wall where is occurring the heat conduction. The specification of the conductors used in the model are given in Table 3.12. The materials and thickness specified are corresponding with the one of the new facility. The containment bottom B.C. considers layers of materials. The number of regions refer to the subdivisions inside a wall. For example, when is expected a high flux is recommended to increase the number of layers at the proximity of the surface in order to have a more precise temperature profile.

[6] Surface-to-Surface Radiation Heat Transfer is managed in other menu.

Table 3.12: Conductor types specifications

Id.	Description	Material	Thickness (cm)	Regions
1	Containment wall	Stainless Steel 1.4462	4	20
2	Containment bottom B.C.	SS 1.4462/ R.C.	54	16
3	Pool walls	Reinforced Concrete	50	11
4	Room walls	Reinforced Concrete	15	9

The material properties were specified at only one temperature as they were not expected to differ greatly in the conditions range. This values are given in 3.13.

Table 3.13: Material properties

Material	Temp. (°C)	ρ (kg/m^3)	k (W/m-°C)	C_p (kJ/kg-°C)
Stainless Steel 1.4462	20	7800	15	0.5
Reinforced Concrete	20	2500	1.8	0.96

- Note: The material properties were obtained from Metalcor GmbH and Properties of Concrete for use in Eurocode 2 (2008).

3.2.11. Radiation Parameters

The inclusion of (surface-to-surface) thermal radiation is done through the Thermal Conductor specifications. This mechanism was only included in the external upper section of the containment that is at the room level. The internal walls of the containment and the external lower section were excluded because is expected that convection plays a more important role. For the specification of the radiation parameters are needed the emissivity of the surfaces and the shape (or view) factors. The emissivities were obtained from [33], and the values were 0.55 for stainless steel (containment exterior) and 0.85 for concrete (room walls). The shape factors depend on the geometries involved (emitter and receiver) and how they "see" each other. In reference [34] are provided guidelines to determine these values. As reference, the values are set between 0-1, where those receivers that cover (or "see") a higher area from the emitter get a higher value. The factors of all the receivers associated with one emitter must sum 1.

3.2.12. T.C. Specification

Once all parameters are defined, it is possible to finalize the thermal conductors specification by selecting the proper values in Table 3.10.

3.2.13. Time Domain

In this menu are specified the total mission time of our simulation, the time step range (minimum and maximum), the time set to print simulation results and other additional options. The time step is mainly controlled by the simulation needs, and it was set between 1e-6 and 1 to not force a specific value. The mission time depended on the simulation case and it was set at 14, 16 (central case) and 19 [h]. The specifications of each simulation case are given in the next chapter.

3.2.14. Solution Options

The main solution options are specified below with a brief description given in the User's Manual:

- **Solution method**: It was set the recommended method, SEMI-IMP. This solution scheme treats velocity and pressure implicitly and treats all transport quantities explicitly. Other options are AUTO-IMP and FRCD-IMP, which differ in how they treat variables, if implicitly or explicitly, and how they manage the time step.
- **Pressure Solution method**: It was set the Conjugate method, as it might offer some advantages with respect to the other available methods (Direct, Sparse, Multigrid, and Block-ITR). This method is generally more efficient for problems with large numbers of cells. It uses an iterative technique that approaches the correct solution monotonically.
- **Differencing scheme**: There are two options, First Order UPwind and Bounded Second Order UPwind scheme (FOUP and BSOUP, respectively). It was set BSOUP as it may provide a higher accuracy and also reduce the numerical diffusion.

3.2.15. Run Options

Finally, in the Run Options are specified the reference pressure, which was set in 101.325 [kPa], the inclusion of Vapor and Liquid phase (the Drop phase was not included as it may increase the already long computational time).

3.2.16. Data acquisition

The data acquisition in GOTHIC is done through the Data Files menu. Here is defined the type of data required (time or space), the location (e.g. control volume) and the property (e.g. pressure). The properties of interest were: pressure, temperature, composition (hydrogen, steam and air concentrations), liquid level, densities and volume fraction.

3.3. Code verification

For the verification step, the following quantities were verified:

- Mass balance of water, air and hydrogen in the containment volume.
- Mass balance of water and air in the pool-room volumes.
- Total energy transferred from the containment.
- Partial pressure of hydrogen inside the containment.

The mass balance of each compound was calculated according to the following equations,

$$M_x^{CV}(t_j) = \sum_{i=1}^{N} V_i \cdot \Theta_i \cdot [\alpha_{l,i}(t_j) \cdot \rho_{l,i}(t_j) + \alpha_{v,i}(t_j) \cdot \rho_{v,i}(t_j) \cdot X_{v,x,i}(t_j)] \tag{3.5}$$

Where:

CV : Selected control volume (1s: containment or 2/3S: pool-room).
i : i-cell in the control volume.
V_i : Volume of cell i.
Θ_i : Volume porosity factor of cell i.
$\alpha_{l,i}$: Liquid volume fraction of cell i.
$\alpha_{v,i}$: Vapor volume fraction of cell i.
$\rho_{l,i}$: Liquid density of cell i.
$\rho_{v,i}$: Vapor density of cell i.
x : Compound of interest, i.e. Water (w), air (a) or hydrogen (h).
$X_{v,x,i}$: Mass fraction of x in the vapor phase v in the i-cell.
t_j : Time j, e.g. 0: initial time, f: end time.

Since the air and hydrogen are non-condensing gases, the liquid phase was assumed to be completely water.

The accumulated amount of water, air and hydrogen was calculated as the mass difference

between the start and end of the simulation ($t_0 = 0$ [s] and $t_f = 55200$ [s], respectively). That is to say,

$$M^{CV}_{x,accum.} = M^{CV}_{x}(t_f) - M^{CV}_{x}(t_0) \tag{3.6}$$

The mass flow of each compound was kept constant along the simulation. However, the beginning and end of the injections have a slope to avoid numerical deviations. In another words, the constant values are not reach instantly but in around 10 seconds. In consequence, to include the mass injected during this short fractions of time, the total mass injected was calculated as trapezoid areas,

$$M^{CV}_{x,net} = \sum_{j=1}^{f} (\dot{m}^{CV}_{x,j,in} + \dot{m}^{CV}_{x,j-1,in}) \cdot (t_{x,j} - t_{x,j-1})/2 \tag{3.7}$$

The deviation of the mass balance was calculated as an error between the accumulated amount inside the control volume with respect to the total entering amount. As air was not injected in the system, the final amount was assessed with the initial one, i.e. as the ratio between the final and the initial amount.

$$Error^{CV}_{MB,x} = \frac{M^{CV}_{x,accum.}}{M^{CV}_{x,net}} \tag{3.8}$$

A similar approach was taken to verify the energy balance inside the containment. The total energy inside the containment at a specific time was calculated with the next equation,

$$E^{1S}(t_j) = \sum_{i=1}^{N} m_{l,i}(t_j) \cdot h_{l,i}(t_j) + m_{v,i}(t_j) h_{v,i}(t_j) \tag{3.9}$$

Where:

CV : Selected control volume (1s: containment or 2/3S: pool-room).
i : i-cell in the control volume.
N : Total number of cells in the control volume.
$m_{l,i}$: Liquid mass in cell i.
$m_{v,i}$: Vapor mass in cell i.
$h_{l,i}$: Liquid enthalpy in cell i.
$h_{v,i}$: Vapor enthalpy in cell i.

t_j : Time j, e.g. 0: initial time, f: end time.

The accumulated energy inside the containment was calculated as the difference of the containment energy at the start and end of the simulation ($t_0 = 0$ [s] and $t_f = 55200$ [s], respectively).

$$E^{1S}_{accum.} = E^{1S}(t_f) - E^{1S}(t_0) \tag{3.10}$$

The total energy that enters the containment during the simulation corresponds to the enthalpy associated with the steam and hydrogen injections, and it was calculated as follows,

$$E^{1S}_{total,in} = M^{1S}_{w,in} \cdot h^{1S}_{w,in} + M^{1S}_{h,in} \cdot h^{1S}_{h,in} \tag{3.11}$$

The total energy that leaves the containment during the simulation was calculated as the difference between the total energy inlet and the accumulated energy, as follows,

$$E^{1S}_{total,out} = E^{1S}_{total,in} - E^{1S}_{accum.} \tag{3.12}$$

As the total energy that leaves the containment corresponds mostly to the latent heat transferred due to the condensation process. These two values may be compared and a deviation can be obtained. It is important to clarify that the total energy outlet includes also sensible heat transfer from the hot non-condensing gases, and the liquid water to the exterior. However, this calculation is more complex to perform. In consequence, it is understood that the deviation obtained may be greater than the real value.

$$E^{1S}_{total,cond.} = M^{1S}_{w,cond.} \cdot h^{1S}_{w,vap.} \tag{3.13}$$

$$Error^{1S}_{EB} = \frac{E^{1S}_{total,cond.} - E^{1S}_{total,out}}{E^{1S}_{total,out}} \tag{3.14}$$

The partial pressure associated to the hydrogen inside the containment was calculated with the ideal gas law as,

$$P_{H_2,calc.} = \frac{N_{H_2}(kmol) \cdot R_u(\frac{kPa \cdot m3}{kmol \cdot K}) \cdot T_{av.}(K)}{V_v(m3)} \tag{3.15}$$

This value was compared with the partial pressure simulated. Since is not possible to distinguish the real partial pressure caused by the hydrogen in the simulation, the adopted value was the pressure difference before and after the hydrogen injection. It is understood that this value includes also some partial pressure of the steam injected during this time frame. Therefore, it is expected that the calculated deviation might be larger than the real one.

$$P_{H_2,sim.} = P^{1S}(t = t_+(H_{2,inj-end})) - P^{1S}(t_-(H_{2,inj-start})) \tag{3.16}$$

The deviation was calculated as follows,

$$Error^{1S}_{P_{H_2}} = \frac{P_{H_2,sim.} - P_{H_2,calc.}}{P_{H_2,calc.}} \tag{3.17}$$

3.4. Design of Experiments and Parametric Study

The boundary conditions for the commissioning tests and the plant model parametric study were determined by a Design of Experiment (DOE) approach. DOE is a structured, organized method for determining the relationship between factors (Xs) affecting a process and the output of that process (Y) [35]. By a DOE method is possible to ensure the generation of valid, defensible, and supportable engineering conclusions [36]. The study areas in which DOE is often applied in engineering are comparative, screening, modeling, optimization, robust design and formulation [37].

Since there is no prior information about the factors affecting the responses (i.e. System Figure of Merits), this design is framed in a screening study. The responses of interest are the peak pressure, peak temperature, peak hydrogen concentration and average condensation rate. While the inputs are those quantities that might have an influence over these responses and that can be controlled during the experimental activities. Considering the capabilities of the plant, the input variables are the steam mass flow rate, water mass flow rate, hydrogen mass flow rate, hydrogen total mass, and water temperature. The levels of each factor are provided in Table 3.14.

Table 3.14: Boundary condition levels

Parameter	Variable	Unit	Low Level	Nominal	High Level
Steam mass flow rate	$\dot{m}_{steam}$	kg/h	300	400	500
Water mass flow rate	$\dot{m}_{water}$	kg/s	3.5	4.3	5.0
Hydrogen mass flow rate	$\dot{m}_{H2}$	g/s	1.50	2.25	3.00
Hydrogen total mass	m_{H2}	kg	2.1	2.8	3.5
Water temperature	T_{water}	°C	15	20	25

As a mean to reduce the number of runs and to allow the distinction of two-factor interactions (higher orders of interaction might be confounded), it was selected a Half-Factorial design. The boundary conditions of each run are specified in Table 3.15 with the inclusion of the mission time. This boundary conditions are used to study the performance of the SMR-PCCS system and to understand the system capabilities from a safety point of view. The results of the parametric study will also be used as a reference for the commissioning tests execution. The plant model settings were not part of the parametric study.

Table 3.15: Boundary conditions of the parametric analysis

Case Id.	Steam mass flow rate	Water mass flow rate	Hydrogen mass flow rate	Hydrogen total mass	Water temperature	Mission time*
-	kg/h	kg/s	g/s	kg	°C	h
0	400	4.25	2.25	2.8	20	16
1	300	3.50	1.50	2.1	25	19
2	500	3.50	1.50	2.1	15	19
3	300	5.00	1.50	2.1	15	14
4	500	5.00	1.50	2.1	25	14
5	300	3.50	3.00	2.1	15	19
6	500	3.50	3.00	2.1	25	19
7	300	5.00	3.00	2.1	25	14
8	500	5.00	3.00	2.1	15	14
9	300	3.50	1.50	3.5	15	19
10	500	3.50	1.50	3.5	25	19
11	300	5.00	1.50	3.5	25	14
12	500	5.00	1.50	3.5	15	14
13	300	3.50	3.00	3.5	25	19
14	500	3.50	3.00	3.5	15	19
15	300	5.00	3.00	3.5	15	14
16	500	5.00	3.00	3.5	25	14

- The mission time was set as approximately 2 hours after the pool filling time. It was not considered as a manipulating factor in the ANOVA analysis.

3.5. Data analysis

The data files were processed in a spreadsheet according with the required value. Some of these data were easily processed, such as, the maximum values of pressure, temperature and hydrogen concentration inside the containment, which values needed only to be localized with a proper function. While others required more work, as the condensation rate. In this case, it was first calculated the total mass of liquid through the multiplication of the cell volume, volume porosity factor, and liquid density of that cell at all times. Then, the condensation rate was calculated as the liquid mass difference at two consecutive times divided by the corresponding time slot.

The results of the parametric study were assessed with an Analysis of the Variance (ANOVA) and the p-value. By these statistic measures was possible to determine whether

the factors had an influence over the responses or not, and the importance in the response variations. The detailed statistics are provided in Appendix B.

4 | Results and Discussions

The present chapter is organized into three main sections. The first section shows the verification of the model, which has the function to assure us that the model equations were implemented and solved correctly. The second section focuses on the phenomena interpretation inside the containment, taking as reference the base case scenario. The third part is dedicated to the parametric analysis, focusing on the evolution of the Figure of Merits (FoM) of the system under different boundary conditions, and the identification of the significant parameters that affects the characteristic system responses.

4.1. Verification of the GOTHIC model

This verification step aims to verify that the equations in the model are correctly implemented and solved. The deviation informed in the following tables serves as an indication of the uncertainties of the solution, however, does not necessarily refers to an error from the real value. Since the real value can only be assessed with experimental data, which is not available for this plant.

In Table 4.1 is shown the verification of the mass balance inside the containment. As the containment is a closed system where mass can only enter, the entering mass of water and hydrogen must be accumulated and the initial mass of air must be invariable. The accumulated mass of water and hydrogen was calculated as the difference between the mass at the end and the beginning of the simulation. This accumulated mass was compared with the mass injected into the volume, imposed in the boundary condition. Hydrogen was the compound with the highest deviation reaching a 0.61%, while water was the lowest with a 0.05%. Understanding the effects that may have this additional mass, it is seen as acceptable, i.e. it will not have a significant effect in the phenomena that will be studied such as compounds stratification, or condensation.

Table 4.1: Mass balance in containment

Parameter	Water	Air	Hydrogen	Total
Initial mass [kg]	0.30	51.65	0.00	51.95
Final mass [kg]	6,137.08	51.91	2.84	6,191.83
Accumulated mass [kg]	6,136.78	0.26	2.84	6,139.87
Total mass, in [kg]	6,133.53	0.00	2.82	6,136.35
Total mass, out [kg]	0.00	0.00	0.00	0.00
Deviation [%]	0.05%	0.50%	0.61%	0.06%

The pool and room control volumes are open between each other, therefore, the mass and energy balance is solved as a continuum. In Table 4.2 is shown the result of the mass verification of the pool-room volume. This system receives liquid water in the pool which amount was imposed in the boundary condition. Also, a pressure boundary condition was imposed in the room to keep the system at atmospheric pressure. In consequence, the deviation of air can be explained by this reason, i.e. the system allowed the exit of mass in order to keep the atmospheric pressure. On one side, it was expected that all the air in the pool would be displaced by the entering of water, and, on the other hand, the expansion of air due to the heating would also cause an additional mass reduction. The total mass and the accumulated water had both a deviation lower than 0.5%, which is considered acceptable for the aim of the simulation.

Table 4.2: Mass balance in pool/room

Parameter	Water	Air	Total
Initial mass [kg]	13.34	2,301.20	2,314.55
Final mass [kg]	218,317.95	1,869.10	220,187.05
Accumulated mass [kg]	218,304.61	-432.10	217,872.51
Total mass, in [kg]	219,347.55	0.00	219,347.55
Total mass, out [kg]	28.01	1,092.89	1,120.91
Deviation [%]	-0.46%	-60.46%	-0.16%

The energy balance was more complex to verify due to the high number of variables involved. Nevertheless, in an attempt to obtain an indication of the model implementation, it was compared the total energy that left the containment with respect to the condensate accumulated (see Table 4.3). The energy that enters the containment corresponds to the enthalpy from the steam and hydrogen boundary conditions. The specific enthalpy of

the steam was 2,675.6 [kJ/kg], and the hydrogen was 4,083.8 [kJ/kg]. The condensate accumulated inside the containment was obtained from the simulation and it was 6,106.83 [kg]. In order to assess the model implementation, it was considered a constant enthalpy of vaporization of 2,256.4 [kJ/kg]. By this methodology, it was obtained a 10% deviation, however, it must be pointed out that not all the energy leaving the containment is due to the condensation of steam, there is also sensible heat transferred from the air, hydrogen and liquid water, which values were not possible to obtain. Therefore, this value is only taken as a reference of the model implementation.

Table 4.3: Energy balance in containment

Parameter	**Total energy**
Parameter	Total energy
Initial Energy [kJ]	131,928
Final Energy [kJ]	1,142,611
Accumulated Energy [kJ]	1,010,684
Total Enthalpy, in [kJ]	16,422,377
Total Enthalpy, out [kJ]	15,411,693
Total Enthalpy, cond. [kJ]	13,779,458
Deviation [%]	-10.59%

Finally, it was verified the partial pressure of hydrogen inside the containment (see Table 4.4). This parameter was also complex to analyze due to the gas mixing inside the containment. Nevertheless, an approximate value was obtained indicating that the pressure calculation is well implemented in the model. The theoretical partial pressure of hydrogen was calculated with the ideal gas law. For this assessment, several values were obtained from the simulation such as the temperature and vapor-occupied volume (at this time, some condensate was already present in the containment). On the other hand, the partial pressure of hydrogen was obtained from the simulation as the difference between the pressure before and after the hydrogen injection, i.e., 722.7 [kPa] and 844.4 [kPa], respectively. With this assessment, it was obtained a deviation of about 3% which is acceptable considering the simplifications made.

Table 4.4: Partial pressure of hydrogen in containment

Parameter	Value
Hydrogen total mass [kg]	2.84
Average Containment vapor volume [m^3]	40.71
Average temperature [°C]	164.49
Estimated pressure from gas ideal law [kPa]	125.71
Estimated pressure from simulation [kPa]	121.75
Deviation [%]	-3.15%

4.2. Analysis of the Base Case Scenario

The initial conditions of the three control volumes, i.e. containment, pool and room, is 101.325 [kPa] and 20 [°C]. All control volumes are initially filled with air. The simulation begins with the LOCA break and the injection of steam into the containment. A few seconds after the break, the pool starts to be filled with water until is completely full. The base case scenario has the following boundary conditions,

- Steam mass flow rate: 400 [kg/h]
- Water mass flow rate: 4.25 [kg/s]
- Hydrogen mass flow rate [1]: 2.25 [g/s]
- Total hydrogen mass: 2.8 [kg]
- Inlet water temperature: 20 [°C]

The Figure 4.1 shows the evolution of the pressure inside the containment at three different heights: 0.25 [m], 5.75 [m] and 11.75[m]. The pressure increases at a fast pace in the beginning as the steam enters the containment, and it reaches a maximum value of around 1200 [kPa] at 3.8 [h] (see "peak 1"). The pressure peaks as a consequence of the competing effects between mass/energy addition, provided by the enthalpy inlet through the steam injection, and mass/energy dissipation, provided by the external cooling through the steam condensation. In other words, the injection of steam increases the number of molecules in the gas phase which increases the pressure, and the condensation reduces the number of molecules in the gas phase which reduces the pressure. Along with this mass transfer process, the continuous steam injection also heats the accumulated mass already inside the containment, which increases the pressure, and the cooling reduces the overall temperature, which reduces the pressure. Once the condensation rate equals or

[1]The injection of hydrogen starts 6 hours after the LOCA break and runs for 0.35 [h].

exceeds the steam injection rate, and the number of molecules in the gas phase starts to decrease, the pressure starts to decrease. The decrement of the pressure is observed until 6.0 [h]. This is the moment when the hydrogen injection begins and the pressure starts to increase again. Given that the hydrogen does not condensate as the steam, the pressure increases at almost a linear rate while the injection runs due to the mass addition. At 6.3 [h] the hydrogen injection stops, and a slightly increment is observed for a short period until the "peak 2", this further increment might occur due to a slight decreasing of the condensation rate. Finally, after the "peak 2", the decreasing rate of the pressure slows down meaning that the condensation process is not as fast as before the hydrogen injection. In consequence, this might be an indication of the effect of non-condensable gases over the condensation rate, as they impose an additional resistance in the boundary layer.

Moreover, after approximately 8 [h] the pressure lines of the levels 0.25 [m] and 11.75 [m] separate from each other. This is a consequence of the additional hydrostatic pressure that the level 0.25 [m] experiences due to the accumulation of condensate at the bottom.

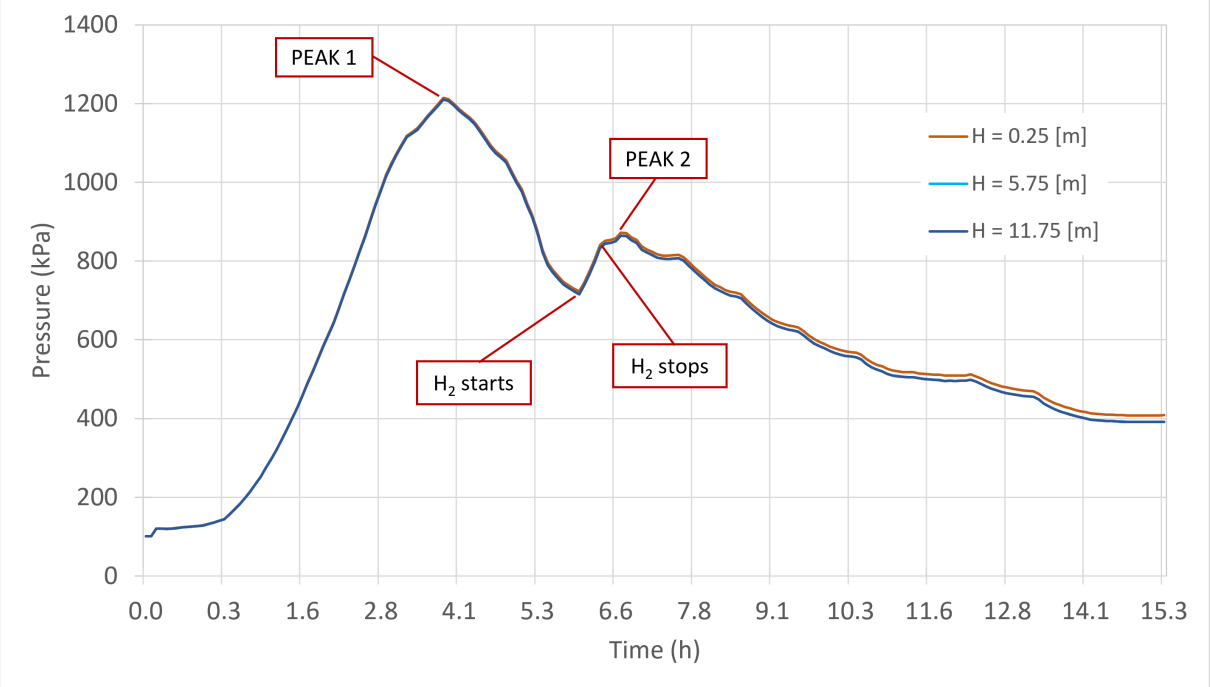

Figure 4.1: Pressure evolution at different heights inside the containment (base case).

The temperature inside the containment is shown at several heights in Figure 4.2. Different temperatures are present at different elevations meaning that there is temperature stratification. The temperature stratification is the result of the buoyancy effect occurring inside the containment, i.e. lighter molecules accumulate at the top and heavier at the

bottom. In contrast to what might be expected before the simulation, it is observed that the top layers are not necessarily the hottest. This is a consequence of the multiple compounds present, namely, air, water and hydrogen. That is to say, if only one compound would be present, the temperature would be aligned from the top, the hottest, to the bottom, the coldest. However, in this mixture of gases it might be possible that hydrogen at a lower temperature has a lower density than steam at a higher temperature. Evolving to what is seen at the end of the simulation (see right-hand data), the temperature at 7.25 [m] is 134.6 [°C], and at 11.25 [m] is only 82.5 [°C].

The steam enters into the containment at 7.25 [m] in the upward direction. Due to this, the layers over 6.25 [m] show a faster increment of the temperature than the layers below. The layers below the injection point are heated up when the steam reaches those regions. As steam fills the containment, the temperature homogenizes and it follows a unique tendency until reaching "peak 1", this is observed from elevation 3.25 [m] to the top. The temperature at "peak 1" is 188 [°C] and it is equivalent to the saturation temperature of the corresponding peak pressure (see T_{sat} line). This means that the regions from 3.25 [m] to the top are in a saturated condition or, better say, in a Liquid-Vapor Equilibrium (LVE). The elevations below 2.25 [m] do not reach the saturated temperature corresponding to the actual pressure, i.e. these lower regions might be rich in air or have liquid water in a sub-cooled condition. In Figure 4.4 is shown the composition at level 2.25 [m], and it is confirmed the presence of air in this zone, but still is richer in steam rather than air. In consequence, this region is characterized by a foggy condition where water liquid droplets are suspended in the air. This means that the cooling process involves not only latent heat during the condensation but also sensible heat to reduce the temperature of the liquid water.

The separation of the superior layers from the saturation line at 6.0 [h] occurs as consequence of the hydrogen injection. The hydrogen enters the containment at 7.25 [m] in the upward direction with a temperature of 25 [°C]. As soon as hydrogen enters, the layers at 10.25 [m] and 11.25 [m] show a reduction of their temperatures indicating that hydrogen accumulates in this region. A similar effect is observed at layers 4.25 [m] and 5.25 [m]. The region between elevations 6.25 [m] and 9.25 [m] follows the tendency of the saturated temperature, indicating that this region might be rich in steam. The composition at different heights is shown in Figure 4.4 and it is seen that hydrogen goes mostly to the uppermost layers and also a portion goes to the bottom over the liquid level. As previously indicated, the temperature stratification occurs due to the buoyancy effect driven by the different densities. Therefore, it is seen that under certain conditions hydrogen and air might be heavier than steam. This feature must be verified with the experimental

activities.

The bottom of the containment at 0.25 [m] reached a maximum temperature of 76 [°C]. This region contains liquid water as seen in Figure 4.6. This temperature confirms that the cooling process also involves sensible heat transfer which allows the further temperature reduction of the liquid water. As the liquid level rises, the next layers at 1.25 [m] and 2.25 [m] are grouped at the same temperature. This means that the liquid portion does not show a remarkable temperature stratification.

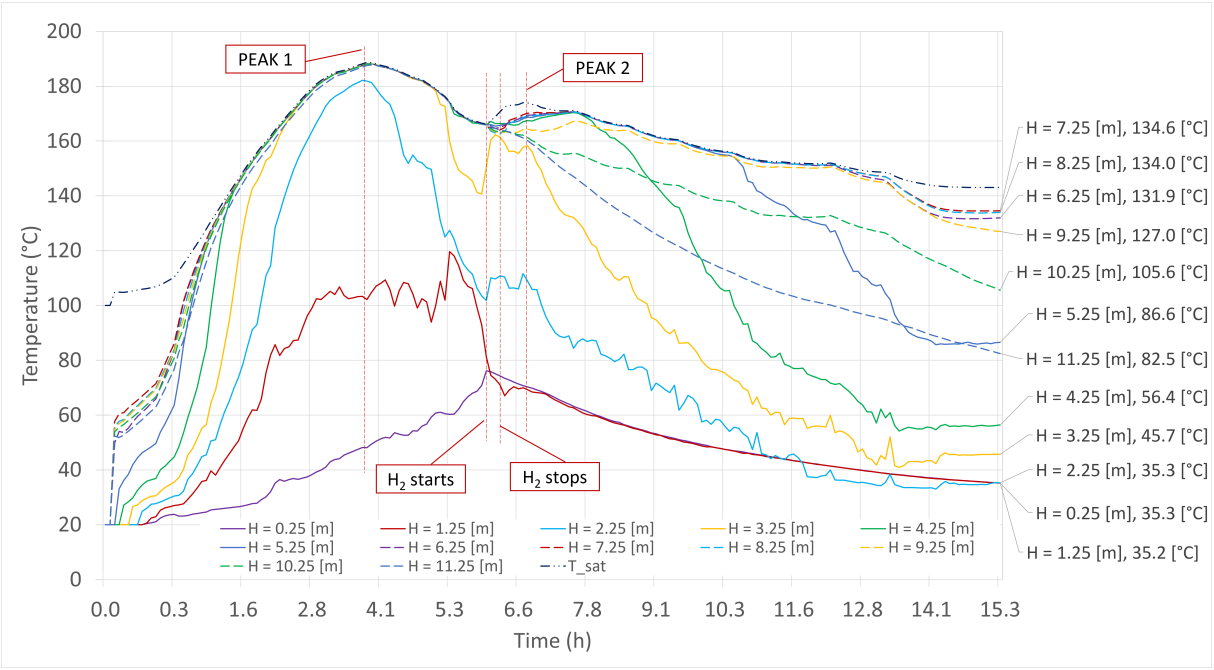

Figure 4.2: Temperature evolution at different heights inside the containment (base case).

An additional representation of the temperature evolution is shown in Figure 4.3. This graph shows the axial temperature profile inside the containment and each line corresponds to the axial temperature at a determined hour. It is observed that the temperature increases and it reaches a maximum at around 4 [h] (solid blue line). At this hour, it is observed the longest isothermal region (or plateau) covering from the elevation 3.25 [m] to the top. This plateau evolves with the time and it represents the rich steam region. The longest plateau is observed during the peak time [2] (corresponding to "peak 1"), while the shortest one is observed at the end of the simulation at 15 [h]. Interestingly, before the peak condition [3] the plateau gets larger by incorporating regions from the bottom, e.g.

[2]The peak time (or characteristic time) is defined in the next section as the time to reach the peak condition, i.e. when the condensation rate equals the steam injection.

[3]Here, the peak condition is defined as a generic term to point out the moment when the pressure and temperature reach their maximum values.

the plateau covers from the top until 5.25 [m] at 1 [h], and later at 4[h] it expands until the elevation of 3 [m]. After the peak time, the plateau starts to lose regions from the bottom, probably due to the condensation of steam, and after 7 [h] it also loses regions from the top, probably due to the start of the hydrogen injection. In another words, the steam rich zone inside the containment expands before the peak and it retracts after the peak.

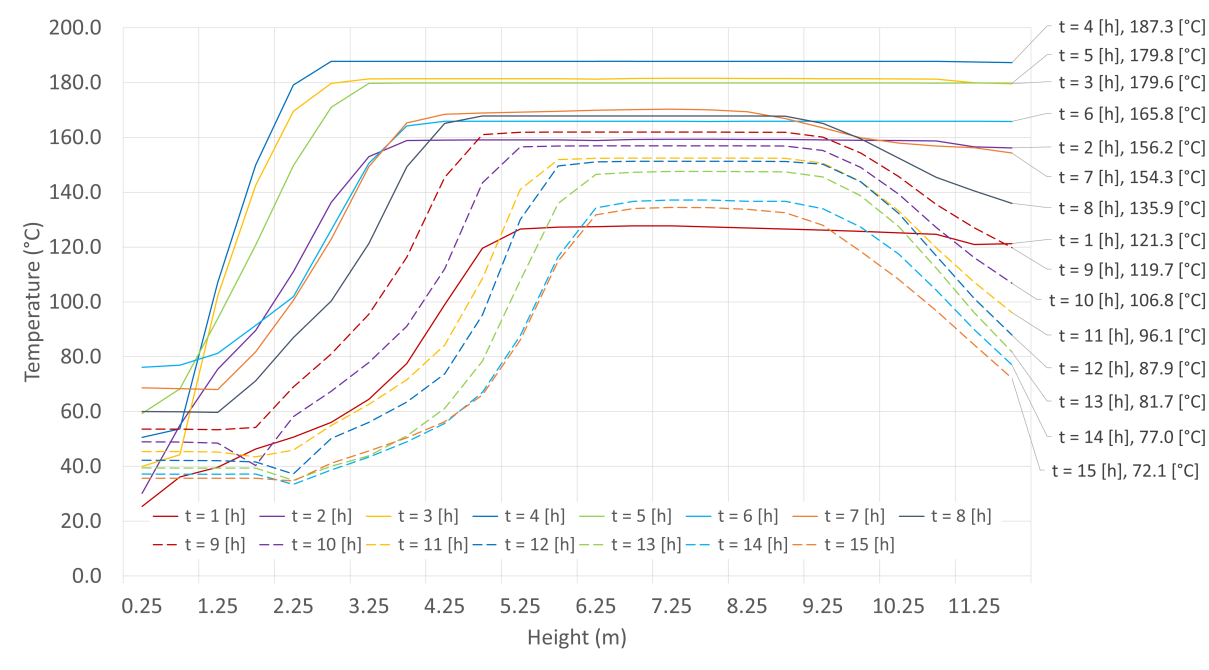

Figure 4.3: Axial temperature profile at different times inside the containment (base case).

On the other hand, there is a possibility that some of the observed temperature stratification might be due to the hydrogen inlet temperature, i.e. as hydrogen is injected at ambient temperature it may cause some temperature reduction at the top of the containment. In a real accident scenario, the hydrogen is produced at the local temperature of the zirconia oxidation at the core. Therefore, it is recommendable to implement a preheater in the line to warm up the hydrogen before it enters the containment.

The gas composition evolution is shown in Figure 4.4 at different elevations. At the beginning only air is present in the containment. When steam enters into the containment, the air goes to the bottom as seen in elevation 2.25 [m]. The concentration of steam reaches 100% in all elevations but not at the bottom, where it only reaches around 85%. The composition stratification occurs due to buoyancy effects in response to the density differences. While the generation of different mixtures along the axial direction responds to turbulence mixtures and mass diffusion effects.

Starting from the upper elevation at 11.75 [m], it is observed that steam is displaced from this position when the hydrogen injection starts at 6 [h], reducing its concentration from 100% to around 9%. It is also observed that following the hydrogen accumulation, some of the air located in the lower region enters, going from almost 0 % to around 10%. At 7.25 [m] is observed an instant reduction of the steam concentration during the time that hydrogen enters into the system since the mass inlet is located at this height. Afterwards, the original composition recovers meaning that hydrogen went to other locations. At around 12 [h] it is observed an increment of the air and hydrogen concentration at this height. This occurs because of the condensation process, i.e. it is not that the region get richer in air and hydrogen but it gets poorer in steam as this condenses. At the end of the simulation, the gas composition at this height was 80% steam, 13% air and 7% hydrogen. At 5.25 [m] is observed that the air and hydrogen increment starts 2 hours before. This means that inside the containment there might be a "condensation front" such as a cloud border that advances from bottom to up as the cooling process works. Furthermore, the cooling process should improve with time as the external pool is filled with water causing that this "front" raises. At the end, the composition at this height was 60% steam, 11% air and 29% hydrogen. Finally, the region over the liquid level at 2.25 [m] [4] is rich in air and hydrogen due to the same prior reason. Here the steam concentration reaches a maximum of 85% at around 4 [h] and then decreases to almost 0%, i.e. the "condensation front" reaches its lowest position at the peak time. This confirms that the isothermal observed in Figure 4.3 corresponds to the rich steam zone inside the containment, and that the position of the lower plateau limit corresponds to the "condensation front".

In summary, the steam rich zone is located in the middle and it gets shorter as the hydrogen accumulates in the top and the "condensation front" raises in the bottom. The "condensation front" can be understood similarly as a cloud border which is not well defined but fuzzy as its composition changes. That is to say, the bottom is rich of air, but there is also some steam present. An indirect measure of this front position can be the plateau observed in a temperature versus elevation plot. Also, hydrogen accumulates mostly in the top and some of it goes to the bottom. For more details, it is provided the concentration evolution of hydrogen, steam and air at several heights in appendix A.

[4]The maximum condensate level reaches 2 [m] height and it is shown in Figure 4.6.

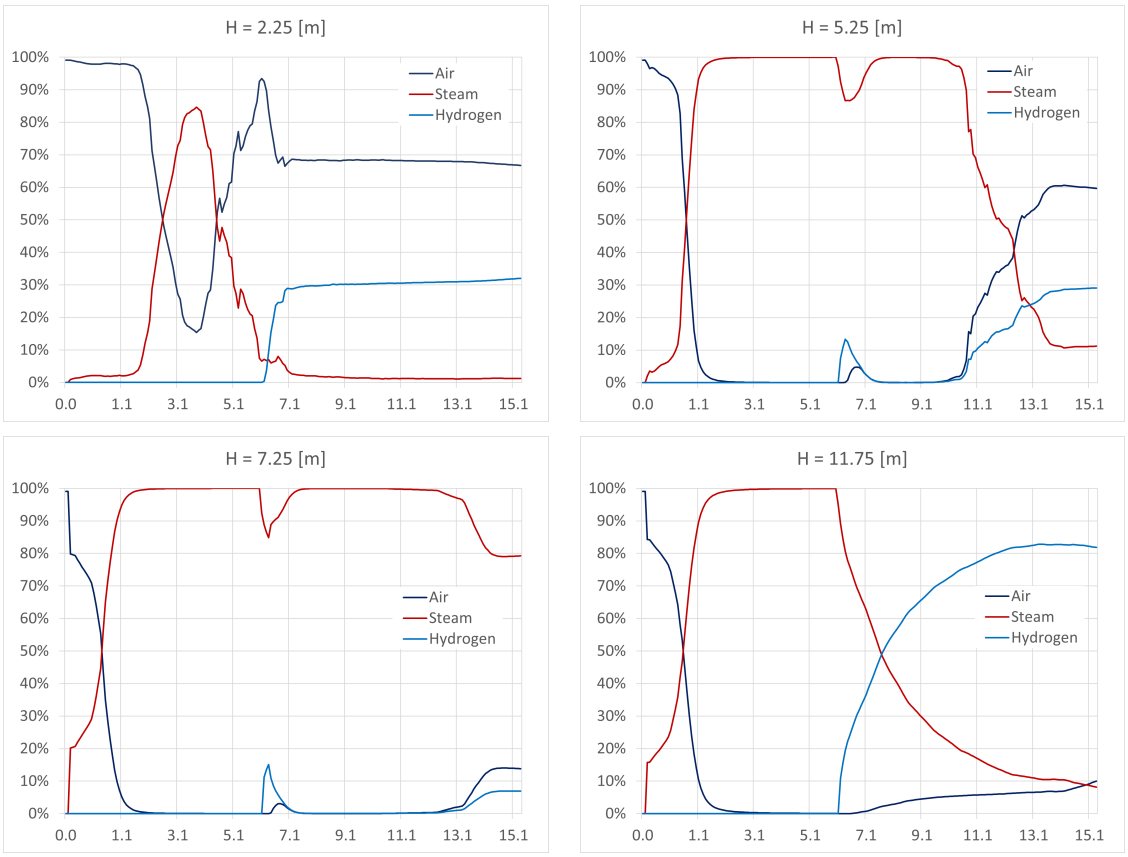

Figure 4.4: Volumetric composition evolution at 4 different elevations inside the containment (base case). X-axis: [h] and Y-axis: [$\%v/v$].

According to the Shapiro diagram (see Figure 1.3), the top section of the containment is located in the detonation region, which can lead to an explosion if an igniter is present. The temperature keeps relatively low in the range of 80-105 [°C] at 15 [h] reducing the risk of auto-ignition. Even though the probability of auto-ignition is low, the presence of any explosive mixture inside the containment should be avoided always. One strategy to reduce this risk is the positioning of Passive Autocatalytic Recombiners (PAR) at this location.

Additionally, the axial hydrogen concentration profile at different hours is shown in Figure 4.5. Each line shows the hydrogen concentration at a specific hour. Here we observe that hydrogen accumulates at the top, with a concentration around 80%, and above the liquid level, with a concentration of 30%. Around 35 minutes after the hydrogen injection finishes (see purple line at 7 [h]), hydrogen is present everywhere in the containment with a predominance in the two indicated regions. In the lower region is observed a plateau of constant concentration. This plateau expands as the "condensation front" raises as explained in the prior paragraph. On the other hand, the top of the containment gets

richer in hydrogen with time as consequence of the displacement of steam. The middle region, that is rich in steam, is not hardly affected during this simulation time. But as the condensation process works it is expected that hydrogen also increases.

Finally, the previous temperature analysis can be complemented, as follows: (i) the region between 6.25 and 9.25 [m] is mostly steam, in this region there is a phase change from vapor to liquid phase, i.e. there is latent heat transfer, reason why its temperature corresponds to the saturated temperature at the corresponding pressure (saturation line in Figure 4.2); (ii) above 10.25 [m] is a non-condensable gas mixture rich in hydrogen, i.e. there is sensible heat transfer, reason why its temperature is lower than the saturated temperature; and (iii) between 2.25 [m] and 5.25 [m] is a non-condensable gas mixture rich in air, i.e. there is sensible heat transfer, reason why its temperature is lower than the saturated temperature.

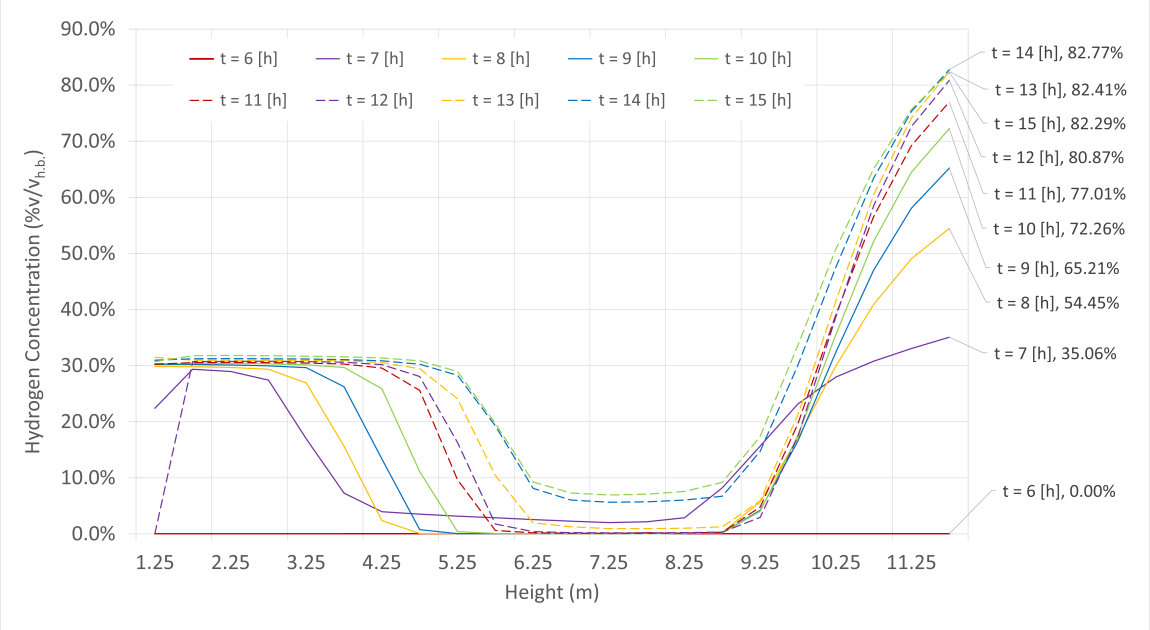

Figure 4.5: Axial hydrogen concentration profile at different times inside the containment (base case).

The condensate accumulation is show in Figure 4.6. This accumulation starts as soon as the steam enters in the containment (see blue line). The blue line indicates the liquid level, which rises faster than the volumetric accumulation due to the geometry of the vessel, i.e. the bottom corresponds to a semi-sphere with a radius of around 1 [m] and, therefore, the cross section changes as the liquid level raises. On the other hand, the volumetric accumulation (see orange line) shows slightly different slopes along the simulation, meaning that the condensation rate varies with time. The total volume of water at

the end of the simulation was 6.3 [m^3] representing a 99.67 % of the total mass of steam injected.

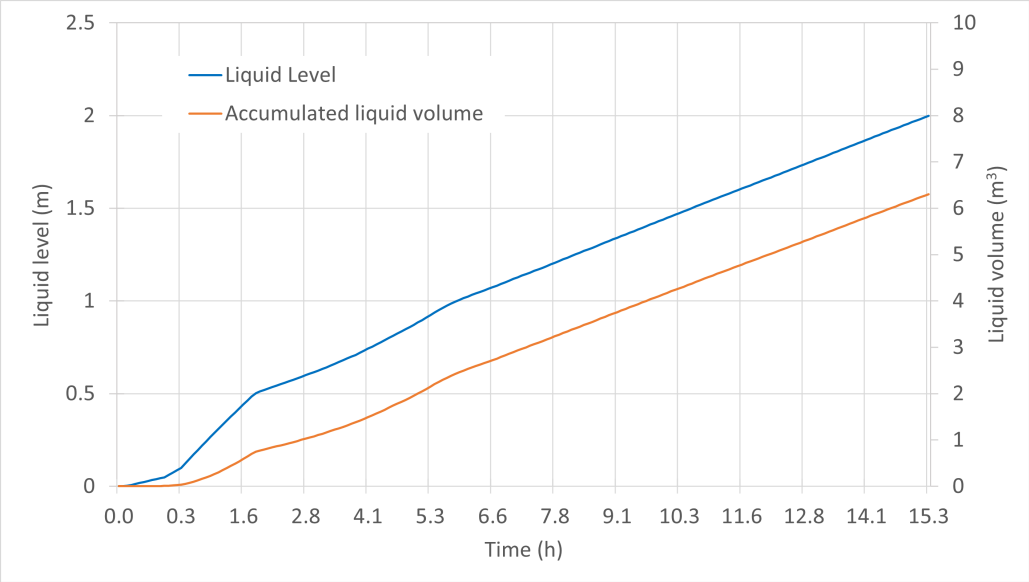

Figure 4.6: Liquid water accumulation inside the containment (base case).

The evolution of the condensation rate with time is shown in Figure 4.7. The condensation rate corresponds to a measurement of the phase change from vapor to liquid phase of the water molecules. In the mid- and long-term, this process is driven by the external cooling of the containment. However, in the beginning the steam condenses as it release its latent heat to the air and containment vessel, which represents the internal heat sink. In other words, the latent heat of the steam is transferred to the immediate surroundings either, air or internal steel structure, causing the instant condensation of steam in the beginning. As consequence, these elements will heat and the condensation rate will reduce because there is less immediate heat sink available to deliver the latent heat. A minimum condensation rate (0.0845 [kg/s] at 2.2 [h]) is reached at around 2.6-2.9 [h] (see "MIN") corresponding with the time that several layers are grouped in the temperature versus time plot (see Figure 4.2). This time can be seen as an "internal inertial time" of the system before the activation of the external cooling [5]. Once the external cooling starts, the condensation rate rises because now the available heat sink is larger than before due to the external heat sink. The condensation rate increases until reaching a maximum (see "MAX", 0.1463 [kg/s] at 5.4 [h]), which is limited by the cooling capability of the system. The time to reach this maximum can be defined as an "external inertial time" which represents the

[5]NOTE: This simplification is introduced in order to separate each effect. In reality, all cooling processes are occurring simultaneously.

time to saturate the external heat sink. This maximum condensation rate represents, in someway, the maximum cooling performance that the natural convection cooling offers. That is to say, if for example the external cooling would be driven by a pump, the speed at which the latent heat from the steam is taken away by the external fluid would accelerate, and therefore a higher maximum condensation rate would be observed. In our case, the system is limited by the natural convection cooling offered by the external air and water. After this maximum level is reached, the condensation rate reduces again and the reason is the same than before, i.e. as the external fluids are heated, the availability of immediate heat sink is reduced what affects the speed of the latent heat transfer. Once the system reach an equilibrium between the energy addition, driven by the steam injection, and the energy dissipation, driven by the external cooling, we observe convergence around the average condensation rate. The average condensation rate was calculated during the steam injection plateau section (in this case, from approximately 0.1 to 15.3 [h]), and for its value was 0.1105 [kg/s], which corresponds to the 99.45 % of the steam injection.

On the other hand, the condensation rate also allows to explain the trend observed in the pressure versus time plot (see Figure 4.1). Here it is clearly seen that both peaks observed during the pressure evolution (see "peak 1" and "peak 2"), occurred when the condensation rate equals the steam injection rate. To explain this point, it is necessary to understand what the pressure is. The pressure is defined as a normal force exerted by a fluid per unit area [38]. In other words, the pressure can be understood as a measure of the number of molecules in the gas phase and the energy carried by them, usually measured with the temperature. In consequence, from the beginning of the simulation until the minimum of the condensation rate (see "MIN"), the accumulation of gas molecules in the containment was accelerated, observed as an accelerated pressure increment in Figure 4.1, where the accumulation of gas molecules corresponds to the difference between the steam injection rate and the condensation rate. Then, when the condensation rate is equal to the steam injection rate, the accumulation of gas molecules change the trend, going from a positive to a negative value, i.e. the number of gas molecules in the system is decreasing. The maximum condensation rate is observed in the pressure versus time plot as a change of the slope. At this point, hydrogen is injected in the system and the reduction of the condensation rate stops. It is known that hydrogen reduces the condensation rate as it implies an additional resistance in the boundary layer. However, as observed here, this statement is not completely true as the condensation rate continue reducing while the hydrogen enters in the system. A reasonable explanation can be that the stratification of gas components inside the vessel suppress this negative effect of the hydrogen on the condensation rate, i.e. as the hydrogen is not well mixed with the steam, it is not an

additional resistance in the boundary layer. What it is observed, is that the stratification delimits the steam to a specific region of the containment, which it does reduce the heat transfer area, affecting in consequence the condensation rate. After "peak 2" the system reaches its equilibrium as explained in previous paragraph.

In summary, we have the following:

- As the condensation rate goes to its minimum, the pressure goes to its maximum, i.e. during this period occurs the fastest gas accumulation rate;
- When the condensation rate equals the steam injection rate, the pressure reaches its maximum, i.e. the accumulation rate of gas molecules is 0;
- When the condensation rate exceeds the steam injection rate, the pressure decreases, i.e. the number of molecules in the gas phase starts to decrease;
- When the condensation rate converges to the average condensation rate, the pressure follows a quasi linear trend, i.e. the accumulation rate of gas molecules keep constant with time.

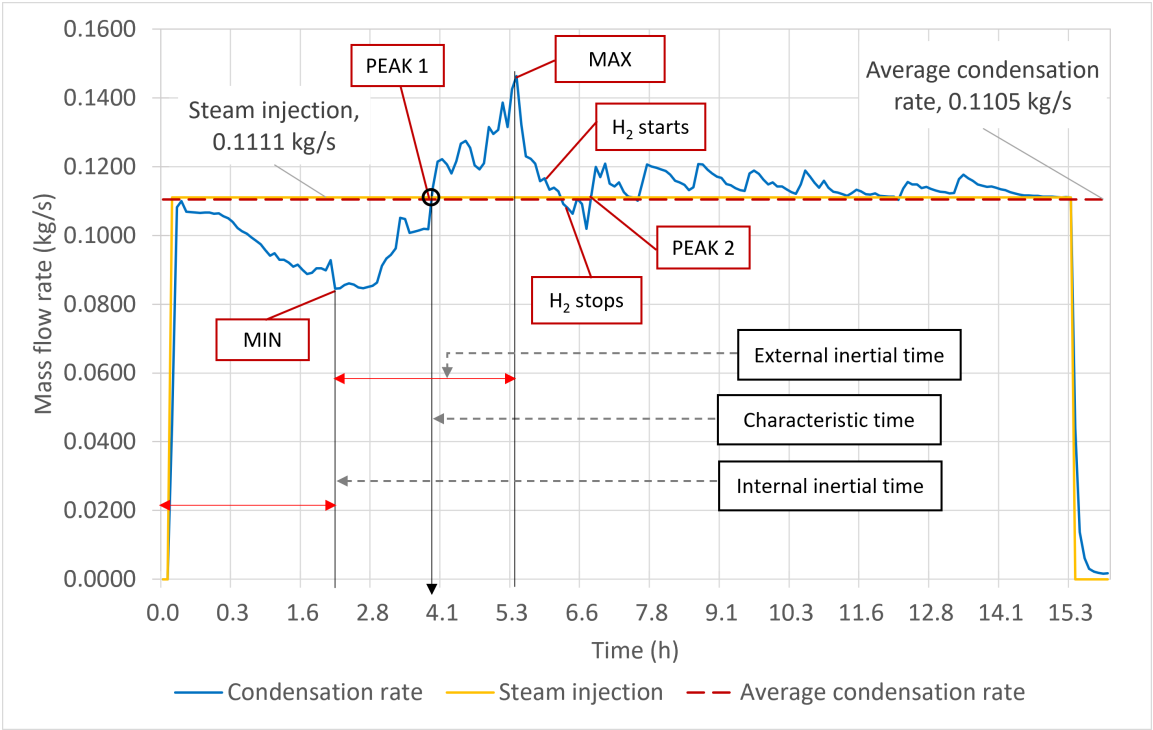

Figure 4.7: Condensation rate evolution inside the containment (base case).

The characteristic time of the system (also, peak time) is defined here as the time at which the condensation rate equals the steam injection rate. This parameter will be important for future discussions.

Figure 4.8 shows the pressure buildup normalized per mole unit of gas inside the containment. The total amount of gas inside the containment corresponds to the sum of air, hydrogen and water vapor at each time. This normalization per mole unit of gas allows to visualize the effects of other variables over the pressure, such as, the temperature and composition. For example, from the graph we have that 1 [kmol] of gas at 0.3 [h] exerts a pressure of 62 [kPa], while 1 [kmol] at 2.8 [h] exerts a pressure of 80 [kPa]. This pressure difference occurs because of the different temperature and composition of the gas at different times. That is to say, a hotter mole unit of gas will exert a higher pressure. A different composition can also affect the pressure, but this topic will be treated in more detail in the next chapter. Previously, it was observed that before the peak time at 3.8 [h] the system increased its temperature (see Figure 4.2), this explains the increment of the normalized pressure build up during this period. However, after the peak time the slope changes and the normalized pressure buildup adopts a slightly constant value of around 83 [kPa/kmol]. Even though the system cools after the peak time, it is not observed a reduction of the the normalized pressure buildup (at least in this scenario). A possible explanation of this behavior is that the cooling effect is covered by the composition effect, and the final result is a constant value. This behavior also tells us that the cooling effect must overcome the underlying composition effect to observe a reduction of the normalized pressure buildup after the peak time (this is observed in some other scenarios).

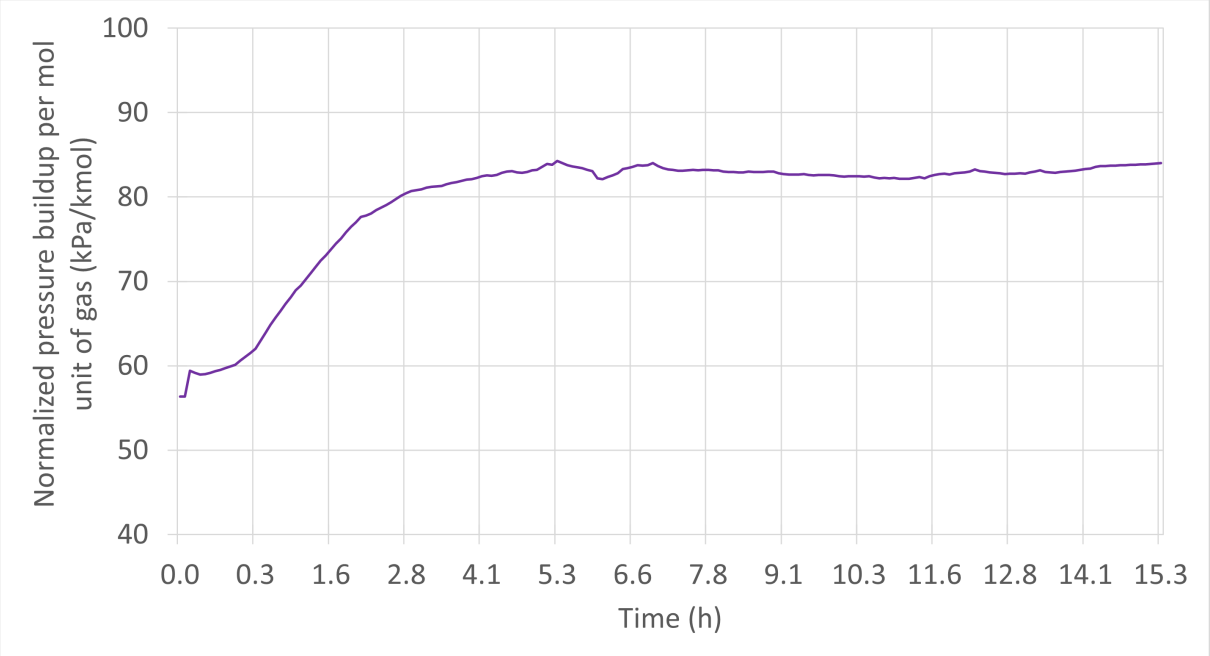

Figure 4.8: Evolution of the pressure buildup normalized to the gas amount inside the containment (base case).

What occurs after the peak time is of primary concern in nuclear safety, because it shows us how the system will evolve in the long-term, meaning days or weeks. In the next section it is seen that the system can evolve with a positive, negative o neutral slope after the peak time. This reflects the cooling capability of the system, i.e. systems with a better cooling capability will show a decreasing slope after the peak time, while systems with an inferior cooling capability will have a positive slope. If the cooling capability of the system is not able to decrease the normalized pressure buildup after the peak time, it means that in the long-term one additional mole unit of gas can exert a higher pressure. That is to say, a system with low number of moles of gas can have a high long-term pressure. As it will be explained, the slope of the curve after the peak is defined by the compressibility factor (see Table 4.7), which depends on the pressure, temperature and composition.

4.3. Parametric study analysis

An analysis of the variance (ANOVA) was performed to determine the statistically significant input variables that explained the variance of the system's responses. The input variables (i.e. steam mass flow rate, water mass flow rate, hydrogen mass flow rate, hydrogen total mass and water temperature) were defined at different levels according to a Half-Factorial design (see Methodology for details). The responses of the system, defined as Figure of Merits (FoM), were the peak pressure, peak temperature, peak hydrogen concentration and average condensation rate. The discussion of each FoM is provided here. In addition, the normalized pressure buildup of each scenario is analyzed.

The peak pressure of each simulation case is provided in Figure 4.9. The peak pressures informed here are the corresponding to "peak 1" of prior section, i.e. the peak reached at the characteristic time. At a first approach, four different levels seem to be common between the different scenarios, i.e. 1815 [kPa], 1425 [kPa], 1015 [kPa] and 780 [kPa]. The base case (Case Id: 0) is a unique case since it does not share any common boundary condition with the other scenarios. The other scenarios share some boundary conditions as defined in Table 3.15. This suggests that the input variables that determine the peak pressure are two, as each variable had two different levels. Table B.1 (see Appendix B) confirms that the two significant parameters are the steam mass flow rate and water mass flow rate with a 95.0% of confidence (i.e. p-values lower than 0.05). This means that the peak pressure is only determined by these two parameters, which reflects the confrontation of two opposite effects, i.e. energy addition and energy dissipation. As explained before, the system reaches the peak pressure when the condensation rate equals the steam injection rate, which in another words is when the energy addition, driven by the steam injection, equals the energy dissipation, driven by the water injection. This can

be seen as an indirect performance of the cooling capability of the system. That is to say, a configuration with a faster cooling capability will produce a lower peak pressure. For example, when the steam injection was high and the water injection was low, i.e. cases Id: 2, 6, 10 and 14, the peak pressure was low. In contrary, when the steam injection was low and the water injection was high, i.e. cases Id: 3, 5, 11 and 15, the peak pressure was high.

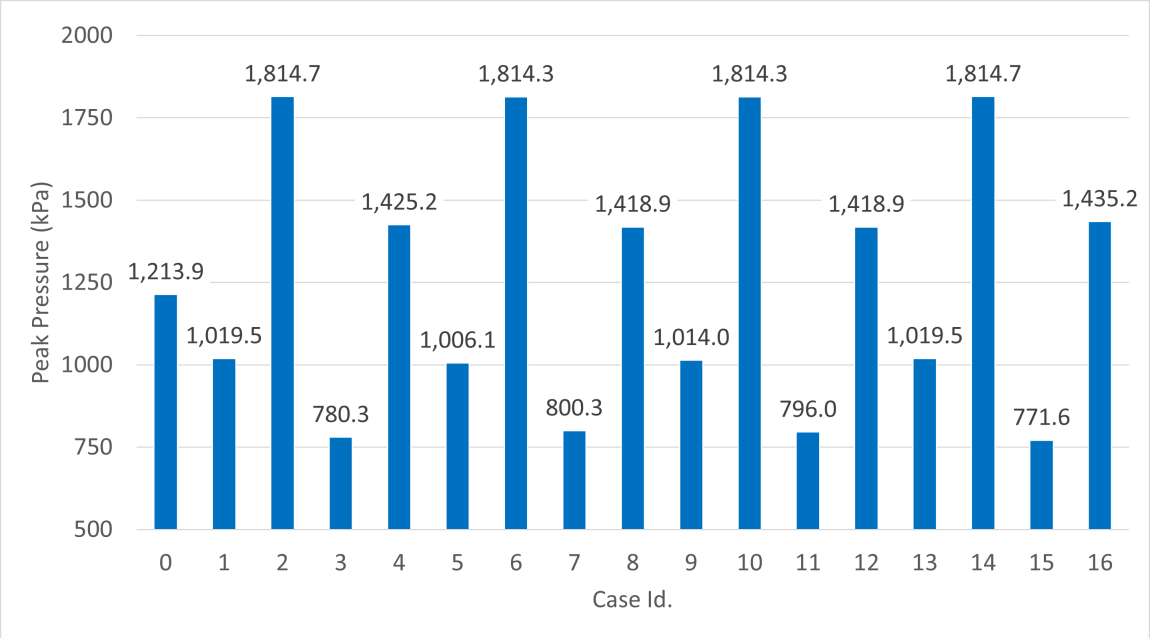

Figure 4.9: Peak pressure for each simulation case.

As expected, the peak temperature corresponds to the saturation temperature of the respective peak pressure in each scenario (see Figure 4.10). This is consequence of the Liquid-Vapor Equilibrium (LVE) of the system, seen as the equilibrium of the steam injection rate and the condensation rate. As before, there are four levels (i.e 207 [°C], 196 [°C], 180 [°C] and 170 [°C]) plus the base case (case Id: 0) present. However, in this case the ANOVA indicates that there are three significant parameters instead of two with a 95.0% of confidence (i.e. p-values lower than 0.05 in Table B.3). The significant parameters that determine the peak pressure are the steam mass flow rate, water mass flow rate and inlet water temperature. The inlet water temperature had a p-value of 0.0495 which in contrast to the 0.0009 of the steam injection or 0.0022 of the water injection is much higher. This means that the influence of the water temperature is lower than the other two parameters, but statistically still play a role and it can affect the overall system evolution. As the peak pressure and peak temperature are coupled due to the LVE condition, and the overall system performance is determined by the opposition effects of

energy addition and energy dissipation, the improvement of the energy dissipation effect through the reduction of the cooling water will affect implicitly the peak pressure, even though this is not directly measured.

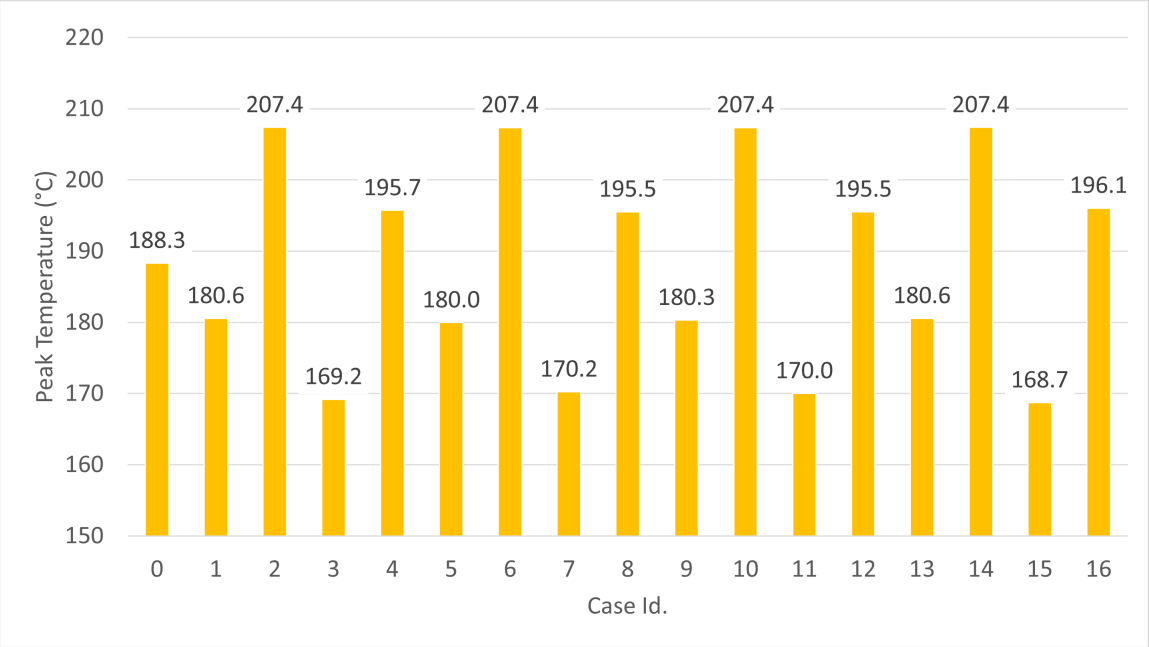

Figure 4.10: Peak temperature for each simulation case.

To study the peak hydrogen concentration it is proposed a normalization with respect to the Hydrogen-to-Steam (H/S) mass flow rate injection. Both results, the normalized and the absolute value are given in Table 4.5. On one side, the absolute value in volumetric concentration [v/v] allows us to understand if the system is in a detonation region as seen in the Shapiro diagram (see Figure 1.3), and on the other side, the normalized value in [v/v:m/m] provides us a base for the comparison between different scenarios. The peak volumetric concentrations of hydrogen were in the range of 73.09-97.77 %v/v meaning that an explosive atmosphere is present in all scenarios. Therefore, to have tools to predict the development of explosive mixtures is critical in nuclear safety. In that context, it is proposed a correlation with the normalized values to determine the peak hydrogen concentration with the initial hydrogen and steam injection. This analysis will be seen later on, after the ANOVA discussion.

Table 4.5: Peak hydrogen concentration and normalized concentration to the inlet Hydrogen-to-Steam mass ratio.

Case Id. -	**Injection H/S mass ratio** m/m	**Injection H/S rel. vel.** m/s	**Peak H_2 Conc.** %v/v	**Norm. Peak H_2 Conc.** v/v:m/m
0	0.0203	-0.7	83.48%	41.22
1	0.0180	-1.7	83.69%	46.49
2	0.0108	-8.9	73.09%	67.67
3	0.0180	-1.7	97.97%	54.43
4	0.0108	-8.9	95.08%	88.03
5	0.0360	7.4	86.46%	24.02
6	0.0216	0.2	76.64%	35.48
7	0.0360	7.4	78.35%	21.76
8	0.0216	0.2	74.77%	34.62
9	0.0180	-1.7	91.70%	50.94
10	0.0108	-8.9	82.29%	76.19
11	0.0180	-1.7	98.62%	54.79
12	0.0108	-8.9	76.79%	71.10
13	0.0360	7.4	97.35%	27.04
14	0.0216	0.2	87.08%	40.31
15	0.0360	7.4	98.77%	27.44
16	0.0216	0.2	79.96%	37.02

Figure 4.11 shows the peak hydrogen concentration in volumetric units and in the proposed normalization units (v/v:m/mm). In contrast to what it was observed for the peak pressure and peak temperature, the peak hydrogen concentration doesn't show a special trend, and neither the normalized peak concentrations. This suggests that the peak hydrogen concentration might involve other parameters in its determination. Table B.5 (see Appendix B) indicates that neither of the input variables is statistically significant in the peak hydrogen concentration. This might be because the input variables do not completely catch the phenomena involved in the determination of this FoM. According to the analysis of the prior section, the peak hydrogen concentration was located in the top of the containment and the accumulation of hydrogen in this section was caused by the buoyancy effects and the condensation of steam. The level of turbulence inside the containment may also affect the speed of the stratification and the peak concentration, however, its level is not captured by the boundary conditions. In consequence, it might

be necessary to perform a different ANOVA for this FoM, for example, a parametric study with the condensation rate as a controlled variable. Finally, it is observed that the volumetric concentrations are not correlated with the normalized concentrations, and it was found that the normalized peak concentration follows a tendency when plotted against the H/S ratio (see Figure 4.12).

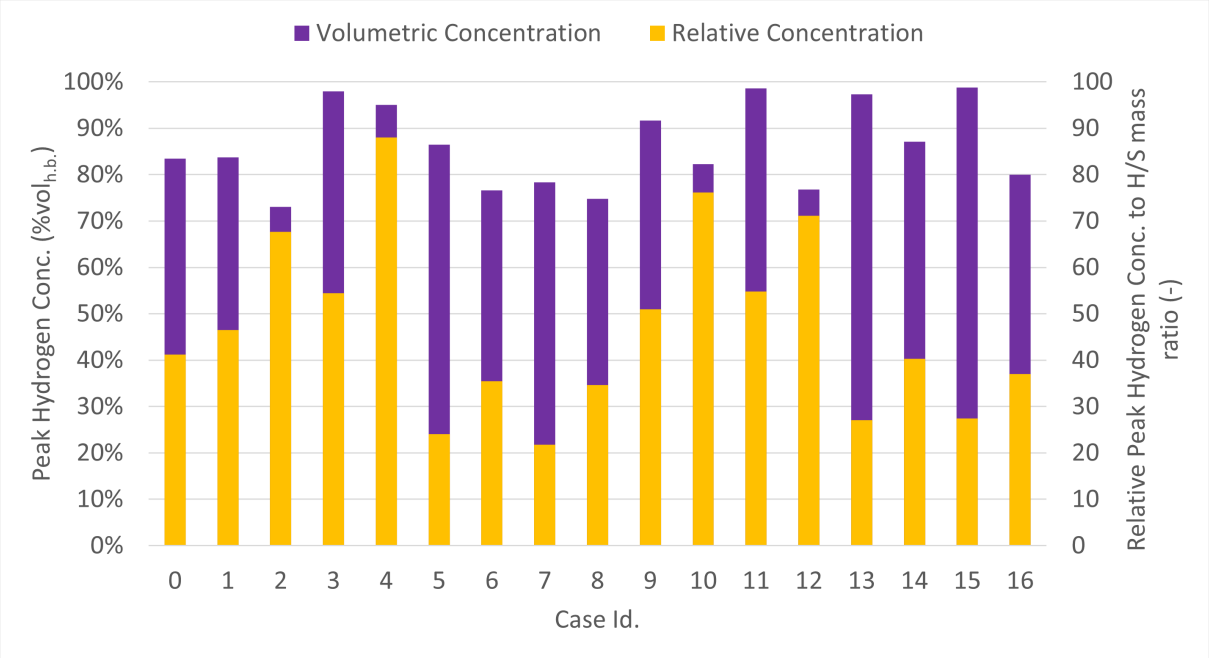

Figure 4.11: Peak hydrogen concentration for each case. (volumetric percentage in humid base)

The normalized peak hydrogen concentration shows a trend when is plotted against the H/S ratio (see Figure 4.12). From Table 4.5 we have that there are four different H/S ratio levels, i.e. 0.0108, 0.0180, 0.0216 and 0.0360, plus the base case level with 0.0230. These five levels are seen in the plot. Also, it is seen that at a same level the normalized peak concentration can be different. For example, when the H/S ratio is 0.0108 the normalized peak concentration can take the values 67.67, 71.10, 76.19 or 88.03. This means that along with the H/S ratio there is another parameter that will ultimately define the peak concentration, e.g. condensation rate or the characteristic time. Unfortunately, it was not possible to decipher in this study which other parameter might determine the normalized peak hydrogen concentration. However, the relation with the H/S ratio is established, and the fitted model given in equation (4.1) has a $R^2 = 0.9318$, which indicates that both variables are correlated.

$$y = (2.1354 \cdot 10^{-2} + 2.1281 \cdot x)^{-1.3736} \tag{4.1}$$

Moreover, this trend also shows that at higher values of the H/S ratio, the normalized peak concentration will change at a slower pace for an equivalent H/S variation. This means that one additional mass unit of hydrogen will have a relative different effect in the normalized peak concentration, depending on the range level of the H/S ratio. For example, when the H/S ratio goes from 0.010 to 0.011, the normalized peak concentration goes from 76.24 to 71.30, i.e. a slope equal to 4934 units, and when the H/S ratio goes from 0.030 to 0.031, the normalized peak concentration goes from 29.46 to 26.93, i.e. a slope equal to 2530. In other words, when the injected mass of hydrogen is very low in comparison with the steam, the system tends to create higher normalized peak concentration, probably due to a stronger tendency to stratification. While, when the hydrogen increases with respect to the steam, the normalized peak concentration will tend to a stable value, i.e. the system will be mixed. In the limit case, when there is no steam present in the containment, it is probably that the evolution to a stratified atmosphere between air and hydrogen will be slower.

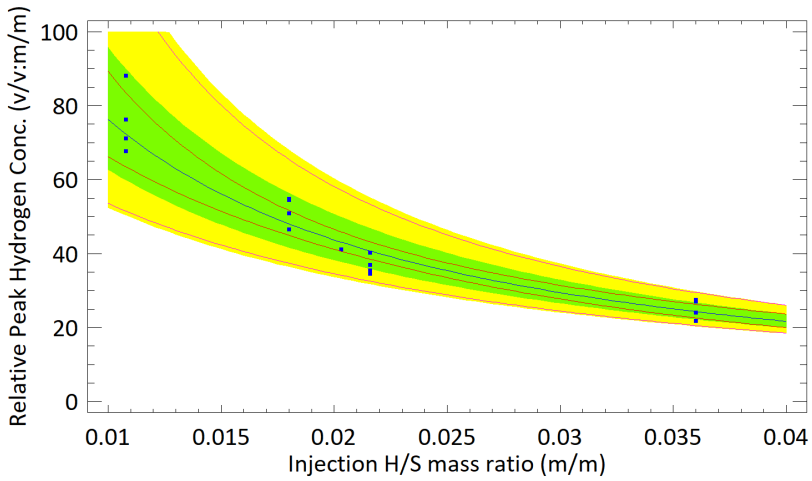

Figure 4.12: Peak hydrogen concentration for each case. (volumetric percentage in humid base)

Figure 4.13 shows the condensation rate curves of each case. It is observed that the curves are grouped mainly in two levels, plus the base case located in between. This suggests that only one input variable determines the condensation rate. Table B.7 confirms that the only significant parameter is the steam mass flow rate with a 95.0 % of confidence. At a first approach, it might sound superficial that the only significant parameter is the steam

injection. However, when understanding that the condensation rate will converge to an average condensation rate in the long term, which is not much different from the steam mass flow rate, it is more clear why this parameter is the only statistically significant. The average condensation rate are informed in Table 4.6, and it is seen that in all simulated cases, this value was over the 99% of the steam mass flow rate. This not only confirms the dependency of the condensation rate with respect to the steam injection rate, but also it confirms the LVE condition.

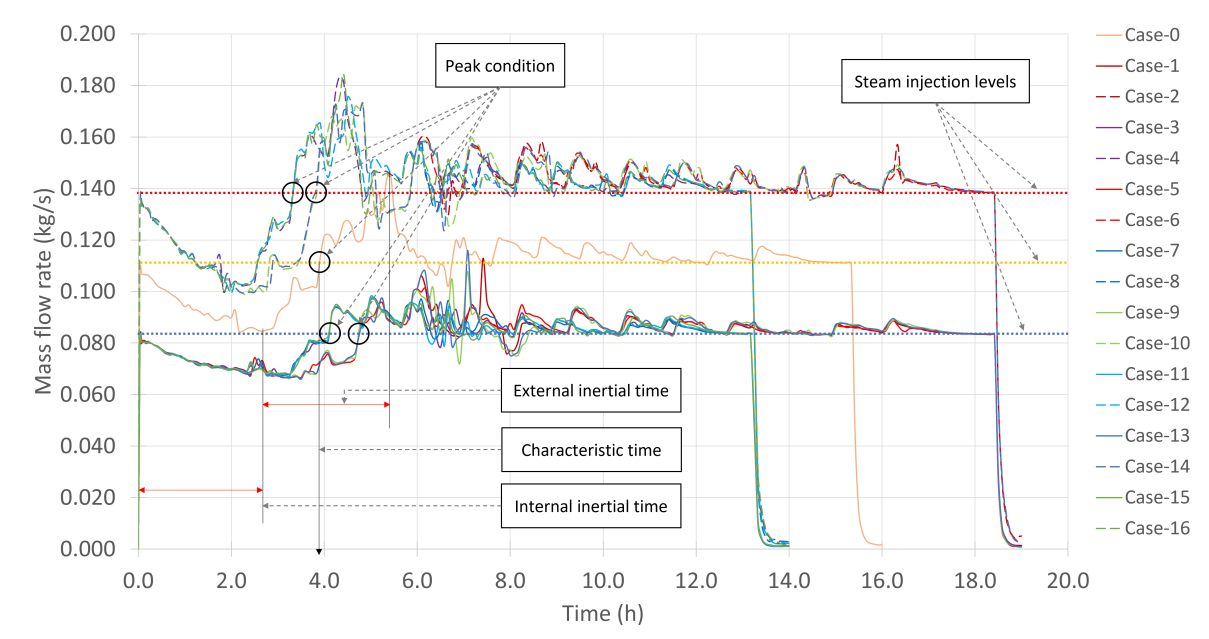

Figure 4.13: Condensation rate evolution of each case.

Now, even though all systems tend to the LVE in the long term, some differences between different scenarios are observed. For example, those cases with a steam injection of 0.0833 [kg/s] (blue point line) show a condensation rate curve less pronounced than the cases with higher steam injection rate, either with, 0.1111 [kg/s] (yellow point line) or 0.1389 [kg/s] (red point line). That is to say, the minimum and maximum of the curves are more restricted when the steam injection rate is lower. Moreover, those cases with a higher steam injection rate reached the peak condition and, consequently, the characteristic time (i.e. when the condensation rate equals the steam mass flow rate) before than those cases with lower steam injection rate. This occurs because as explained in the prior section, the condensation rate is an indirect measure at which the latent heat is dissipated into the environment, being the immediate environment (internal heat sink) the responsible of the formation of a minimum, and the transition to a fully developed natural convection cooling regime the responsible of a maximum. Therefore, when the steam injection rises

the internal heat sink is heated faster causing that the minimum is reached before, i.e the internal inertial time is shortened.

Table 4.6: Average condensation mass flow rate of each case and its percentage with respect to the steam injection.

Case Id. -	**Average Condensation Rate** (kg/s)	**Percentage with respect to the steam injection mass flow rate** %
0	0.1105	99.4552%
1	0.0829	99.5047%
2	0.1381	99.4252%
3	0.0827	99.2555%
4	0.1378	99.2414%
5	0.0830	99.5866%
6	0.1379	99.3016%
7	0.0828	99.4137%
8	0.1380	99.3875%
9	0.0829	99.4671%
10	0.1378	99.1844%
11	0.0827	99.2431%
12	0.1380	99.3395%
13	0.0829	99.4512%
14	0.1380	99.3721%
15	0.0827	99.2957%
16	0.1378	99.2355%

Figure 4.14 shows the previously defined normalized pressure buildup for all cases. It is observed that after the peak time (which occurred between 3.3 - 4.8 [h] depending on the case), the normalized pressure buildup has a positive, negative or neutral slope. That means that one additional unit of gas may exert a higher, comparable or lower pressure than the prior units of gas already present in the system. As previously indicated, the possible parameters that may have an influence on the pressure are the temperature and the composition. However, after the peak time the temperature of the system reduces, and consequently, the slope should be negative. This means that is the effect of the composition which ultimately determines the sign of this slope.

In order to understand these effects, it was developed an expression of the normalized pressure buildup by using the compressibility factor definition. The compressibility factor

(see equation 4.2 [33]) is usually seen as an indicator of the deviation from the ideal gas behaviour. However, in a more profound perspective it is an indicator of the forces acting between different molecules in a mixture. That is to say, different molecules can have intermolecular forces that makes them to separate or to get closer, affecting other properties, such as, the density of the mixture.

$$Z \equiv \frac{PV}{nRT} \tag{4.2}$$

An average compressibility factor of the gas phase was calculated and plot for all the simulated cases. It was also plotted the pressure evolution to compare both trends. These plots are found in Appendix C. From the plots, it can be observed that a couple of cases when the peak pressure was reached, the compressibility factor reached a minimum and changed its tendency. This occurred always when the peak pressure was over 1124.8 [kPa], which can be considered as a break point. In the other cases, the compressibility factor continue decreasing for a while.

By reordering equation (4.2), and deriving with respect to time, we obtain an expression of the normalized pressure rate as a function of the temperature-, volume-, and Z-rate. We know that R, Z, V and T are always positive values, and that dV_{gas}/dt is negative (i.e. the gas space inside the containment reduces with time due to the condensation accumulation. See equation (4.16)).

$$\frac{P}{n} = \frac{ZRT}{V}, \tag{4.3}$$

$$\frac{d(P/n)}{dt} = R\frac{d(ZT/V)}{dt}, \tag{4.4}$$

$$\frac{1}{R}\frac{dP_u}{dt} = Z\frac{d(T/V)}{dt} + (T/V)\frac{dZ}{dt}, \tag{4.5}$$

$$\frac{1}{R}\frac{dP_u}{dt} = \frac{Z}{V}\frac{dT}{dt} - \frac{ZT}{V^2}\frac{dV}{dt} + \frac{T}{V}\frac{dZ}{dt}, \tag{4.6}$$

$$\tag{4.7}$$

In consequence, by performing a sign analysis of each term, it can be inferred that the term that determines the slope of the normalized pressure buildup after the peak time is the compressibility factor, i.e. $dP_u/dt > 0$ when $dZ/dt > 0$, and $dP_u/dt < 0$ when $dZ/dt < 0$.

Table 4.7: Direction of the terms affecting the normalized pressure buildup rate at different moments.

Period	dP_u/dt	$\frac{Z}{V}\frac{dT}{dt}$	$-\frac{ZT}{V^2}\frac{dV}{dt}$	$\frac{T}{V}\frac{dZ}{dt}$
Before Peak	+	+	+	-
After Peak ($P_{peak} < 1124.8$ [kPa])	-	-	+	-
After Peak ($P_{peak} > 1124.8$ [kPa])	+	-	+	+

The compressibility factor can be predicted for real gas mixtures using advanced equations-of-state, such as Peng Robinson or Soave-Redlich-Kwong [33]. The compressibility factor is a function of temperature, pressure and composition, and therefore it is coupled with the system conditions. Although it is out of the scope of this thesis, it is also foreseen the possibility of determining a range of initial conditions that might lead to a long term safe condition, i.e. a negative slope of the normalized pressure buildup after the peak. For example, by coupling the compressibility factor with the mass and energy balance of the system.

Continuing with the analysis of Figure 4.14, it is also possible to associate the post-peak slope with the cooling capability of the system. That is to say, those cases characterized by a fast heat dissipation present a negative slope, while those with a slow heat dissipation present a positive slope. In consequence, there should exist a break point of the cooling capability that determines if the system will evolve with a positive slope or a negative one.

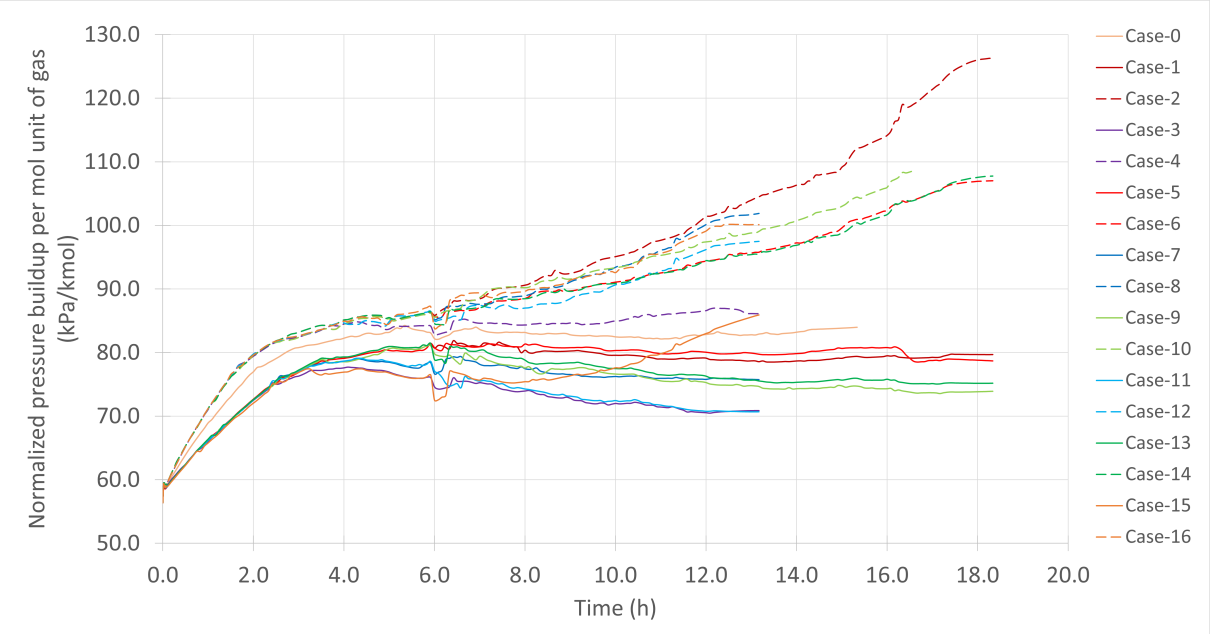

Figure 4.14: Normalized pressure buildup comparison

Table 4.8 reports the slopes after the peak. These slopes were obtained by a linear regression with the data from the peak condition until the 12 hours (see Appendix C). The unit of the slope is [kPa/kmol-s], which corresponds to the rate of the normalized pressure buildup after the peak.

These values[6] were plotted against the volumetric energy of the gas phase at the peak condition (see Figure 4.15). The volumetric energy of the gas phase (Q_v^*) is defined here as the internal energy of the gas divided by the volume of gas (see equation (4.8)). Its units are $\frac{kJ}{m^3}$. The break point (i.e. when the normalized pressure buildup rate is equal to 0) was calculated and it corresponds to a volumetric energy of 13720 [kJ/m^3] (the break point in pressure units is 1124.8 [kPa]). This means that if our system has a volumetric energy over 13720 [kJ/m^3], a positive slope of the normalized pressure buildup after the peak can be expected.

$$Q_{v,g}(t) = \frac{U_{gas}(t)}{V_{gas}(t)} \tag{4.8}$$

[6]Only those normalized pressure buildup rates with a R^2 over 0.5 were considered

Table 4.8: Normalized post-peak pressure buildup rates for each case.

Case Id. -	**Norm. Pressure Buildup Rate** (kPa/kmol-s)	**R^2 of linear regression** -
0	-2.573E-05	0.193
1	-9.246E-05	0.763
2	5.500E-04	0.971
3	-2.514E-04	0.965
4	6.928E-05	0.586
5	-2.308E-05	0.154
6	3.355E-04	0.979
7	-1.187E-04	0.802
8	4.862E-04	0.949
9	-2.133E-04	0.925
10	4.552E-04	0.981
11	-3.075E-04	0.951
12	3.467E-04	0.899
13	-1.944E-04	0.906
14	3.198E-04	0.952
15	1.677E-04	0.429
16	4.540E-04	0.944

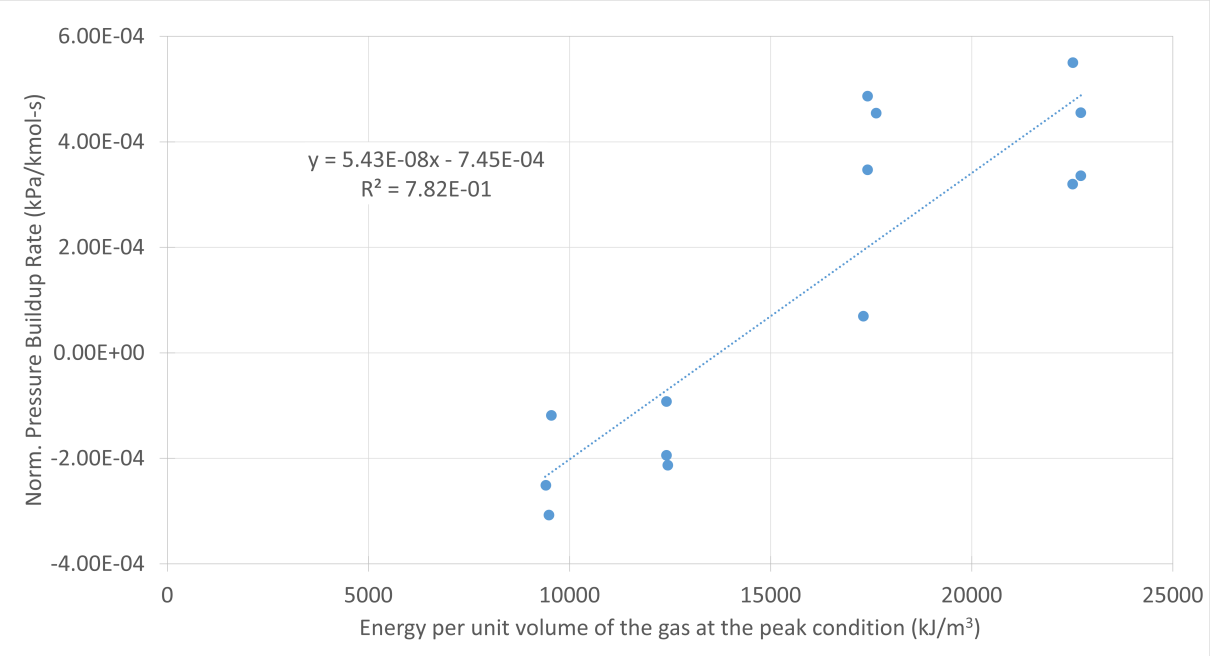

Figure 4.15: Normalized post-peak pressure buildup versus volumetric energy of the gas phase at the peak condition.

Here, it is developed an equation to estimate the volumetric energy of the gas phase at the peak condition. Starting with an energy balance of the gas phase inside the containment (the control volume is the gas phase itself, not the containment). We have,

$$\frac{dE_{gas}(t)}{dt} = \dot{Q}_{g,in}(t) - \dot{Q}_{g,out}(t) \tag{4.9}$$

As the energy of the gas is actually the internal energy (given that other types of energy can be neglected), and replacing the definition of the volumetric energy, we have the following,

$$\frac{dE_{gas}(t)}{dt} = \frac{dU_{gas}(t)}{dt} = \frac{d(Q_{v,g}(t) \cdot V_{gas}(t))}{dt} \tag{4.10}$$

The inlet energy corresponds to the enthalpy of the steam injection, and assuming that our system is in a Liquid-Vapor equilibrium the outlet energy should be equal to the condensation rate times the heat of vaporization. In consequence, our energy balance can be written as follows,

$$\frac{d(Q_{v,g}(t) \cdot V_{gas}(t))}{dt} = \dot{m}_{steam} \cdot h_{steam,in} - \dot{m}_{cond} \cdot \Delta h_{vap} \tag{4.11}$$

Now, by taking into consideration that the average condensation rate is almost equal to the steam mass flow rate (see Table 4.6), and that the instant condensation rate is equal to the steam injection at the characteristic time (t^*: peak or characteristic time). It is possible to obtain an approximated solution of the equation as follows,

$$\frac{d(Q_{v,g}(t) \cdot V_{gas}(t))}{dt} = \dot{m}_{steam} \cdot h_{steam,in} - \dot{m}_{steam} \cdot \Delta h_{vap} \tag{4.12}$$

$$\int_0^* d(Q_{v,g} \cdot V_{gas}) = \int_0^* \dot{m}_{steam} \cdot (h_{steam,in} - \Delta h_{vap}) dt \tag{4.13}$$

$$(Q_{v,g} \cdot V_{gas})^* - (Q_{v,g} \cdot V_{gas})_0 = \dot{m}_{steam} \cdot (h_{steam,0} - \Delta h_{vap,0}) \cdot (t^* - t_0) \tag{4.14}$$

$$\tag{4.15}$$

From the initial conditions of the system, we can determine that $(Q_{v,g} \cdot V_{gas})_0 = 10899.4$ [kJ] (containment initially filled with air at 20 [°C]). And, knowing that the gas volume decreases with the condensate rate as,

$$\frac{dV_{gas}(t)}{dt} = \frac{-\dot{m}_{cond}(t)}{\rho_{cond}(t)} \tag{4.16}$$

We have that,

$$V^*_{gas} \approx V_0 - \frac{\dot{m}_{steam}}{\rho_{cond}} \cdot t^* \tag{4.17}$$

Finally, the expression to estimate the volumetric energy of the gas phase at the peak condition is,

$$Q^*_{v,g} = \frac{\dot{m}_{steam} \cdot (h_{steam,0} - \Delta h_{vap,0}) \cdot t^* + Q_{v,0} \cdot V_0}{V_0 - \frac{\dot{m}_{steam}}{\rho_{cond}} \cdot t^*} \tag{4.18}$$

Where the steam can be estimated during a real accident condition.

Figure 4.16 shows a plot of the observed values versus the predicted ones to assess the model. The deviation of the slope from the 45° line shows that the model is not accurate in all the range of values. That is to say, it overestimates the volumetric energy when is below 17000 [kJ/m^3] and it underestimates it over this value. One possible source of this error can be the exclusion of the sensible heat exchange in the model, or, even, the consideration of constant thermodynamic data. Nevertheless, the predicted values are in the range of the observed ones which anticipates a good behavior. One big open question

is about the calculation of the characteristic time, which must still be calculated through simulations.

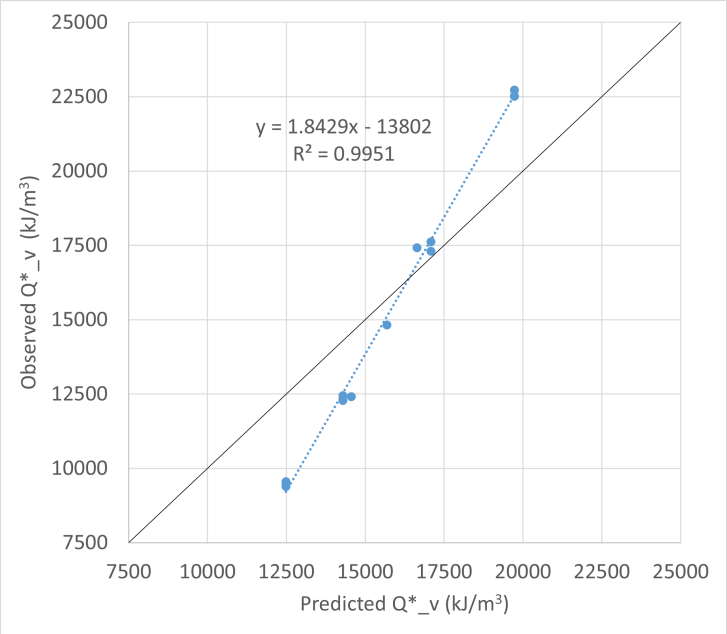

Figure 4.16: Observed vs predicted plot for the proposed model of the volumetric energy at the peak condition of the gas phase

5 | Recommendations

With respect to the experiments that will be carried out at Becker Technologies GmbH. A couple of recommendations can be provided:

- Preheat the helium injection (as hydrogen replacement) to avoid additional stratification caused by the experimental conditions.
- To verify the validity of the normalized pressure buildup by performing experiments over and below the break point, for example, cases 2 and 11.
- To verify the relationship for the normalized hydrogen concentration by performing experiments with very low and very high H/S mass ratio.
- To verify the simulated compound stratification (from top to bottom): hydrogen-rich, steam-rich, and air-rich regions.

6 | Conclusions

The main conclusions from the analysis of the base case scenario and the parametric study are:

1. The pressure evolution is governed by the transient balance between steam injection and condensation. Pressure increases when mass and energy addition due to steam inflow dominate over removal mechanisms, and it decreases once condensation and cooling become dominant. Therefore, the pressure peak represents the point at which the system transitions from injection-dominated to condensation-dominated behavior.

2. The temperature distribution inside the containment is governed by buoyancy effects, and the turbulent and diffusive mixing among steam, air, and hydrogen. The presence of multiple gas species alters the expected thermal stratification, i.e. hottest point at the top to the coldest at the bottom, since density differences depend not only on temperature but also on composition. The highest temperature is observed in the upper-middle region of the vessel, corresponding to a steam-rich zone. This occurs because certain gas mixtures with lower temperatures accumulate at the top of the containment, forming a hydrogen-rich region. Additionally, the temperature of the steam-rich region follows the saturation temperature associated with the peak pressure, indicating that the mixture is in a saturated condition, i.e., in Liquid–Vapor Equilibrium (LVE).

3. The gas composition stratification occurs due to buoyancy effects in response to the density difference between different mixtures. The generation of mixtures along the axial direction responds to turbulent mixing and mass diffusion effects. As a result, a steam-rich zone develops in the middle, a hydrogen-rich zone accumulates at the top, and an air-rich zone remains at the bottom. The interface between the steam-rich and lower air-rich zones can be described as a "condensation front," analogous to a cloud border, which is not sharply defined but fuzzy in composition. This front level rises over time as condensation progresses, reducing the extent of the steam-rich region and allowing hydrogen and air to redistribute.

4. The condensation rate can be described by three different periods that helps to understand its trend. The first period corresponds to the heating of the internal heat sink, composed of the internal air and containment vessel. During this period the condensation rate slows down, due to the consumption of immediate heat sink to release the steam latent heat, and it reaches a minimum value at the defined "internal inertial time". After this, the condensation rate accelerates, due to the expansion of the available heat sink provided by the activation of the external containment cooling, until reaching a maximum value at the defined "external inertial time", which represents the limitations provided by the natural convection cooling process. Between the transition from the minimum to the maximum value, the condensation rate equals the steam injection rate, point that coincides with the peak pressure and peak temperature, at the defined "characteristic or peak time". After the maximum value, the condensation rate slows down and converge to the steam injection rate, indicating that the system is evolving to a quasi Liquid-Vapor Equilibrium (LVE) state.

5. The parametric study confirms several of the previous hypotheses regarding the significant variables influencing the appearance of the peak pressure and peak temperature, namely the steam and water injection rates, as well as the inlet water temperature. However, the most notable finding is that the condensation rate depends almost exclusively on the steam injection rate, while hydrogen has no statistically significant effect. This behavior arises from the stratification of the gas mixture, i.e. in a well-mixed atmosphere, hydrogen could increase resistance in the condensation boundary layer, but in a large-scale containment where stratification occurs, steam- and hydrogen-rich regions separate, eliminating this additional resistance. This was observed with the trend of the condensation rate, which continued evolving to the LVE with the steam injection rate independently of the hydrogen injection. Nevertheless, hydrogen can indirectly influence global condensation by displacing steam to lower regions, which reduces the available condensation area.

6. The normalization of the pressure with respect to the mass of gas present in the containment indicated that to reach a long-term safe condition, defined as a condition where one additional molecule of gas would exert a lower pressure than the former ones, is achieved for values lower than a break point, which is a representative parameter of the cooling capability of the system. The break point was defined as a limiting value of the volumetric energy (of the gas phase) that can sustain a system without running away. The break point for the PCCS-SMR of Becker Technologies, for a natural convection cooled system, is 13.720 $[kJ/m^3]$.

7. The following correlation to estimate the break point was developed. It only depends on the initial conditions of the system, the steam injection rate (which can be estimated during an accident scenario), and the characteristic time.

$$Q^*_{v,g} = \frac{\dot{m}_{steam} \cdot (h_{steam,0} - \Delta h_{vap,0}) \cdot t^* + Q_{v,0} \cdot V_0}{V_0 - \frac{\dot{m}_{steam}}{\rho_{cond}} \cdot t^*} \tag{6.1}$$

Bibliography

[1] Davide Papini, Davor Grgić, Antonio Cammi, and Marco Ricotti. Analysis of different containment models for iris small break loca, using gothic and relap5 codes. *Nuclear Engineering and Design*, 241(4):1152–1164, 2011.

[2] Nuclear Energy Agency. *Relevant thermal hydraulic aspects of advanced reactors design: status report*. OECD Publishing, Paris, 1996.

[3] International Atomic Energy Agency. *Safety related terms for advanced nuclear plants*. Technical Document No. 626. IAEA, Vienna, 1991.

[4] International Atomic Energy Agency. *Small Modular Reactors - Catalogue 2024*. A Supplement to: IAEA Advanced Reactors Information System (ARIS). IAEA, Vienna, 2024.

[5] US Nuclear Regulatory Commission. 0968 - r107p - ap1000 introduction to differences: 05.2 - pcs text (passive containment cooling system), 2011. URL `https://www.nrc.gov/docs/ml1122/ML11221A115.pdf`.

[6] Kent Welter, José Reyes Jr, and Adam Brigantic. Unique safety features and licensing requirements of the nuscale small modular reactor. *Frontiers Energy Research*, 11: 1160150, 2023.

[7] International Atomic Energy Agency. *Status of advanced light water cooled reactor designs*. Technical Document No. 968. IAEA, Vienna, 1996.

[8] International Atomic Energy Agency. *Natural circulation data and methods for advanced water cooled nuclear power plant designs*. Technical Document No. 1281. IAEA, Vienna, 2000.

[9] Nuclear Energy Agency. *The Fukushima Daiichi Nuclear Power Plant Accident: OECD/NEA Nuclear Safety Response and Lessons Learnt*. OECD Publishing, Paris, 2013.

[10] Tokyo Electric Power Company, Inc. *Fukushima Nuclear Accident Analysis Report*. TEPCO, Tokyo, 2012.

[11] International Atomic Energy Agency. *Safety of Nuclear Power Plants: Design.* Specific Safety Requirements No. 2 (rev.1). IAEA, Vienna, 2016.

[12] Hassan Nawaz Butt, Muhammad Ilyas, Masroor Ahmad, and Fatih Aydogan. Assessment of passive safety system of a small modular reactor (smr). *Annals of Nuclear Energy*, 98:191–199, 2016.

[13] International Atomic Energy Agency. *Fundamental Safety Principles.* Safety Fundamentals No.1. IAEA, Vienna, 2006.

[14] International Atomic Energy Agency. *Implementation of Accident Management Programmes in Nuclear Power Plants.* Safety Reports Series no. 32. IAEA, Vienna, 2004.

[15] Dan Gabriel Cacuci. *Handbook of Nuclear Engineering*, chapter 15. Springer, New York, 2010.

[16] International Atomic Energy Agency. *Deterministic safety analysis for nuclear power plants.* Specific Safety Guide No. 2 (rev.1). IAEA, Vienna, 2019.

[17] International Atomic Energy Agency. *Advances in Small Modular Reactor Technology Developments.* A Supplement to: IAEA Advanced Reactors Information System (ARIS). IAEA, Vienna, 2022.

[18] Palash K. Bhowmik, Scott J. Ormiston, Joshua P. Schlegel, and Debasish Chowdhury. State-of-the-art and review of condensation heat transfer for small modular reactor passive safety: Computational studies. *Nuclear Engineering and Design*, 410:112366, 2023.

[19] Palash K. Bhowmik, Joshua P. Schlegel, and Shripad Revankar. State-of-the-art and review of condensation heat transfer for small modular reactor passive safety: Experimental studies. *International Journal of Heat and Mass Transfer*, 192:122936, 2022.

[20] International Atomic Energy Agency. *IAEA nuclear safety and security glossary.* Non-serial Publications. IAEA, Vienna, 2022.

[21] International Atomic Energy Agency. *Approaches and tools for severe accident analysis for nuclear power plants.* Safety Reports Series No.56. IAEA, Vienna, 2008.

[22] International Atomic Energy Agency. *Hydrogen Phenomena During Severe Accidents in Water Cooled Reactors.* Training Course Series No. 72. IAEA, Vienna, 2021.

[23] Nuclear Energy Agency. *Best Practice Guidelines for the Use of CFD in Nuclear Reactor Safety Applications – 2024 Update*. OECD Publishing, Paris, 2025.

[24] B. Boyack, R. Duffey, G. Wilson, P. Griffith, G. Lellouche, S. Levy, U. Rohatgi, W. Wulff, N. Zuber, and U.S. Nuclear Regulatory Commission. *Quantifying reactor safety margins: Application of code scaling, applicability, and uncertainty evaluation methodology to a large-break, loss-of-coolant accident.* NUREG/CR-5249 EGG-2552 R4. US NRC, Washington DC, 1989.

[25] Yili Yang, Yuxin Wang, Yusheng Liu, and Shengfei Wang. Phenomena identification ranking table (pirt) study for suppression containment of small modular reactor using new methodology. *International Journal of Advanced Nuclear Reactor Design and Technology*, 5(2):104–113, 2023.

[26] F. Morin, P. Olita, S. Lorenzi, S. Marciano, M.E. Ricotti, C. Lombardo, A. Wielenberg, F. Weyermann, and C. Herrer. Elaboration of simplified pirt transients for smr pwr. Technical report, CEA, CIRTEN, ENEA, GRS and IRSN, 2020.

[27] Nuclear Energy Agency. *State-of-the-Art Report (SOAR) on Containment Thermal-hydraulics and Hydrogen Distribution*. OECD Publishing, Paris, 1999.

[28] S. Schwarz, K. Fischer, A. Bentaib, J. Burkhardt, J. Lee, J. Duspiva, D. Visser, J. Kyttälä, P. Royl, J. Kim, P. Kostka, and R. Liang. Benchmark on hydrogen distribution in a containment based on the oecd-nea thai hm-2 experiment. *Nuclear Technology*, 175(3):594–603, 2011.

[29] *GOTHIC Containment Analysis Package - User Book (NAI 8907-02)*. Numerical Applications, Inc., Palo Alto, CA, version 7.2b(qa) edition, March 2009.

[30] *GOTHIC Containment Analysis Package - Qualification Report (NAI 8907-09)*. Numerical Applications, Inc., Palo Alto, CA, version 7.2b(qa) edition, March 2009.

[31] *GOTHIC Containment Analysis Package - Technical Book (NAI 8907-06)*. Numerical Applications, Inc., Palo Alto, CA, version 7.2b(qa) edition, March 2009.

[32] Adrian Bejan. *Convection Heat Transfer*, chapter 4. John Wiley & Sons, New Jersey, 4th edition, 2013.

[33] Don W. Green and Marylee Z. Southard. *Perry's Chemical Engineers' Handbook*. McGraw-Hill Education, New York, 8th edition, 2008.

[34] Center for Chemical Process Safety. *Guidelines for Vapor Cloud Explosion, Pressure*

Vessel Burst, BLEVE, and Flash Fire Hazards, chapter Appendix A. John Wiley & Sons, New Jersey, 2nd edition, 2010.

[35] James E. Roughton and Nathan Crutchfield. *Job Hazard Analysis - A Guide for Voluntary Compliance and Beyond*. Elsevier, USA, 2008.

[36] US National Institute of Standards and Technology. Data collection for process modeling, 2025. URL `https://www.itl.nist.gov/div898/handbook/pmd/section3/pmd31.htm`.

[37] L.A. Román-Ramírez and J. Marco. Design of experiments applied to lithium-ion batteries: A literature review. *Applied Energy*, 320:119305, 2022.

[38] Mehmet Kanoglu Yunus Cengel, Michael Boles. *Thermodynamics*, chapter 1. MC Graw Hill, New York, 2019.

A | Appendix A: Containment's composition evolution of the base case

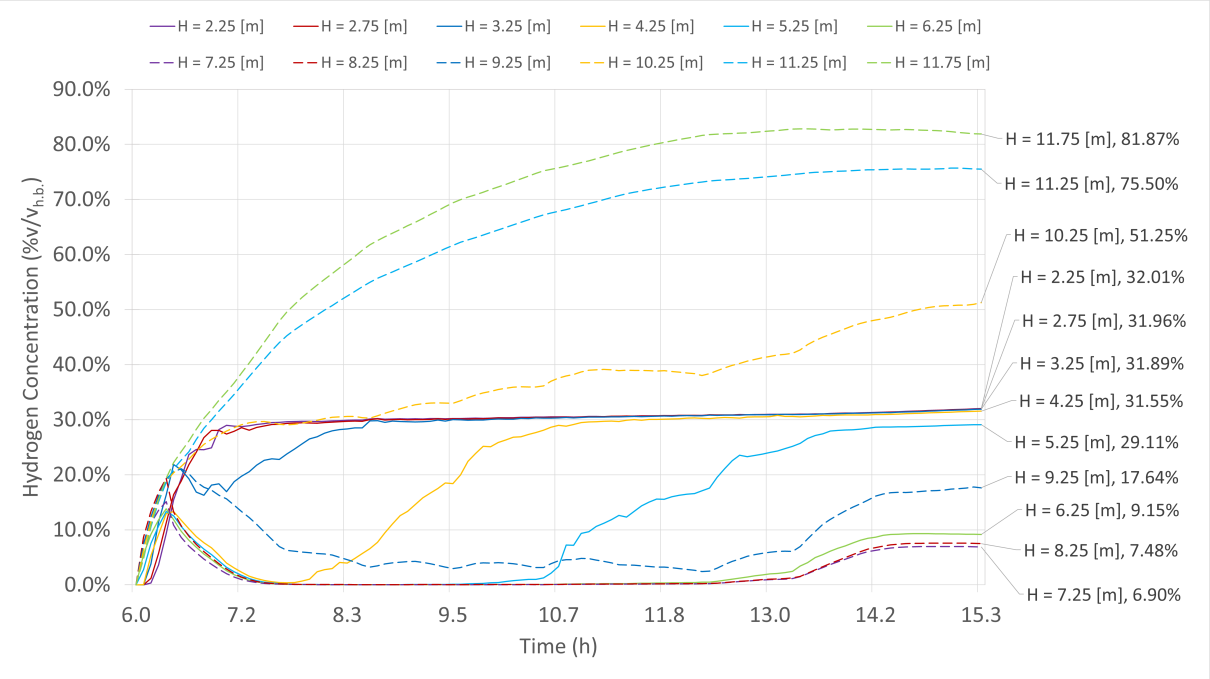

Figure A.1: Hydrogen concentration evolution at different heights inside the containment (base case).

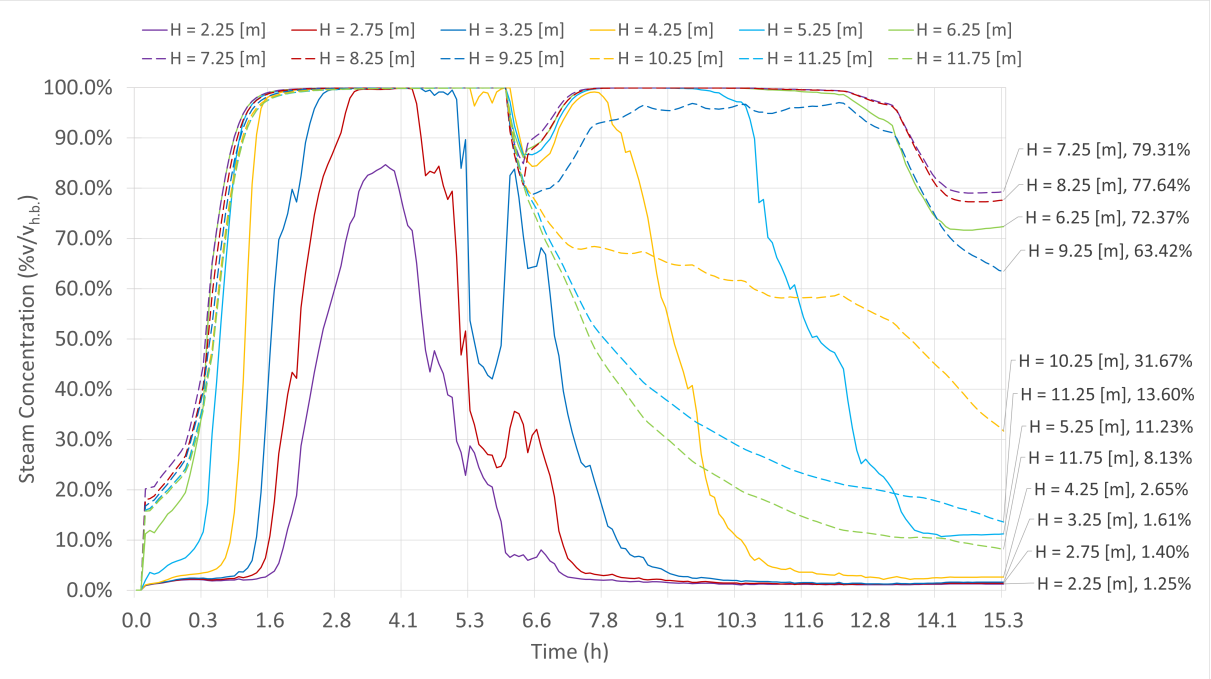

Figure A.2: Steam concentration evolution at different heights inside the containment (base case).

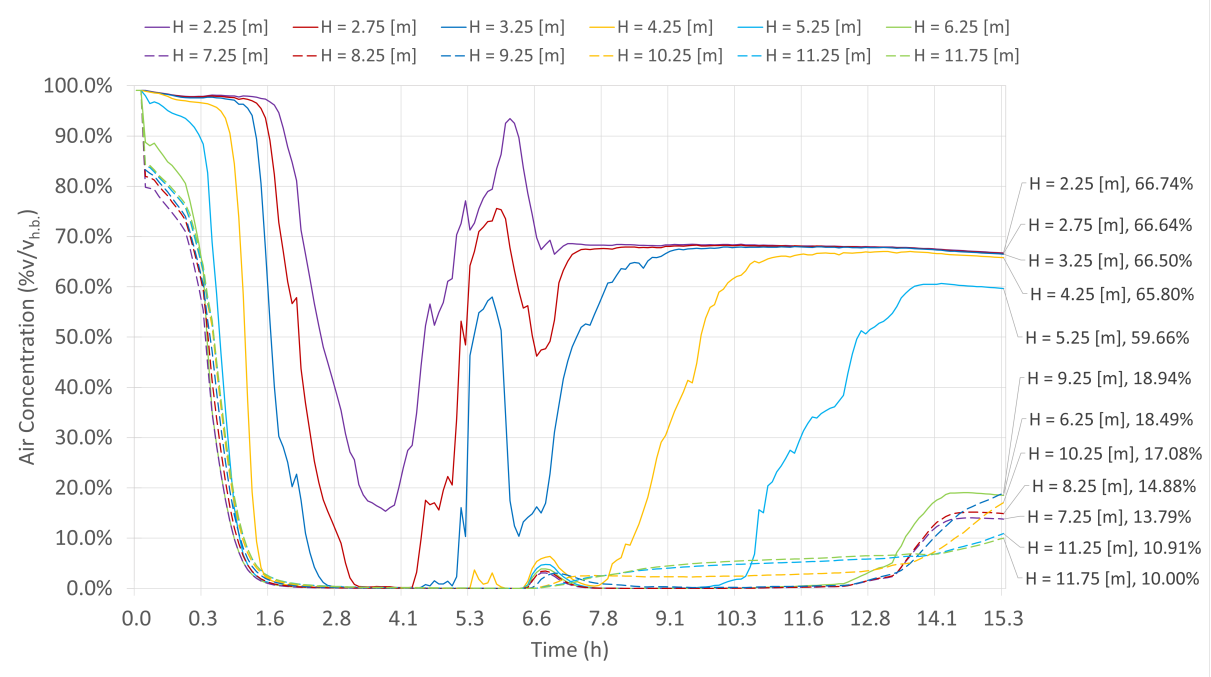

Figure A.3: Air concentration evolution at different heights inside the containment (base case).

B | Appendix B: ANOVA of the System's FoM

The ANOVA table partitions the variability of each Figure of Merit (peak pressure, peak temperature, peak hydrogen concentration and average condensation rate) into separate pieces for each of the effects (boundary conditions). It then tests the statistical significance of each effect by comparing the mean square against an estimate of the experimental error. When the P-values are less than 0.05 is an indication that they are significantly different from zero at the 95.0% confidence level.

The second table shows each of the estimated effects and interactions. The largest variance inflation factor (V.I.F.) equals 1.0. For a perfectly orthogonal design, all of the factors would equal 1. Factors of 10 or larger are usually interpreted as indicating serious confounding amongst the effects.

Table B.1: Analysis of variance for peak pressure

Source	Sum of Squares	Df	Mean Square	F-Ratio	P-Value
A:Steam mass flowrate	2.07E+06	1	2.07E+06	1021.45	0.0199
B:Water mass flowrate	381559	1	381559	188.68	0.0463
C:Hydrogen mass flowrate	0.36	1	0.36	0	0.9915
D:Hydrogen total mass	1.6384	1	1.6384	0	0.9819
E:Water temperature	452.413	1	452.413	0.22	0.7187
AB	26308.8	1	26308.8	13.01	0.1722
AC	31.5282	1	31.5282	0.02	0.9209
AD	13.9502	1	13.9502	0.01	0.9472
AE	108.472	1	108.472	0.05	0.8551
BC	11.56	1	11.56	0.01	0.952
BD	7.3984	1	7.3984	0	0.9615
BE	150.553	1	150.553	0.07	0.8304
CD	0.245025	1	0.245025	0	0.993
CE	59.8302	1	59.8302	0.03	0.8916
DE	2.60822	1	2.60822	0	0.9771
Total error	2022.28	1	2022.28		
Total (corr.)	2.48E+06	16			

Table B.2: Estimated effects for peak pressure

Effect	Estimate	Stnd. Error	V.I.F.
average	1257.49	10.9068	
A:Steam mass flowrate	718.62	22.4849	1
B:Water mass flowrate	-308.852	22.4849	1
C:Hydrogen mass flowrate	-0.3	22.4849	1
D:Hydrogen total mass	0.64	22.4849	1
E:Water temperature	10.635	22.4849	1
AB	-81.1	22.4849	1
AC	2.8075	22.4849	1
AD	1.8675	22.4849	1
AE	-5.2075	22.4849	1
BC	1.7	22.4849	1
BD	-1.36	22.4849	1
BE	6.135	22.4849	1
CD	-0.2475	22.4849	1
CE	3.8675	22.4849	1
DE	0.8075	22.4849	1

Standard errors are based on total error with 1 d.f.

Table B.3: Analysis of variance for peak temperature

Source	Sum of Squares	Df	Mean Square	F-Ratio	P-Value
A:Steam mass flowrate	2829.18	1	2829.18	484716.49	0.0009
B:Water mass flowrate	505.35	1	505.35	86580.57	0.0022
C:Hydrogen mass flowrate	0.004225	1	0.004225	0.72	0.5512
D:Hydrogen total mass	0	1	0	0	1
E:Water temperature	0.9604	1	0.9604	164.54	0.0495
AB	0.748225	1	0.748225	128.19	0.0561
AC	0.0529	1	0.0529	9.06	0.2042
AD	0.027225	1	0.027225	4.66	0.2761
AE	0.390625	1	0.390625	66.92	0.0774
BC	0.0121	1	0.0121	2.07	0.3865
BD	0.030625	1	0.030625	5.25	0.262
BE	0.319225	1	0.319225	54.69	0.0856
CD	0.0361	1	0.0361	6.18	0.2434
CE	0.1156	1	0.1156	19.81	0.1407
DE	0.003025	1	0.003025	0.52	0.6028
Total error	0.00583676	1	0.00583676		
Total (corr.)	3337.23	16			

Table B.4: Estimated effects for peak temperature

Effect	Estimate	Stnd. Error	V.I.F.
average	188.246	0.0185294	
A:Steam mass flow rate	26.595	0.0381994	1
B:Water mass flow rate	-11.24	0.0381994	1
C:Hydrogen mass flow rate	-0.0325	0.0381994	1
D:Hydrogen total mass	0	0.0381994	1
E:Water temperature	0.49	0.0381994	1
AB	-0.4325	0.0381994	1
AC	0.115	0.0381994	1
AD	0.0825	0.0381994	1
AE	-0.3125	0.0381994	1
BC	0.055	0.0381994	1
BD	-0.0875	0.0381994	1
BE	0.2825	0.0381994	1
CD	-0.095	0.0381994	1
CE	0.17	0.0381994	1
DE	0.0275	0.0381994	1

Standard errors are based on total error with 1 d.f.

Table B.5: Analysis of variance for peak hydrogen

Source	Sum of Squares	Df	Mean Square	F-Ratio	P-Value
A:Steam mass flow rate	0.0475349	1	0.0475349	70.16	0.0756
B:Water mass flow rate	0.00302775	1	0.00302775	4.47	0.2813
C:Hydrogen mass flow rate	0.00246264	1	0.00246264	3.63	0.3075
D:Hydrogen total mass	0.0135199	1	0.0135199	19.95	0.1402
E:Water temperature	0.000178891	1	0.000178891	0.26	0.6978
AB	0.000307126	1	0.000307126	0.45	0.6228
AC	3.16406E-05	1	3.16406E-05	0.05	0.8645
AD	0.00698478	1	0.00698478	10.31	0.1922
AE	0.00956973	1	0.00956973	14.12	0.1656
BC	0.0178022	1	0.0178022	26.27	0.1227
BD	0.00584078	1	0.00584078	8.62	0.209
BE	2.67806E-05	1	2.67806E-05	0.04	0.8751
CD	0.0140245	1	0.0140245	20.7	0.1377
CE	0.00761693	1	0.00761693	11.24	0.1845
DE	3.63006E-05	1	3.63006E-05	0.05	0.8552
Total error	0.000677568	1	0.000677568		
Total (corr.)	0.129642	16			

Table B.6: Estimated effects for peak hydrogen

Effect	Estimate	Stnd. Error	V.I.F.
average	0.860053	0.00631324	
A:Steam mass flow rate	-0.109013	0.0130151	1
B:Water mass flow rate	0.0275125	0.0130151	1
C:Hydrogen mass flow rate	-0.0248125	0.0130151	1
D:Hydrogen total mass	0.0581375	0.0130151	1
E:Water temperature	0.0066875	0.0130151	1
AB	-0.0087625	0.0130151	1
AC	0.0028125	0.0130151	1
AD	-0.0417875	0.0130151	1
AE	0.0489125	0.0130151	1
BC	-0.0667125	0.0130151	1
BD	-0.0382125	0.0130151	1
BE	0.0025875	0.0130151	1
CD	0.0592125	0.0130151	1
CE	-0.0436375	0.0130151	1
DE	0.0030125	0.0130151	1

Standard errors are based on total error with 1 d.f.

Table B.7: Analysis of variance for average condensation rate

Source	Sum of Squares	Df	Mean Square	F-Ratio	P-Value
A:Steam mass flowrate	0.012144	1	0.012144	825794.72	0.0007
B:Water mass flowrate	6.25E-08	1	6.25E-08	4.25	0.2875
C:Hydrogen mass flowrate	2.50E-09	1	2.50E-09	0.17	0.751
D:Hydrogen total mass	1.00E-08	1	1.00E-08	0.68	0.561
E:Water temperature	4.00E-08	1	4.00E-08	2.72	0.347
AB	2.25E-08	1	2.25E-08	1.53	0.4328
AC	2.50E-09	1	2.50E-09	0.17	0.751
AD	0	1	0	0	1
AE	4.00E-08	1	4.00E-08	2.72	0.347
BC	0	1	0	0	1
BD	2.50E-09	1	2.50E-09	0.17	0.751
BE	2.50E-09	1	2.50E-09	0.17	0.751
CD	2.50E-09	1	2.50E-09	0.17	0.751
CE	2.50E-09	1	2.50E-09	0.17	0.751
DE	0	1	0	0	1
Total error	1.47E-08	1	1.47E-08		
Total (corr.)	0.0121442	16			

Table B.8: Estimated effects for average condensation rate

Effect	Estimate	Stnd. Error	V.I.F.
average	0.110382	2.94118E-05	
A:Steam mass flow rate	0.0551	6.06339E-05	1
B:Water mass flow rate	-0.000125	6.06339E-05	1
C:Hydrogen mass flow rate	0.000025	6.06339E-05	1
D:Hydrogen total mass	-0.00005	6.06339E-05	1
E:Water temperature	-0.0001	6.06339E-05	1
AB	0.000075	6.06339E-05	1
AC	-0.000025	6.06339E-05	1
AD	0	6.06339E-05	1
AE	-0.0001	6.06339E-05	1
BC	0	6.06339E-05	1
BD	0.000025	6.06339E-05	1
BE	0.000025	6.06339E-05	1
CD	-0.000025	6.06339E-05	1
CE	0.000025	6.06339E-05	1
DE	0	6.06339E-05	1

Standard errors are based on total error with 1 d.f.

C | Appendix C: Pressure and Compressibility Factor Evolution

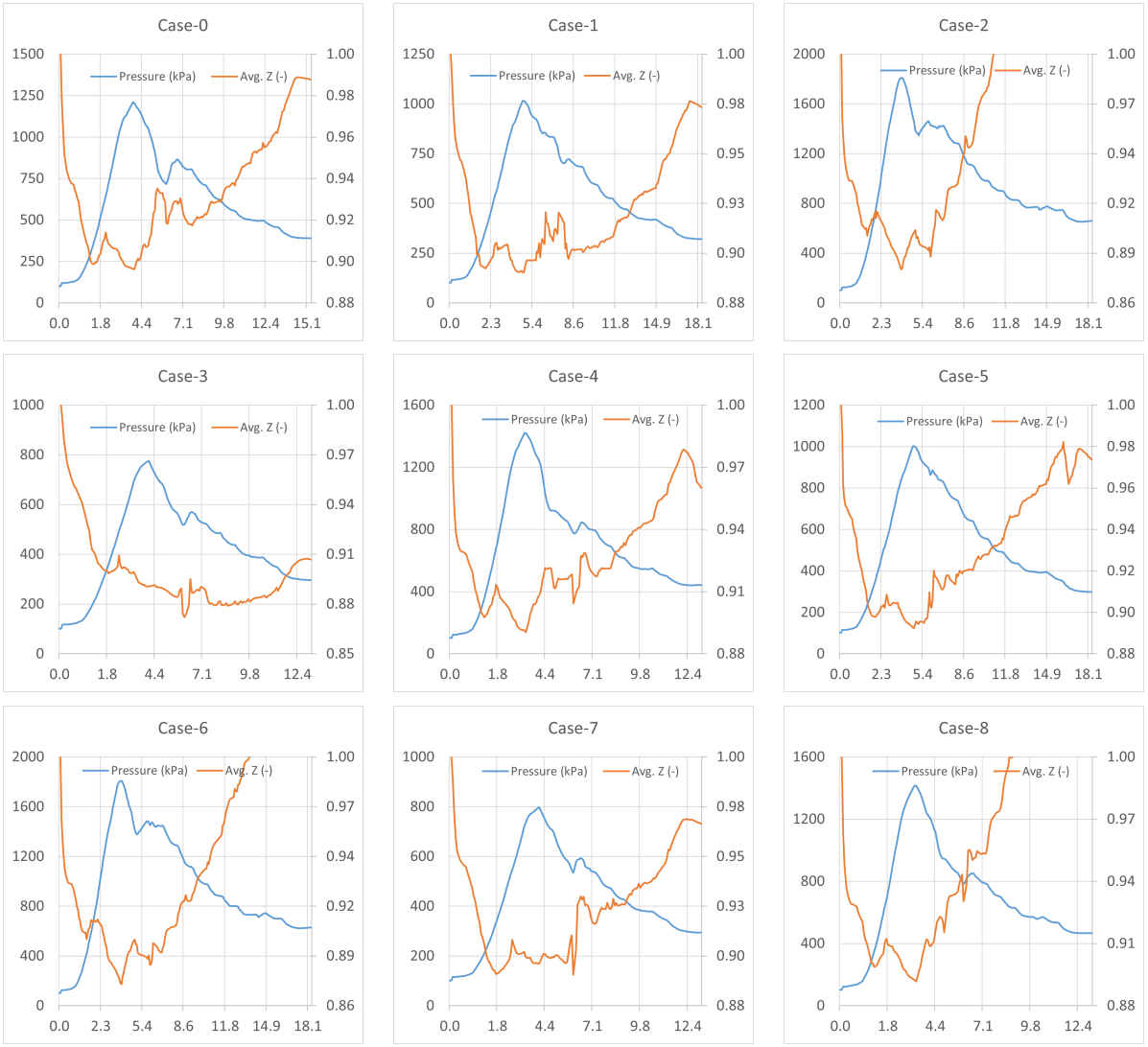

Figure C.1: Comparison between pressure and compressibility factor evolution. Cases 0-8

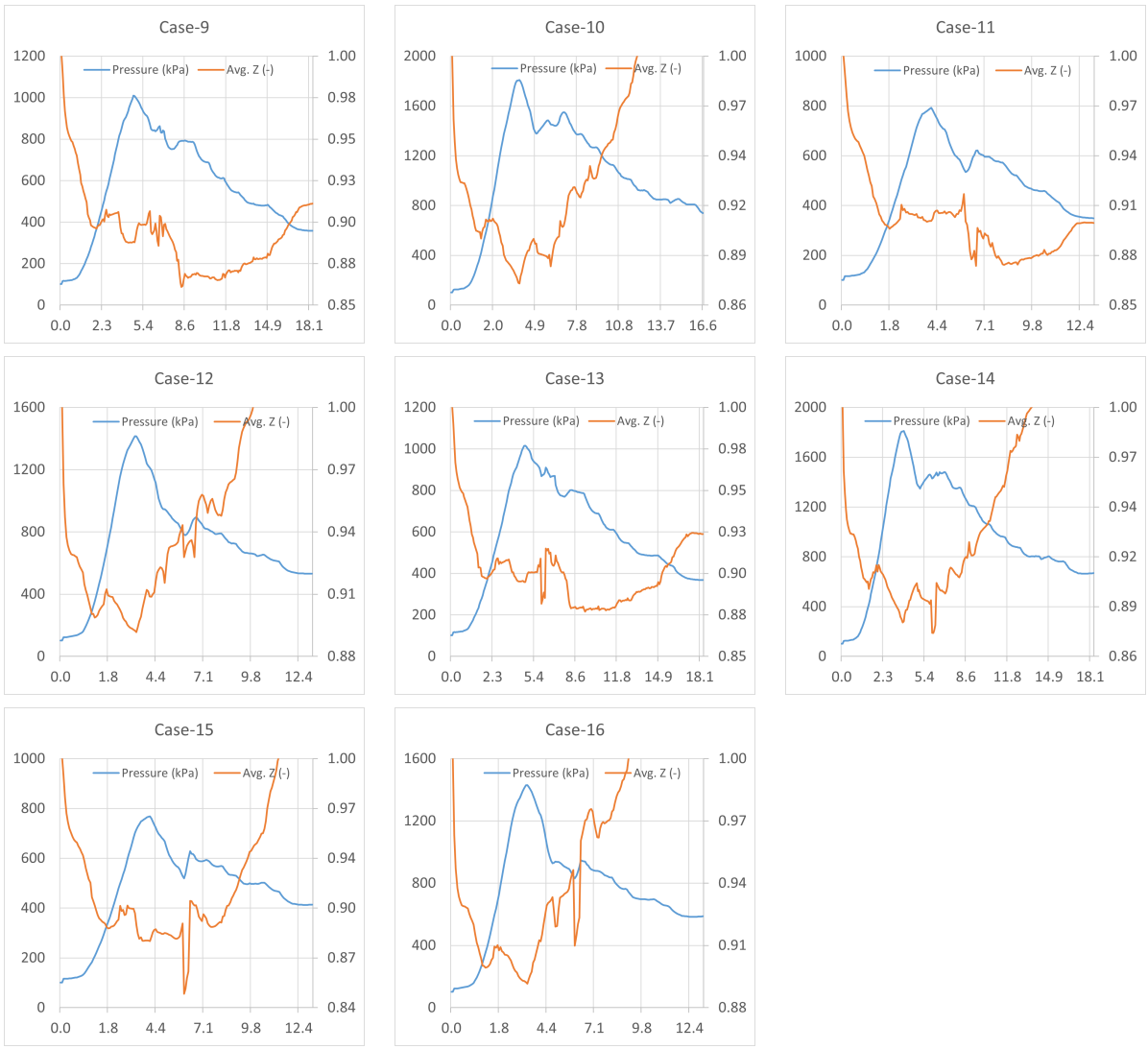

Figure C.2: Comparison between pressure and compressibility factor evolution. Cases 9-16

D | Appendix D: Linear regression plots of normalized pressure

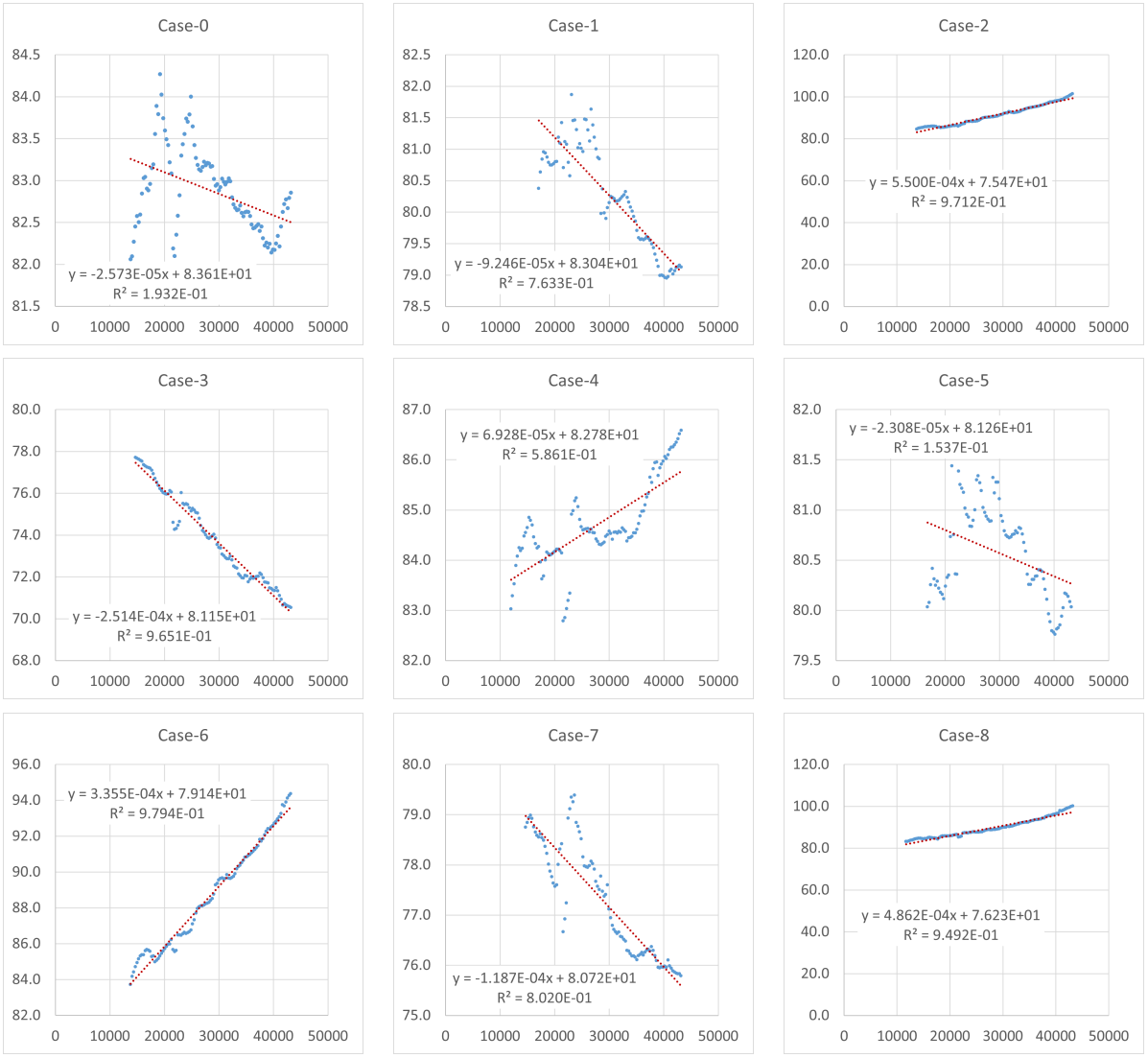

Figure D.1: Linear regressions for pressure buildup between peak condition and 12 hours. Cases 0-8

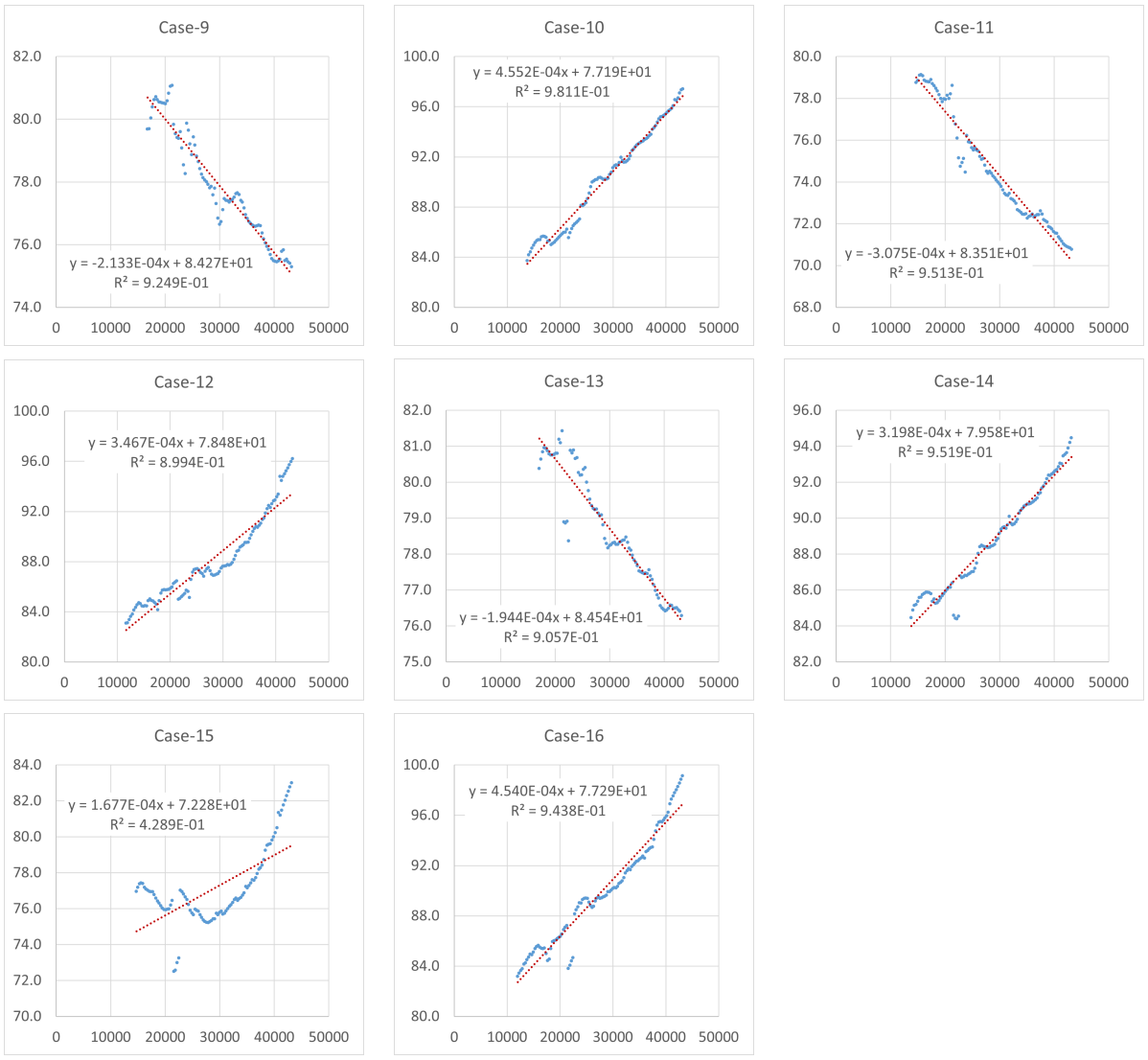

Figure D.2: Linear regressions for pressure buildup between peak condition and 12 hours. Cases 9-16

E | Appendix E: Average Compressibility Factor evolution

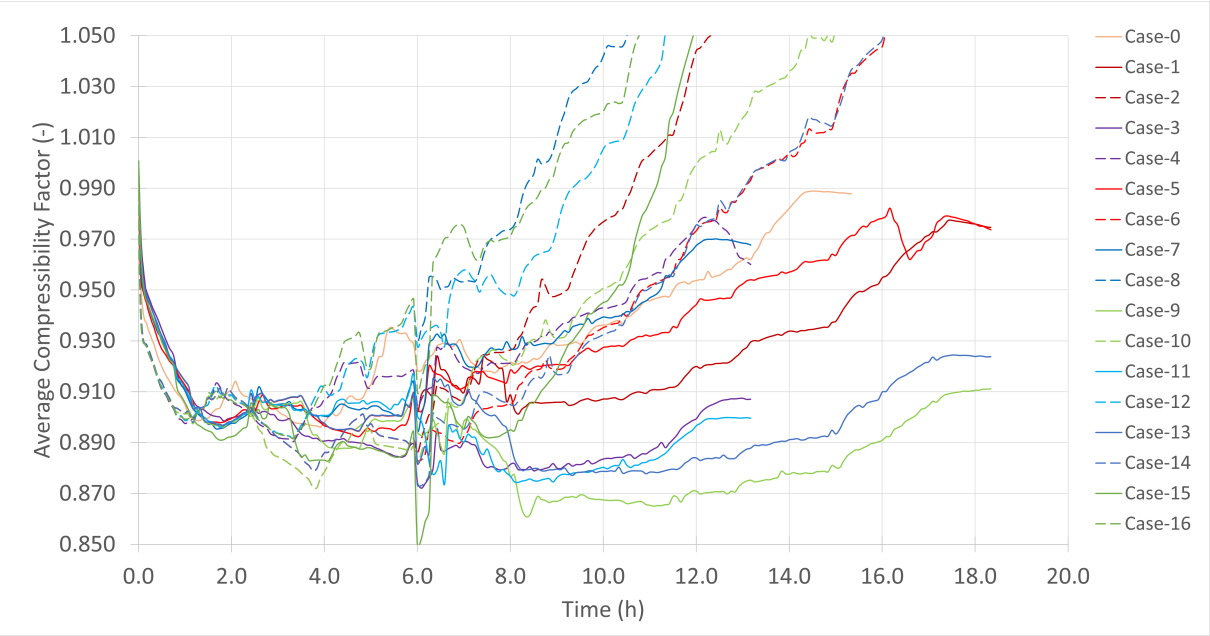

Figure E.1: Average compressibility factor for all cases

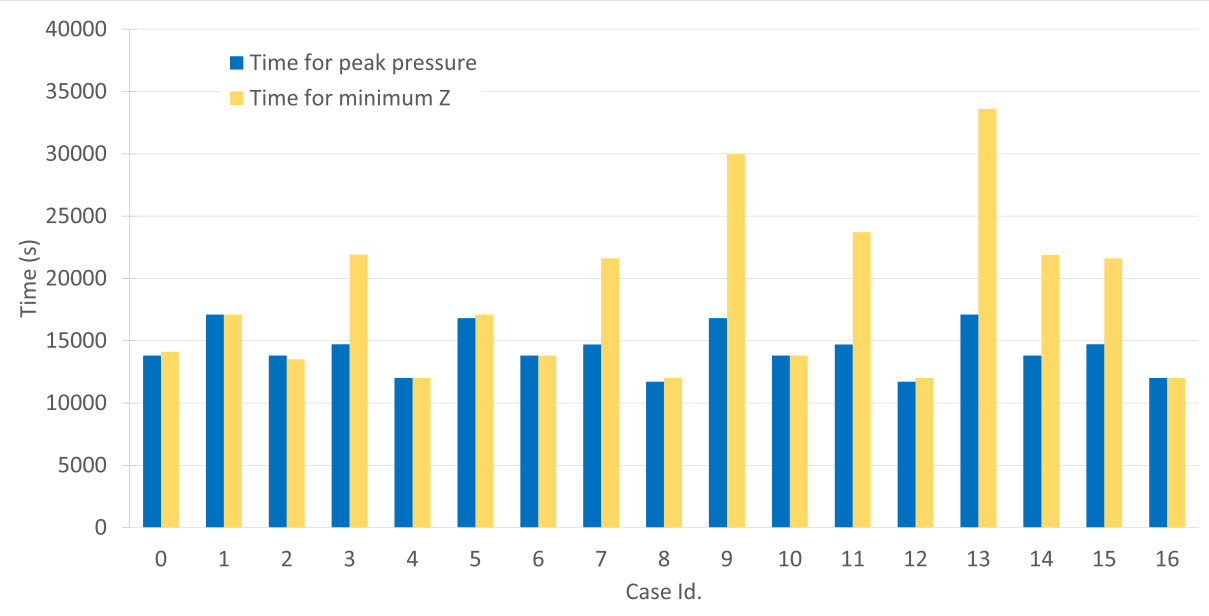

Figure E.2: Comparison of time for peak pressure and minimum compressibility factor for all cases

List of Figures

List of Tables

List of Symbols

Variable	Description	SI unit
A_b	External surface area at fluid interface	m^2
A_f	Portion of total area in contact with adjacent fluid	m^2
A_i	Internal surface area between conductors	m^2
C^c	Mass source from hydrogen combustion	kg/s
C^e	Energy source from hydrogen combustion	W
D	Diameter	m
D^c	Mass diffusion coefficient (incl. turbulence)	m^2/s
D^e	Thermal diffusion coefficient	m^2/s
D^e_{cn}	Thermal conductivity	W/(m·K)
D_h	Cell hydraulic diameter	m
D_{sg}	Binary diffusion coefficient (steam-gas)	m^2/s
E^c	Mass source from engineered safety equipment	kg/s
E^e	Energy source from engineered safety equipment	W
$\vec{E^m}$	Momentum source from engineered safety equipment	N
H	Height	m
M_s	Steam molecular weight	kg/mol
$m_{l,i}$	Liquid mass in cell i	kg
$m_{v,i}$	Vapor mass in cell i	kg
N	Total number of cells in control volume	–
P	Static pressure	Pa
s^c	Mass source per unit area at wall A_w	$kg/(m^2s)$
s^e	Energy source per unit area at wall A_w	W/m^2
$\vec{s^m_\phi}$	Momentum source per unit area at wall A_w	N/m^2
S^c	Mass source per unit area at interface A_I	$kg/(m^2s)$
S^e	Energy source per unit area at interface A_I	W/m^2
$\vec{S^m_\phi}$	Momentum source per unit area at interface A_I	N/m^2

Variable	Description	SI unit
T_1	Containment wall temperature	K
T_2	Building wall temperature	K
T_∞	Fluid temperature	K
t_j	Time j (0: initial, f: final)	s
V_{cn}	Conductor volume	m^3
V_i	Volume of cell i	m^3
$\vec{g}$	Gravitational acceleration	m/s^2
$\vec{n}$	Outward normal vector to surface dA	–
$\vec{u}$	Velocity	m/s
h	Enthalpy	J/kg
$h_{l,i}$	Liquid enthalpy in cell i	J/kg
$h_{v,i}$	Vapor enthalpy in cell i	J/kg
h	Heat transfer coefficient	$W/(m^2K)$
ke	Kinetic energy	J/kg
$\bar{c}$	Molar concentration (boundary layer)	mol/m^3
ρ	Density	kg/m^3
$\rho_{l,i}$	Liquid density of cell i	kg/m^3
$\rho_{v,i}$	Vapor density of cell i	kg/m^3
α	Volume fraction	–
$\alpha_{l,i}$	Liquid volume fraction of cell i	–
$\alpha_{v,i}$	Vapor volume fraction of cell i	–
β	Thermal expansion coefficient	1/K
χ_g	Volume concentration of non-condensing gas	–
ΔT	Temperature difference	K
ϵ	Emissivity	–
Γ''_d	Condensation rate per unit area	$kg/(m^2s)$
λ_t	User specified multiplier	–
ν	Kinematic viscosity	m^2/s
ϕ	Phase (v: vapor, l: liquid, d: drops, i: ice)	–
Ψ	Area porosity factor	–
σ	Stefan–Boltzmann constant	$W/(m^2K^4)$
$\boldsymbol{\sigma_\phi}$	Stress tensor	Pa
Θ	Volume porosity factor	–
Θ_i	Volume porosity factor of cell i	–
ζ	Vapor component (s, n, g)	–